THE UNIVERSITY OF QUEENSLAND

AUSTRALIA

Cooperative Localization and Tracking of Resource-Constrained Mobile Nodes

by
Vikram Kumar
M. Tech. (CSE)

A thesis submitted for the degree of Doctor of Philosophy at
The University of Queensland in 2018
School of Information Technology and Electrical Engineering

Abstract

Tracking mobile nodes is a topic of significant scientific and commercial interest. However, due to the high energy consumption of GPS receivers, high-frequency, long-term tracking of resource-constrained mobile nodes remains challenging. Cooperative position tracking has been proposed to improve energy efficiency, however most existing schemes perform opportunistic cooperation and optimize for either energy or accuracy. In this thesis, a cooperative tracking algorithm is proposed using planned cooperation, where a cluster head centrally coordinates resource usage among cluster members. This technique assumes the existence of a reasonably stable cluster of mobile nodes carried by groups of people, animals, or vehicles. Several variants of the proposed cluster-based tracking algorithm are investigated, which differ based on how a node estimates its position after receiving a position update from the cluster head. These techniques include estimating a node's position to be the same as the position update, or using a Kalman filter to incorporate inertial measurement sensor data as well as the received position updates.

A second group of localization techniques estimates position based on RSSI-based range estimates from a subset of nodes using GPS to estimate their position. Multilateration is used to estimate node positions based on these ranges. The theoretical bounds (Cramer-Rao Lower Bounds) for localization performance are derived in a practical scenario where both neighbouring node positions and RSSI range estimates have errors following normal (position) and log-normal (range) probability distributions. Targeting resource-constrained nodes, two different self-localization algorithms are proposed which use these different error distributions. The two algorithms vary in computational complexity and localization performance. In simulated experiments, the proposed self-localization algorithms reduce the root mean square error and bias-norm up to 50% while reducing computation time by 80% compared to previously published algorithms.

Finally, a multi-mode tracking algorithm is proposed building on the proposed cluster-based tracking and self-localization algorithms. This algorithm uses either individual mea-

surements, group estimates, or multilateration-based estimates based on the current status of the group and the desired energy or accuracy performance. This multi-mode tracking algorithm is as accurate as individual GPS tracking while using up to 50% less energy when evaluated on position tracks of nodes generated using Reynolds' flocking model. Overall, the proposed algorithms show significant improvements in localization and tracking of mobile nodes compared to the current state-of-the-art.

Declaration by author

This thesis is composed of my original work, and contains no material previously published or written by another person except where due reference has been made in the text. I have clearly stated the contribution by others to jointly-authored works that I have included in my thesis.

I have clearly stated the contribution of others to my thesis as a whole, including statistical assistance, survey design, data analysis, significant technical procedures, professional editorial advice, financial support and any other original research work used or reported in my thesis. The content of my thesis is the result of work I have carried out since the commencement of my higher degree by research candidature and does not include a substantial part of work that has been submitted to qualify for the award of any other degree or diploma in any university or other tertiary institution. I have clearly stated which parts of my thesis, if any, have been submitted to qualify for another award.

I acknowledge that an electronic copy of my thesis must be lodged with the University Library and, subject to the policy and procedures of The University of Queensland, the thesis be made available for research and study in accordance with the Copyright Act 1968 unless a period of embargo has been approved by the Dean of the Graduate School.

I acknowledge that copyright of all material contained in my thesis resides with the copyright holder(s) of that material. Where appropriate I have obtained copyright permission from the copyright holder to reproduce material in this thesis and have sought permission from co-authors for any jointly authored works included in the thesis.

Publications during candidature

Conference papers

- V. Kumar, R. Arablouei, R. Jurdak, B. Kusy, and N. Bergmann, "Multi-mode Tracking of a Group of Mobile Agents," in *Proceedings of IEEE 20th International Symposium on Wireless Personal Multimedia Communications (WPMC)*, 17-20 December 2017, Yogyakarta, Indonesia. (https://arxiv.org/pdf/1711.02348.pdf)

- V. Kumar, R. Arablouei, R. Jurdak, B. Kusy, and N. Bergmann, "RSSI-based self-localization with perturbed anchor positions," in *Proceedings of IEEE 28th Annual International Symposium on Personal, Indoor, and Mobile Radio Communications (PIMRC)*, 8-13 October 2017, Montreal, Canada. (http://dx.doi.org/10.1109/PIMRC.2017.8292600)

- V. Kumar, N. Bergmann, I. Ahmad, R. Jurdak, and B. Kusy, "Cluster-based position tracking of mobile sensors," in *Proceedings of IEEE International Conference on Wireless Sensors (ICWiSe)*, 10-12 October 2016, Langkawi, Malaysia. (http://dx.doi.org/10.1109/ICWISE.2016.8187754)

Publications included in this thesis

No publications included. Although,

- Chapter 3 is heavily based on the publication "V. Kumar, N. Bergmann, I. Ahmad, R. Jurdak, and B. Kusy, "Cluster-based position tracking of mobile sensors," in *Proceedings of IEEE International Conference on Wireless Sensors (ICWiSe)*, 10-12 October 2016, Langkawi, Malaysia."

Contributor	**Statement of contribution**
Vikram Kumar	Conception and design (90%) Analysis and interpretation (85%) Drafting and production (85%)
Neil Bergmann	Conception and design (5%) Analysis and interpretation (5%) Drafting and production (5%)
Izanoordina Ahmad	Conception and design (5%) Analysis and interpretation (5%) Drafting and production (0%)
Raka Jurdak	Conception and design (0%) Analysis and interpretation (5%) Drafting and production (5%)
Brano Kusy	Conception and design (0%) Analysis and interpretation (0%) Drafting and production (5%)

- Chapter 6 is heavily based on the publication "V. Kumar, R. Arablouei, R. Jurdak, B. Kusy, and N. Bergmann, "RSSI-based self-localization with perturbed anchor positions," in *Proceedings of IEEE 28th Annual International Symposium on Personal, Indoor, and Mobile Radio Communications (PIMRC)*, 8-13 October 2017, Montreal, Canada."

Contributor	Statement of contribution
Vikram Kumar	Conception and design (90%) Analysis and interpretation (85%) Drafting and production (85%)
Reza Arablouei	Conception and design (10%) Analysis and interpretation (5%) Drafting and production (5%)
Raka Jurdak	Conception and design (0%) Analysis and interpretation (5%) Drafting and production (5%)
Brano Kusy	Conception and design (0%) Analysis and interpretation (5%) Drafting and production (0%)
Neil Bergmann	Conception and design (0%) Analysis and interpretation (0%) Drafting and production (5%)

- Chapter 7 is heavily based on the publication " V. Kumar, R. Arablouei, R. Jurdak, B. Kusy, and N. Bergmann, "Multi-mode Tracking of a Group of Mobile Agents," in *Proceedings of IEEE 20th International Symposium on Wireless Personal Multimedia Communications (WPMC)*, 17-20 December 2017, Yogyakarta, Indonesia.".

Contributor	Statement of contribution
Vikram Kumar	Conception and design (90%) Analysis and interpretation (85%) Drafting and production (85%)
Reza Arablouei	Conception and design (10%) Analysis and interpretation (5%) Drafting and production (5%)
Raka Jurdak	Conception and design (0%) Analysis and interpretation (5%) Drafting and production (5%)
Brano Kusy	Conception and design (0%) Analysis and interpretation (5%) Drafting and production (0%)
Neil Bergmann	Conception and design (0%) Analysis and interpretation (0%) Drafting and production (5%)

Manuscripts included in this thesis

No manuscripts included.

Contributions by others to the thesis

No contributions by others.

Statement of parts of the thesis submitted to qualify for the award of another degree

None

Research Involving Human or Animal Subjects

No animal or human subjects were involved in this research.

Acknowledgements

There are a number of people who deserve to be both acknowledged and thanked for their support and assistance during my exciting and successful journey as PhD student. I would like to first express my sincere gratitude to my supervisors Prof. Neil Bergmann, Prof. Raja Jurdak, Dr. Branislav Kusy and Dr. Reza Arablouei for the continuous support and immense knowledge throughout my PhD journey. My supervisors have routinely gone beyond their duties to firefight my worries, concerns, and anxieties, and have worked to instill great confidence in both myself and my work. I could not have imagined having better advisors and mentors for my PhD study. I would also like to extend my special thanks to the research group and colleagues from CSIRO for always being there when I needed any help. I am deeply grateful to Dr. Dhirendra Sharma (Associate Professor, UIIT, Himachal Pradesh University, Shimla, India), Prof. Vikram Singh (Department of Computer Science at Chaudhary Devi Lal University, Sirsa, Haryana, India), and Prof. K.L Bansal (Department of Computer Science, Himachal Pradesh University, Shimla, India) for their guidance throughout my PhD journey.

I am grateful to the Govt. of India for providing me financial assistance under National Overseas Scholarship scheme. With their financial assistance, I am able to make it this far in the program and is able to reach my goal as a doctoral student.

I am thankful to my family members and relatives. Words can not express how grateful I am to my mother, father, mother-in-law, father-in-law, and late grandparents, for all of the sacrifices to ensure my success in this journey. Their prayers for me was what sustained me thus far. Encouragement received from my sisters and brothers-in-law, throughout this journey was remarkable and deserve a special thanks. A lot of love and thanks to their sweet kids Paru, Shivu, Kaun, and Chantu for always cheering me up. Definitely, a heartiest thanks to my cousins and friends for their continuous inspirations.

Lastly, a wholehearted thanks to my beloved wife Dr. Babita for her sacrifices, motivation, and love, throughout this complex journey of PhD. Without her, I would not be who I am today.

Financial support

The financial support received from the Government of India under the National Overseas Scholarship scheme for tuition fees and living allowance is gratefully acknowledged.

Top-up scholarship and additional financial support for attendance at conferences from School of ITEE, University of Queensland, and from CSIRO/Data61 is also gratefully acknowledged.

Keywords

Localization, self-localization, multilateration, wireless sensor networks, cooperative localization, RSSI, weighted least-squares.

Australian and New Zealand Standard Research Classifications (ANZSRC)

- ANZSRC code: 080504, Ubiquitous Computing, 60%
- ANZSRC code: 090609, Signal Processing, 40%

Fields of Research (FoR) Classification

- FoR code: 0805, Distributed Computing, 60%
- FoR code: 0906, Electrical and Electronic Engineering, 40%

Table of Contents

List of Figures

List of Tables

List of Mathematical Notations used in the thesis

x	a lower-case letter represents a scalar variable
$\tilde{x}$	a letter with a tilde accent represents the noisy value of original variable x
$\hat{x}$	a letter with a hat accent represents an estimated value of variable x
$\bar{e}$	a letter with an overbar represents an approximate value
$\mathbf{r}$	a lower-case bold letter represents a vector
$\mathbf{r_i}$	ith element of vector $\mathbf{r}$
$\mathbf{F}$	an upper-case bold letter represents a matrix
$\mathbf{F_{ij}}$	element located in the ith row and jth column of matrix
$(.)^T$	denotes the vector/matrix transpose
$(.)^{-1}$	denotes the matrix inverse
$\frac{\partial(.)}{\partial v}$	represent the partial derivative with respect to the variable v
Var(.)	returns the variance of a scalar argument
Cov(.)	returns the covariance matrix of its vector argument
Tr (.)	is the matrix trace operator
$\mathcal{N}(\mu, \sigma)$	represents the normal distribution with mean μ and standard deviation σ

List of Abbreviations used in the thesis

A-GPS assisted-GPS.

AOA angle of arrival.

BC bias compensated.

CBT cluster-based tracking.

CEKF complementary extended Kalman filter.

CH cluster head.

CKF cooperative Kalman filter.

CoMon cooperative ambience monitoring platform.

CRLB Cramer-Rao lower bound.

CSIRO Commonwealth Scientific Industrial Research Organization.

CTLS constrained total least-squares.

DoD Department of Defense.

DR dead reckoning.

EKF extended Kalman filter.

EWTLS element-wise total least-squares.

FIM Fisher information matrix.

GNSSs global navigation satellite systems.

GPS global positioning system.

GSM global system for mobile communication.

HNL heuristic non-linear.

HPL heuristic pseudo-linear.

IEEE Institute of Electrical and Electronics Engineers.

IMU inertial measurement unit.

INS inertial navigation system.

KF Kalman filter.

LEAP low energy assisted positioning.

MCU microcontroller unit.

MDS multidimensional scaling.

MEMS microelectromechanical system.

ML maximum likelihood.

PDR pedestrian dead reckoning.

RAPS reliable anchor pair selection.

RMSE root mean square error.

RSSI received signal strength indicator.

SDP semidefinite programming.

SLSQP sequential least squares programming.

SOCP second order cone programming.

SPEAR source position estimation for anchor position uncertainty reduction.

SPEAR-S source position estimation for anchor position uncertainty reduction with single measurement.

TDOA time difference of arrival.

TLS total least-squares.

TOA time of arrival.

TTFF time to first fix.

WLAN wireless local area network.

WLS weighted least-squares.

WSN wireless sensor networks.

Chapter 1

Introduction and Motivation

Localization and tracking of mobile nodes is useful for both industrial and scientific purposes. For example, in the industrial context, Google traffic updates and driving directions are interesting applications using location data. In the scientific context, tracking animal's location improves our knowledge of their movement range and foraging behaviour. The Batmon project [1] of Commonwealth Scientific Industrial Research Organization (CSIRO) is an example of a project which depends on localisation. Indeed, this Batmon project is a primary motivation behind my thesis. It involves continental-scale fruit bat monitoring to understand their movement and its influence on the spread of bat-borne diseases. Bats harbour viruses such as Hendra, Lasaa, and Ebola which are transmitted through the bat's bite, urine or aerosolization of saliva and may lead to the death of victims [2–6]. On the positive side bats play an important role in the native ecology [7, 8].

More broadly, localization and tracking of livestock (e.g., cattle, goats, and pigs in commercial farms), wildlife (e.g., deer, dingoes), humans (e.g., workers, cyclists), and mobile assets (gas cylinders, tools) also have scientific and industrial importance. These applications involve long-term tracking of sensor nodes fitted with battery operated tracking devices. In most of these applications, the node movements are uncontrolled. Therefore, device maintenance (e.g. battery replacement) may be laborious or even impossible. Hence, the tracking device should be fitted with the maximum possible energy resources and it should use them efficiently. However, to preserve the natural movements of the tracked animals, the allowed maximum size and weight of the tracking devices is restricted, and this limits the available computational power and energy resources. The satellite-based global positioning system (GPS) is commonly used for outdoor localization and tracking. However, for resource-

constrained devices, GPS-receivers are still relatively expensive in energy use. For example, Camazotz, the tracking device used in the Batmon project, uses a CC430 system on chip (SoC) with GPS, inertial, acoustic, air pressure and temperature sensors, two solar panels, a 300mAh Li-Ion battery operating at 3.7V (3996J), with a total weight of just under 30g [9]. Its battery is sufficient only for one year with 25 GPS-based position updates per day (0.43J/GPS activity, GPS(74mW) and processor (13.2mW) use for 5s). This tracking period and resolution may not be sufficient for Batmon and other similar applications.

However, in many applications, nodes exhibit grouping behaviour. The grouping behaviour presents an opportunity to distribute the GPS sensing load and share the GPS-based position among the group members. Load sharing will potentially increase the tracking life (reduced energy usage) of nodes but this comes at the expense of increased position error. The energy-accuracy trade-off of sharing the GPS positioning information and sensing load among the group members is the focus of this thesis.

This thesis considers the problems of outdoor localization and tracking of uncontrolled nodes having grouping behaviour. Such groups may be dynamic in nature which means there may exist different clusters of nodes during the tracking period. The size and number of nodes in a cluster formed depends on the radio communication range. The nodes are assumed to have resource-constrained tracking devices similar to Camazotz. Each node in a group is considered as an independent entity but the node will participate in a group activity to either increase the tracking life-time or localization accuracy. In a group activity, member nodes share the GPS sensing load, received signal strength indicator (RSSI) measurements, and other sensor information such as accelerometer and magnetometer readings. The GPS has errors in its positioning from a number of sources such as errors in ephemeris data, satellite clock, multipath or errors in the receiver itself (thermal noise, software issues) [10]. Similarly, the RSSI measurements also have noise from sources such as multipath, radio-interference, obstructions or model inaccuracy leading to errors in distance estimation among nodes [11]. Considering the use of microelectromechanical system (MEMS)-based components, the measurements from inertial-sensors also have noise. My thesis considers these different kinds of errors in position measurement in group activity and investigates the possible solutions to either increase the tracking period or improve the self-localization accuracy or both. The evaluation presented is based on simulated group movement behaviour generated through the well-known Reynolds flocking algorithm [12]. The energy model used is based on the reported

energy consumption of Camazotz [9]. All the simulation framework and algorithms required to perform the experiments are designed using Python. The four specific contributions made in this thesis are outlined in the following paragraphs.

First, this thesis presents a cluster-based tracking (CBT) algorithm. CBT distributes the GPS sampling load and shares the position information among the cluster members in a planned manner using a cluster head (CH). Three variants of CBT are evaluated, namely "CBT-Standard", "CBT-cooperative Kalman filter (CKF)" and "CBT-CKF with Accelerometer and Magnetometer". The results are compared with an algorithm in which a node samples its own GPS every time it requires a position update, referred to here as the Individual algorithm. Evaluations reveals that CBT can reduce the position error up to 43% for a given energy budget compared to the Individual algorithm. Similarly, CKF with Acc.&Mag can reduce the energy usage up to 27% while staying within the position error performance range of Individual algorithm.

Second, this thesis presents the Cramer-Rao lower bound (CRLB) for the variance of the position estimate using a multilateration technique. In multilateration, there are two types of nodes. The first type, referred to as "blind nodes" are the nodes whose position is not yet known. The second type, referred to as "anchor nodes" are the nodes that have an estimate of their current locations (e.g., using GPS) and are in the communication range of the blind nodes. Given the anchor node positions and the distance estimates between blind nodes and anchor nodes, the blind node position is the intersection of circles whose origins are located at the anchor positions and whose radii are equal to the distances between anchor nodes and the blind node. This work extends previously published results in the literature. The presented CRLB considers more realistic assumptions about errors, i.e., a zero-mean normal distribution of errors in anchor positions and a log-normal distribution of errors in distance estimates. The former assumption is due to GPS-based positioning and the latter is due to the distance estimation using RSSI measurements [13, 14].

Third, this thesis presents two self-localization algorithms targeting resource-constrained devices. Both the algorithms are heuristic in nature and are named heuristic non-linear (HNL) and heuristic pseudo-linear (HPL) algorithms. HNL minimizes a non-linear, weighted sum-square-error cost function in an iterative manner. The cost function consists of the weighted square of the difference between the distance inferred from an RSSI measurement and the Euclidean distance between the blind node and the anchor node to which the RSSI

measurement corresponds. The square-error terms are weighted by their variances, which are estimated by taking into account perturbations in both RSSI measurements and anchor node position information. The results are compared with an existing iterative algorithm, named source position estimation for anchor position uncertainty reduction (SPEAR), considering similar noise assumptions in measurements [15]. Compared to SPEAR, the proposed HNL algorithm has advantages in both root mean square error (RMSE) and computational time. HNL only took one-sixth of the computational time and gives up to 27% less RMSE compared to SPEAR.

The proposed HPL algorithm gives a closed form solution. HPL first approximates the problem's original non-linear system of equations with a linearized system of equations. Next, HPL uses a weighted least-squares (WLS) solution to solve the system of linear equations. The weights are estimated by taking into account the statistical properties of the perturbations in both RSSI and anchor position information. Finally, HPL calculates and compensates for the bias in the solution caused by noisy anchor positions and RSSI measurements. To the best of my knowledge, there is no existing algorithm considering similar noise assumptions to the ones made here and providing a closed form solution. HPL results are compared with the "Hyperbolic" algorithm [16]. The Hyperbolic algorithm considers similar noise assumptions on distance estimates while assuming perfect knowledge of anchor node positions and provides a closed form solution. The proposed HPL algorithm considerably improves the Hyperbolic algorithm both in term of RMSE and bias without any extra computational burden. HPL shows up to 50% lower RMSE compared to the Hyperbolic algorithm and reduces the bias close to zero.

Fourth, the thesis presents a multi-mode tracking algorithm. To maximize position accuracy, this algorithm chooses the best between HPL, CBT and Individual tracking for the localization at an instance based on the group size and available resources. For a given energy budget, multi-mode tracking reduces the mean tracking error by up to 20% in comparison to CBT. Additionally, the proposed multi-mode tracking algorithm is as accurate as the Individual-based tracking while using around 50% less energy.

The rest of the thesis is organized as follows. Chapter 2 covers the literature survey on energy-efficient localization and tracking algorithms and presents the research questions addressed in this thesis. Chapter 3 describes the CBT algorithm for sharing the GPS sensing load among a group of mobile nodes in planned cooperation. Chapter 4 gives the derivation of

the theoretical bound on the localization variance. Chapters 5 and 6 propose HNL and HPL algorithms to approach the theoretical bounds derived in Chapter 4. Chapter 7 describes the multi-mode tracking algorithm and evaluates its energy-accuracy performance. Finally, Chapter 8 presents the conclusions drawn from this thesis work along with the original contributions made and possible future directions.

Chapter 2

Literature Review, Gaps, and Research Questions

Localization refers to the process of estimating the location of a device or node. An application may need 2D or 3D location information. When the location information is tracked along with time, then the process is referred as tracking. The field of localization and tracking is vast. It ranges from an airplane navigation to localization/tracking of honey bees [17, 18]. Following are the basic parameters categorizing the localization field.

- Outdoor Versus Indoor: Outdoor localization refers to locating a node in open areas such as a sea, forest, street, and road. Indoor localization refers to node positioning inside a building, bus, airplane, etc.

- Self Versus Target: The process in which a node estimates its own location is called self-localization. However, the process of estimating the location of another node (generally referred as a target node) is called target localization. For example, finding the location of an object using radar is target localization, whereas if the same object uses its GPS or the radar information to estimate its location, then it's self-localization.

- Resource-constrained Versus Resource-rich: The term resource may refer to a computational resource or an energy resource or both. The availability of resources for location calculation can have a significant impact on the accuracy of the estimated location. A resource-rich node, e.g. a car, may have enough battery and computational power to run a complex optimization algorithm and estimate its location, whereas resources available in a tracking device fitted on a honey bee may be minuscule.

- Centralized Versus Distributed: This category specifies where the processing related to localization takes place. In centralized localization, all the position estimation-related processing happens at a single central location. Whereas, in distributed localization, the tasks involved in the location estimation are divided among a set of processing nodes in a network. Distributed processing is one way to deal with the problem of constrained resources.

- Online Versus Offline : In online localization, the location is estimated and provided to an application on a real-time basis e.g. Google driving directions. In offline localization, raw location information is recorded and processed at a later time. Offline localization generally serves analytic purposes such as tourist movement history.

This thesis is focused on outdoor, self-localization of resource-constrained mobile nodes in 2D. The resource limitations are considered in both energy and computational power. The processing is assumed to be at the node itself (centralized) and the location is calculated on a real-time basis (online).

The rest of chapter is organized as follows. Section 2.2 discusses global navigation satellite systems (GNSSs) and the GPS operation followed by high energy consumption issues of GPS as a challenge in localization and tracking of resource-constrained devices. Section 2.1 covers various mobility models. Section 2.3 presents radiolocation technologies and multilateration along with the challenges posed by errors in various measurements required for multilateration. Section 2.4 covers the literature addressing the high-energy consumption issue of GPS by duty-cycling it. Section 2.5 discusses the literature related to the multilateration-based localization addressing the measurement error problem. Next, section 2.6 presents a summary of the reviewed literature along with the identified research gaps. Finally, Section 2.7 presents various research questions addressed along with a short comment on the methodology to answer those research questions.

2.1 Mobility Models

Mobility models describes the movement of mobile noes, and how their location, velocity and acceleration change over time. The various movement models relevant to this thesis are discussed below.

2.1.1 Random Walk

This term was first coined by Karl Pearson in [19]. The Random Walk model, also referred to as the Brownian Motion, was originally proposed to emulate the unpredictable movement of particles in physics. The Random Walk model is a memoryless mobility process where the information about the previous status is not used for the future decision. A basic example of a random walk is the random walk on the integer number line which starts at 0 and at each step moves $+1$ or -1 with equal probability. Other examples such as path traced by a molecule in liquid and the search path of a foraging animal can also be approximated as a random walk.

2.1.2 Random Waypoint

This model was first proposed by Johnson and Maltz in [20]. This mobility model is a simple and straightforward stochastic model. In this model a node randomly chooses a waypoint (destination point) which are uniformly randomly distributed on the system area. The node then moves with constant speed on a straight line to this point. Once arrived, the node pause for a random time, and then chooses a new destination and speed. This process repeats again and again.

2.1.3 Reynolds flocking

In 1987, Craig Reynolds proposed a distributed flocking movement model [12]. This model consist of three simple steering behaviors parameters (separation, alignment, cohesion) which describe how an individual node in a flock maneuvers based on the positions and velocities its nearby flockmates. The separation value decides the steer to avoid crowding local flockmates. The alignment value defines the steer towards the average heading of local flockmates. The cohesion value decides the steer to move toward the average position of local flockmates. By chossing the different values for these steering behaviors one can simulate different types of the flocking behaviour.

2.2 GNSSs and GPS

GNSSs are commonly used for outdoor localization. The Department of Defense (DoD) of the United States started the first GNSS project, presently known as GPS, for military purposes, which, later on, was made available for civilian use. Initially, GPS made available for civilian use was purposefully degraded, with accuracy of about 100m, using selective availability, which was later removed. At present, consumer grade GPS is able to obtain an accuracy in the range 1m to 10m [21]. For specialized applications such as surveying, centimetre level accuracy is possible [22]. In addition to GPS, Russia's Global Orbiting Navigation Satellite System and the European Union's Galileo are global operational GNSSs. This thesis is focused on GPS, due to its current dominance in applications worldwide.

2.2.1 GPS Working

The GPS system consists mainly of three segments namely the space segment, control segment and user segment as shown in Fig. 2.1 [22, 23].

Space Segment

This segment consists of the GPS satellites which send radio signals from space. There are total 24 satellites in six orbital planes. The satellite signals include ranging signals and navigation messages. The ranging signals are meant to estimate the distances between GPS receiver on the earth and the satellites transmitting the signal. The GPS satellites transmit two types of ranging codes differentiated based on the accuracy: the Precision or P-code and the Coarse Acquisition or C/A-code, designed for military and civilian purpose respectively. C/A-code messages are less accurate, easier to acquire but easier to jam than the P-code. The navigation messages include ephemeris data and almanac data. The ephemeris data contains the position of each satellite in orbit. The almanac data is used to calculate the time and status of the entire satellite constellation.

Control Segment

This segment consists of five satellite tracking stations located around the world. It tracks the GPS satellites and provides them with periodic updates, correcting their ephemeris constants and clock-bias errors on a daily basis.

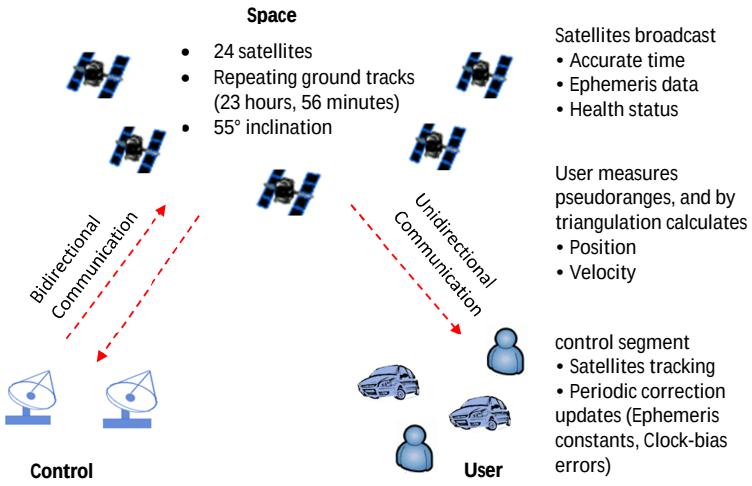

Figure 2.1: GPS system segments: Space, Control and User

User Segment

This segment consists of the GPS receivers, the ones located in the users' devices. GPS receivers convert satellite signals into position, and velocity estimates.

The GPS receiver calculates its position using multilateration. Multilateration requires a minimum number of reference points with their location known (satellites in this case) and the distance between the visible satellites and the GPS receiver (user interested in finding the location). To estimate the distance, the GPS receiver generates a set of codes identical those transmitted by the system's satellites and calculates the time delay between its codes and the codes received from the GPS satellites by determining how far it has to shift its own codes to match those transmitted by the satellites. Then the travel time is multiplied by the speed of light to estimate distances between the receiver and the satellites, called pseudoranges. Rather than require strong clock synchronization between the receivers and the atomic clocks on the satellites, the receiver clock offset is also one of the estimated parameters. To calculate the four parameters of position (x,y,z) and clock offset, readings from four satellites are needed.

2.2.2 GPS Errors

The Euclidean distance between a node's actual position and GPS-based positioning is called the GPS error. There are multiple sources of GPS error such as atmospheric delays, multipath, satellite clock, ephemeris errors, and receiver noise which includes receiver kinematics and receiver hardware quality [10]. The GPS-based positioning error can be calculated

as a function of pseudorange errors on the satellite set. It is a common assumption that each error source in range estimation is independent and follows a normal distribution on a large enough set of samples. Another known condition is that the sum of all errors for each satellite is equal to the total pseudorange errors. Given these conditions, the pseudorange error estimate can be described using a normal distribution following the central limit theorem. In addition, the error in each axis (x, y, z) of the GPS-based position estimation can also be described using a normal distribution with zero mean [24].

2.2.3 Time to First Fix and GPS Start Modes

In resource-constrained devices the time to first fix (TTFF) plays an important role due to its direct relationship with energy consumption, and the larger the TTFF, the higher the energy consumption. GPS positioning involves iterative refinement of the position estimate before it settles down and reports final position. In this iterative process, TTFF is the time required by the GPS to finish its first position estimate. This involves startup, satellite signal acquisition, navigation data and time required to perform the calculation. TTFF depends on the start types (cold, warm and hot) of the GPS. These types are differentiated based on the navigational data already available on the GPS receiver memory.

Cold Start

The cold start refers to a state when GPS is not active for a long time (probably weeks duration) and it does not have any valid ephemeris or almanac data in its memory. The cold start time may vary from the 30s to 45s depending on the manufacturer [25].

Warm Start

In warm start, the GPS receiver is supposed to have valid almanac data, the previous position of the receiver, and the time which allows the receiver to predict the visible satellites. This helps in faster acquisition of the signal and ephemeris data. The warm start takes around 25s to 35s, which again varies with manufacturer [25].

Hot Start

A hot start is performed if the receiver has valid ephemeris in addition to the data in the warm start. Then a receiver only needs ranging signals from satellites which take around 1s to 5s [25].

2.2.4 Energy Consumption: A Problem

The energy-consumption value calculated for the hot start of Camazotz is around 0.4J (explained in Chapter 1) [9]. This is relatively high for resource-constrained devices. For example, the Camazotz battery (3996J) is only sufficient for one year with 25 GPS-based position updates per day. Both the tracking period and resolution is not sufficient for applications in Batmon [1] or other localization/tracking applications such as tracking of livestock (e.g., cattle, goats, pigs in commercial farms), wildlife (e.g., dear, dingoes), humans (e.g., workers, cyclists), and mobile assets (cylinders, tools) which also have scientific and industrial importance.

An obvious solution to increase the tracking period and resolution is to increase the available battery resources. One option is to increase the battery size. Increasing the available battery size will increase the weight of the tracking devices. However, there are limitations in both size and weight of tracking devices which can be used in order to ensure the natural movement of the nodes. Therefore, the only option left is to efficiently use the available resources.

GPS dominates the energy consumption among other components such as radio, microcontroller unit (MCU), inertial sensors in tracking devices [26, 27]. Hence, it becomes natural to focus on efficient use of the GPS. The above applications of interest consist of nodes with grouping behavior. The grouping nature of the nodes carries the potential to increase the tracking period. The node's individual GPS can be duty-cycled by distributing the GPS-sensing load among the group members. However, it is not clear how to distribute the GPS-sensing load efficiently and what is the resulting tracking error range. In addition, what is the energy-accuracy trade-off and how does this trade-off vary with a range of sampling intervals?

This thesis investigates how GPS can be used to either increase the tracking period or accuracy or both in applications having resource-constrained nodes but which exhibit some

group behaviour. A significant amount of the literature is dedicated to duty-cycling the GPS and increasing the tracking period while maintaining or improving the accuracy. The relevant literature is discussed in the section 2.4.

2.3 Radiolocation Technologies and Multilateration

The size of wireless sensor networks (WSN) can range up to hundreds or thousands of nodes. For such large networks, it may not be possible to equip every node with GPS. Generally, such networks contain a small percentage of nodes with independent positioning sensors such as GPS receivers [28–33]. The rest of the nodes use information from neighbouring nodes to estimate their positions using radiolocation technologies such as angle of arrival (AOA), time of arrival (TOA), time difference of arrival (TDOA) and multilateration (described later in the section). In addition to large static WSNs, radiolocation technologies are useful in localization and tracking resource-constrained mobile nodes as shown in this thesis.

For a given node, neighbouring nodes considered in this thesis are the nodes within its direct radio communication range. This thesis uses the term "blind node" for a node which does not know its current location information and needs to localize itself using cooperative localization. The term "anchor node" is used for a node which knows its current position and is in the communication range of blind nodes. Several techniques using radio signals to determine the position of an object are described in the following sections [28, 29, 34–37].

2.3.1 Angle of Arrival

The knowledge of angle between anchor nodes and a blind node can be used in blind node localization [38–41]. Given an anchor node's (sensing device) position, orientation and range to the blind node, it only requires single measurement of bearing to calculate blind node position as shown in Fig. 2.2.

When range measurements are not available then the blind node position can be calculated using angles from two or more geographically distinct positions as shown in Fig. 2.3.

There are two basic methods for measuring angle or arrival. The first is to use a directional antenna and rotate it seeking maximum signal strength and the second is to use an antenna with a steerable beam to search for the direction of maximum signal strength. The details

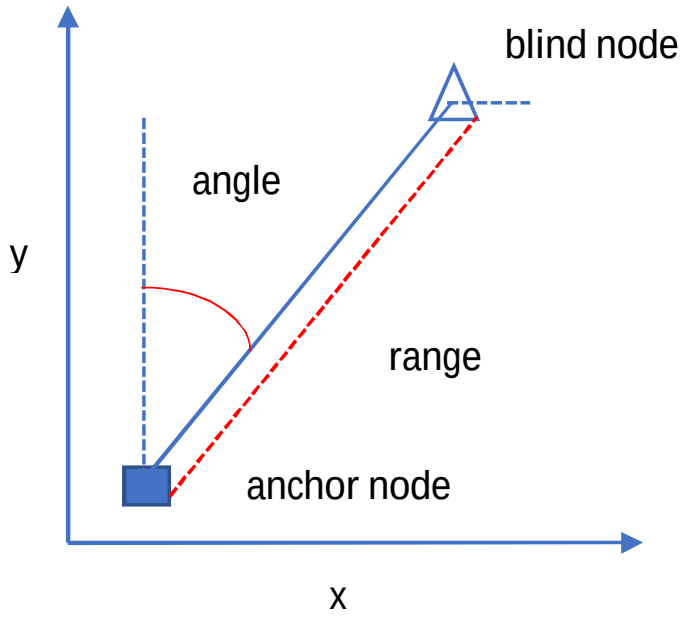

Figure 2.2: Blind node localization using range and angle measurements from one anchor

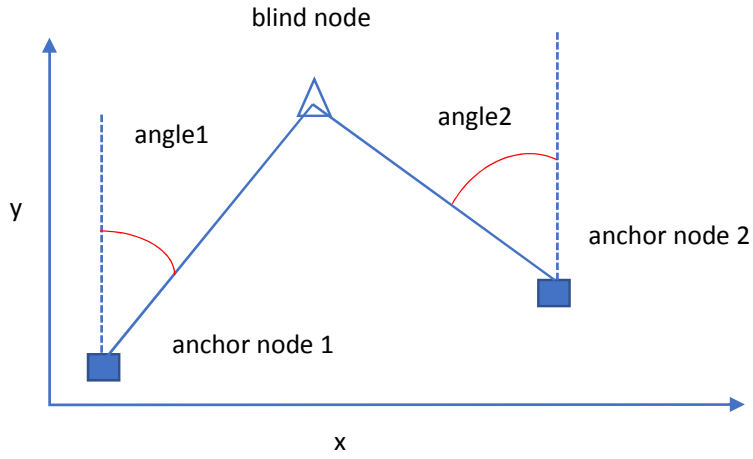

Figure 2.3: Blind node localization using angle measurements from two anchors

of AOA localization can be found in [42, 43]. A comparative study of advanced methods (ESPRIT, JADE, and SAGE) for joint estimation of TOA and DOA is given in [44].

2.3.2 Time of Arrival

TOA is the time at which a blind node first receives a radio signal transmitted by an anchor node. The measured time is used to calculate the propagation time between anchor node and blind node. The propagation time multiplied by the signal propagation speed gives the distance or range between an anchor node and blind node. The presence of additive noise and multipath signals, and the need for accurate clock synchronization makes the time of flight estimation challenging [45–48]. Recently proposed ultrawideband-based localization systems

such as Ubisense, BeSpoon, and DecaWave can deal with multipath and clock synchronization issues efficiently [49]. However, such additional hardware is not typically yet available on low-cost sensor nodes.

2.3.3 Time Difference of Arrival

In this technique, a blind node sends signals to multiple anchor nodes located at known locations. The anchor nodes record the arrival time of the signal and the blind node location is estimated by the difference of the recorded arrival time stamps. In contrast to TOA, TDoA does not require the exact time when the signal was transmitted. TDoA measurements involve the challenges of time synchronization of anchor nodes and signal detection [50, 51].

2.3.4 Backscatter Communication

Backscatter Communication has demonstrated the viability of astonishingly low-power tags or battery-less communications. Backscatter system picks up TV or cellular signals using antenna and converts them into electricity, which it then uses to reflect a Morse code-like version of that signal. Similar antennas on other devices in turn detect that coded, reflected signal, and can respond accordingly. Recently, researchers have explored localization using Backscatter Communication [52, 53].

2.3.5 Radio Signal Strength Indicator

RSSI denotes the measured power of a radio signal at a receiver. It can be measured by a receiver during normal data communication without any additional energy, bandwidth or hardware requirement and is mostly reported in the logarithmic unit dB or dBm (dB relative to 1 mW power). Given transmit power, receiver antenna gains, and signal path loss as a function of distance, RSSI can be used to estimate transmit distance. The RSSI measurement is available during normal packet reception and does not require any additional hardware like other ranging techniques e.g. AOA, TDOA, and TOA. In addition, RSSI is included in Institute of Electrical and Electronics Engineers (IEEE) 802.11, ZigBee and supported by a number of commercially available radios. These reasons constitute the basis for the use of the RSSI-based ranging technique in this thesis.

In an idealized environment, RSSI follows the free space radio propagation model. The

radio signal strength is linearly related to the inverse square of the distance d between the transmitter and the receiver. The received power $P_r(d)$ at distance d follows the Friis equation [54] given as

$$P_r(d) = \left(\frac{\lambda}{4\pi d}\right)^2 P_t G_t G_r \tag{2.1}$$

where λ is the transmitter signal wavelength in meters, P_t is the transmitted power, G_t and G_r are transmitting and receiving antennas gains, respectively.

RSSI is not a particularly accurate estimator of distance, so RSSI-based location techniques need to account for this accuracy. In practice, both the signal propagation and received power suffers from several factors such as fading, interference, obstruction, absorption, and multipath. Therefore, rather than a strict deterministic relationship, individual measurements of RSSI are typically assumed to come from a probabilistic distribution. RSSI in such environments is generally modeled using a parameterisable log-normal shadowing path loss model [55] given as

$$P_r(d) = P_r(d_0) - \eta 10 \log_{10}\left(\frac{d}{d_0}\right) + n_p \tag{2.2}$$

where, d_0 is the reference distance, $P_0(d_0)$ denotes the received power at distance d_0, η is the path-loss exponent, and n_p is the normal random variable (zero mean, parameterisable variance) that accounts for fading effects. The distance estimate $\hat{d}$ of actual distance d using this model is then a random variable:

$$\hat{d} = d \exp\left(-\alpha n_p\right) \tag{2.3}$$

where, $\alpha = \frac{\log 10}{10}$. In (2.3), n_p is a normal distributed variable within an exponential which makes the distance estimates $\hat{d}$ a log-normal distributed variable (experimentally verified in [56]).

In addition to free space, the radio propagation model described in (2.2) is applicable in different environments such as outdoor and indoor both with and without line-of-site. The path-loss exponent η is one of the most important parameter which has been considered widely in radio propagation model analysis. It can take a range of values in different environment as given in Table 2.1 [57, 58].

Environment	Path-loss exponent
Free Space	2
Urban area cellular radio	2.7 to 3.5
Showed urban cellular radio	3 to 5
Inside building line-of-site	1.6 to 1.8
Obstructed inside buildings	4 to 6
Obstructed inside factories	2 to 3

Table 2.1: Path-loss exponent for different environment

A number of authors have verified the radio propagation model given in (2.2) in different set of environments [59–61]. In our lab, one of other students in our team undertook experiments using sensor nodes similar to those planned for this work [62, 63]. The authors of [62, 63] verified the RSSI model given in (2.2) by performing field experiments. They conducted a large number of dense outdoor experimental measurements at different distances and transmit powers using Camazotz [9], the CSIRO's in-house developed tracking platform, to verify the path-loss model and estimate its parameters. Th parameters for the CC2420 ZigBee module are based on results published in [64]. They used $d_0 = 1$m and measured RSSI every 5m up to 45m and estimated various radio propagation parameters as $p_{0(\text{dBm})} = -33.44$, and $\eta = 3.567$, which are used in my experiments as well.

2.3.6 Multilateration: A Problem With Measurement Errors

This thesis is focused on 2D RSSI-based localization using multilateration. In multilateration, a blind node requires anchor nodes position and distances to them in order to calculate its position. Given accurate anchor node positions and distances, blind node position is just the intersection of circles with the origin located at anchor node positions and radius equal to the corresponding distances Fig. 2.4. For example, the left-hand side of Fig. 2.4 shows three anchor nodes A,B,C with their positions given by coordinates $(x1, y1), (x2, y2), (x3, y3)$ which are known exactly and one blind node D with unknown position coordinate (x, y). The accurate distances between the anchor nodes and the blind node are represented as $d1, d2, d3$. Given the accurate distances and accurate anchor node information, the blind node position is simply the intersection of circles denoted by the red dot. This is solvable using simple trigonometry.

As discussed above, neither the distance estimates nor the anchor positions are error free. In that situation, the left-hand side figure turns to the one given on right-hand side, where

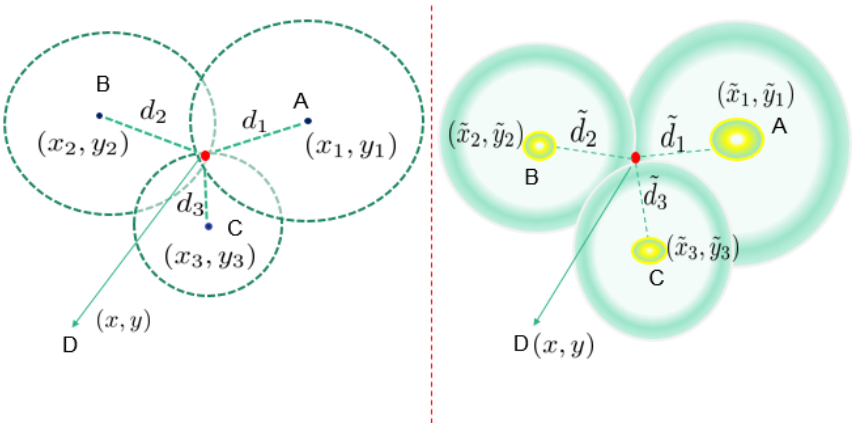

Figure 2.4: Multilateration: the left figure shows multilateration given perfect knowledge of anchor positions and distance information and the right figure shows multilateration when both anchor positions and distance measurements have errors.

the intersection of circles has uncertainty The solution to the blind node position estimation problem depends upon the nature of the errors assumed in distance and anchor position estimates.

This thesis considers a blind node localization problem (formally defined in Section 4.1, Chapter 4) where errors in the distance estimates follow a log-normal distribution and anchor positions errors follow a normal distribution. The former assumption is due to the underlying RSSI-based distance estimation and the latter is due to GPS-based anchor position. The literature related to the multilateration problem is discussed in Section 2.5.

2.4 Literature: GPS Duty-Cycling

As described in section 2.2.4, this section covers the literature on the problem of how GPS can be used to either improve the tracking period or accuracy or both in applications having resource-constrained nodes that exhibit some group behaviour.

Discussion of the attempts to reduce the GPS energy consumption in localization and tracking are categorized as follows:

- **Standalone GPS Duty-Cycling**: This category consists algorithms using approaches such as periodic, application-specific customization, object behaviour modeling, use of low-power MEMS-based sensors (accelerometer, magnetometer, gyroscope) and dynamic selection of localization technology.

- **Computation Offloading to Cloud/Central-server**: This category covers the algorithms using ideas of using existing cellular network infrastructure, energy-hungry

computation offloading and information storage such as roadmap, Wi-Fi/cellular network coverage, and trajectories.

- **Multisensor Data Fusion** This category covers the algorithms focusing on information fusion from multiple independent localization sources. The common methods in use are Kalman filter and its extensions, complementary filters, and particle filters.

- **Cooperative GPS Duty-Cycling**: This category covers the algorithms which consider resource and information sharing with neighbouring nodes within the radio communication range to improve the localization error and the energy usage.

2.4.1 Standalone GPS Duty-Cycling

An obvious solution to the GPS energy consumption problem is to decrease its sampling frequency. This saving comes at the cost of increased positioning error. The approach used in [65–67], looks at the problem of "when to localize" rather than how to localize. Tilak [67] proposed two approaches, one adaptive and one proactive, to decide the position sampling interval. The adaptive algorithm calculates the position sampling interval using recently observed motion of the nodes. A node estimates its velocity based on the distance traveled and time taken in last two sampling points. The node uses this velocity estimate for traveled-distance estimation and decides its next sampling point at a pre-calculated distance. The predictive algorithm uses a model-based movement prediction for velocity estimation. Both the algorithms give significant energy savings compared to tracking using a periodic (constant) sampling interval.

An algorithm named EnTracked, which uses an accelerometer to detect motion or non-motion states and GPS speed reading for better speed estimation is given in [68]. EnTracked consists of three modules: an application requiring position data, the EnTracked-server, and the EnTracked-client. The application module requests the data from the EnTracked-server module which formulates the position query according to the application specific error and uncertainty requirements of a client. The EnTracked-client module implements the client logic: if the currently available position reading meets the position uncertainty requirement of the application then supply the same position value otherwise compute a new position. A new GPS reading is not requested until positional uncertainty crosses an application specific tolerance limit. EnTracked saves up to 50% energy in comparison to an algorithm using

periodic sampling.

The subsequent version of EnTracked named EnTrackedT focuses on energy efficient trajectory tracking [69, 70]. This version simplifies the trajectory by ensuring it is within some known corridor boundary. EnTrackedT uses three strategies namely heading aware strategies (using a compass); distance aware strategies (using GPS-based speed); and movement aware strategies (using an accelerometer). EnTrackedT further reduces the energy consumption by 40% to 60%. The reduction depends upon the position uncertainty limit which varies up to 500m.

The authors of [71] investigate the best localization source for an object with a fixed energy budget. Their algorithm named EnLoc characterizes the optimal localization accuracy for a given energy budget using a node's movement history. EnLoc requires area maps containing the locations of Wi-Fi access points, global system for mobile communication (GSM) towers, and GPS performance profiles to achieve the reported performance. The algorithm, reliable anchor pair selection (RAPS) given in [72] uses a node's spatio-temporal history and knowledge of GPS accuracy fluctuations in urban areas. It uses a cell tower-RSS blacklisting database to detect when GPS is unavailable (e.g., indoor) and avoid turning on the GPS in such cases. In RAPS, GPS is turned ON only when estimated uncertainty in the position exceeds the maximum threshold and the accuracy level of the GPS in that area is acceptable. RAPS achieves around 30% energy saving compared to periodic sampling with a similar error profile. The major energy saving of RAPS comes by avoiding GPS activation when it's likely to be unavailable or available with poor performance. A drawback of RAPS is the requirement of spatio-temporal history and an RSSI database of cell towers. The energy saving of RAPS may differ for high deviations from the historical movement patterns.

A mobile phone middleware for energy and context-aware location-based services is given in [73]. These authors noticed the lack of on-the-fly adjustment of GPS duty-cycling in the Android stack. Hence, they proposed middleware with a dynamic scheduler, mobility profiling, batch transmission and energy-aware features. The mobility profiling module creates user profiles and predicts their activity based on their movement history of available GPS points. The proposed middleware predicts the probability of a user remaining in the same profile and adjusts the GPS duty-cycling accordingly. The complex nature of the proposed middleware makes it unsuitable for the resource-constrained nodes.

The above-mentioned works make it clear that the smart use of GPS and low-power

inertial-sensors significantly improves both energy and accuracy. A direct performance comparison among these algorithms is not straightforward. These algorithms differ in term of resource requirements; one needs cell-tower databases, another need maps and another makes use of travel history. In addition, these algorithms consider different tracking or localization scenarios. In my view, these algorithms are complementary to each other and could be combined if relevant resources or information is available. Generally, the energy and accuracy improvements reported compared to periodic sampling vary from 30% to 50%. The range of improvements depends on the tracking scenario, available information, resources and tracking requirements.

2.4.2 Computation Offloading to Cloud/Central-Server

Offloading the computationally intensive task in localization to an external server is another approach for energy-efficient localization. A major limitation of algorithms using such an approach is the unavailability of connectivity to the cloud at all locations. This limits the algorithms use in localization and tracking of uncontrolled mobile nodes considered in this thesis. However, following is a review of some interesting algorithms using such an approach.

The algorithm named assisted-GPS (A-GPS) uses existing cellular networks to predict and convey the possible visible GPS satellites information to a node [74]. A-GPS greatly reduces the search space and shortens the time-to-first-fix from minutes to seconds. The algorithm achieves an accuracy of 50m indoors and 15m outdoors. However, the algorithm is unsuitable for the localization in areas with no cellular coverage.

The authors of [75] explore a GPS computation black box. Their proposed algorithm named low energy assisted positioning (LEAP) shifts the delay-tolerant and energy-hungry GPS computational stages to a cloud server. Therefore, GPS is switched on for a second or less to collect the sub-millisecond level propagation delay for the signal of each satellite. LEAP infers the other information necessary to perform the GPS-based position calculation from nearby objects e.g. cellular towers. This results in 80% energy saving compared to traditional GPS positioning algorithms. A LEAP extension, named Co-GPS, uploads raw GPS signal to a cloud and performs signal processing their itself [76]. Co-GPS uses the earth elevation database to generate landmarks for reference and removes the reference object requirement. An issue with Co-GPS is its energy and accuracy trade-off. For accurate localization, it requires a huge data upload which may reduce the potential energy gains.

Trajectory simplification is an approach to reduce communication overhead by reducing sensing data transferred during location updating. The idea behind trajectory simplification is to replace the obtained positions with a smaller subset (snapshot), the one which is minimal in size while still reflecting the overall motion information. It is useful for applications which need mobile node's trajectory information instead of a single position. The authors of [65] proposed to reduce the data transmissions by decreasing the number of location updates. The authors of [77] proposed an Inter-Frame Coding (IFC) algorithm which exploits spatio-temporal localities to compress trajectory based locating sensing data. In addition, offline localization (data processing at central server) can be cheap, but is not suitable when real-time results are needed and Internet connectivity is not available.

2.4.3 Multisensor Data Fusion

Significant research has been undertaken to improve position estimates by fusing the noisy GPS measurements and noisy measurements from MEMS-based navigation sensors or other sources of position information such as Wi-Fi.

The authors of [78] proposed an algorithm to fuse the differential-GPS [79] and dead reckoning (DR)-based estimations. In DR, the authors use a pedometer and compass to estimate displacement and direction respectively. They use an extended Kalman filter (EKF) to process the GPS-based and DR-based position estimation. Simulation-based results reveal that the proposed algorithm reduces the horizontal position error of differential-GPS from 5m to 2m (60% reduction).

In [80], the authors use MEMS-based inertial sensors (accelerometer, gyroscope, and magnetometer) for pedestrian navigation and exploit the complementary nature of gyroscope and magnetometer to improve DR. The magnetometer-based azimuth estimations are more sensitive to the local disturbances in the magnetic field measurements caused by nearby permanent magnets, electric currents, or large iron bodies but are stable over time. Whereas, gyroscopes-based azimuth estimations are independent of the location, but drift continuously with time. Therefore, the authors use the gyroscope derived azimuth to identify magnetic disturbances and the magnetic compass to determine the bias of the gyroscope and the initial orientation, even when no GPS signal is available. They refine the direction estimate by applying a Savitzky-Golay filter and a Kalman filter (KF). This algorithm also achieves a position accuracy of around 5m.

The authors of [81] describe a MEMS-based navigation system without using GPS. This system uses accelerometer signals for step detection, a magnetometer for azimuth angle calculation and a multi-layer neural network for the step-length estimation. It performs final estimation using a modified receding horizon Kalman finite impulse response filter. Another middleware for Android-based mobile phones to track the position using GPS, accelerometer, and magnetometer is given in [82]. The authors use sensors of a mobile phone (accelerometer and magnetometer) to track the position in-between two consecutive GPS samples. The time between two consecutive GPS activations is based on the error accumulation in the sensor-based position estimation. To compute the sensors-based location, the authors use Vincenty's formulae and low-pass filters to process the noisy sensor signals. GPS is used as both the starting point for sensor-based location and an error correction mechanism to reduce the drift in sensor-based estimation. Their middleware reduces GPS usage around 20% while ensuring a predefined maximum position uncertainty limit.

A vehicle localization framework using a smartphone's inertial sensors is given in [83]. This framework uses a DR approach to compute the position based upon the pipelined processing of velocity, acceleration, and directional components. This framework focuses on accurate positioning. However the high-frequency sampling of even an accelerometer and a magnetometer can also lead to high energy utilization [27]. This work lacks details of the energy and accuracy gains with their approach. The authors of [84] present a GPS-inertial navigation system (INS) map matching algorithm using curve-to-curve matching after Kalman filtering to correct mismatch and eliminate redundancy.

For indoor environments, the authors of [85] present a tracking algorithm which fuses information from wireless local area network (WLAN), pedestrian dead reckoning (PDR) and map information. The authors evaluate a complementary extended Kalman filter (CEKF) and a particle filter to fuse the information from the available sources. Their algorithm achieves errors less than 3m in distance and 12° in heading for particle filters compared to 4m in distance and 12° for the CEKF. The authors of [86] proposed a navigation system for a smartphone using WiFi, PDR, and landmarks such as turns, elevators, escalators, stairs, and doors. This system use smartphone sensors (accelerometer, magnetometer, gyroscope, barometer) and WiFi to identify landmarks. To makes the system suitable for resource-constrained nodes the sensor fusion problem is formulated in a linear perspective and uses a KF instead of a particle filter. The framework achieves an average localization accuracy of

1m.

In summary, the literature suggests improvements in tracking accuracy by fusion of different sources of information with suitable fusion methods. The GPS integration with an INS reduces the GPS duty-cycling roughly in the range of 50%. However, INS requires high sampling of inertial sensors for such results and as observed in [27] continuous high sampling of inertial sensors is also energy expensive. The addition of information from sources such as landmarks, map, and pedometer further improve the navigation performance. However, the computation time to run such algorithms is a few seconds, as observed in [85], and this may not be suitable for resource-constrained devices with long-term tracking requirements.

2.4.4 Cooperative GPS Duty-Cycling

Inspired by the social and group nature of humans, researchers have also investigated the possibility of position or energy improvement by sharing sensor measurements within a group of mobile nodes. The algorithms using this approach are referred as cooperative algorithms. In cooperative algorithms, the measurements such as GPS, inertial measurement unit (IMU), and distance are shared among neighbouring nodes through communication interfaces such as low-power radio, Bluetooth, and Wi-Fi.

The authors of [87] present a cooperative GPS duty-cycling algorithm using a Wi-Fi ad-hoc network while ensuring an application-specific upper error bound. In this algorithm, each node tracks its own position uncertainty and whenever a node approaches the uncertainty limit, it requests a position update from neighbouring nodes. In case of a fruitful reply, the node updates its position with the received information, otherwise it activates its own GPS for a position update. The authors use real data traces of visitors in the Epcot theme park in Florida to evaluate the algorithm. The results are compared with an algorithm in which a node relies only on the locally available information and does not use any kind of cooperation. The algorithm reduces energy consumption in the range of 30% to 40%. However, the reduction is strongly dependent on parameters such as communication range and maximum tolerable position uncertainty.

The cooperative ambience monitoring platform (CoMon), a novel cooperative ambiance monitoring platform is proposed in [88]. This platform addresses the energy problem through opportunistic cooperation among nearby mobile nodes using Bluetooth. It uses following for cooperative activity:

- Contact stability profile: CoMon maintains the history of contacts along with their duration. It uses this information to decide whether to initiate cooperative activity with a particular node or not.

- Differentiation between acquaintances and strangers: CoMon maintains this information to decide whether to share the activity data with a particular user or not.

- Profit and loss analysis ability: The node's personal ability to make profit and loss analysis is based on factors such as the following. What is being shared with a neighbour? What is each node getting in return from the other? What chances are there to end up with a beneficial cooperation?.

CoMon concentrates on general resource sharing among devices. Complex negotiations process make CoMon unsuitable for resource-constrained mobile nodes.

In [89], the authors propose a GPS duty-cycling algorithm based on radio contact logging and inertial sensors. The algorithm uses short-range radio communication as a means of reducing position uncertainty of a node. If the sum of the neighbouring node position uncertainty and distance to that node is less than the node's own position uncertainty, the node updates its position estimate with its neighbour's position, otherwise it activates its own GPS. The algorithm also uses an accelerometer to detect movement versus a stationary state of a node. This avoids activation of the GPS in the stationary state resulting in better energy efficiency. This algorithm saves 50% energy compared to the individual algorithm while meeting the application specific positioning criteria. In another work [27], the authors propose movement-pattern-based and group-based motion sensors duty cycling algorithms. The authors use empirical data traces of cattle to evaluate the performance of the algorithms. The movement-based algorithm yields 78% improvement in overall node energy consumption, and the group-based method results in an additional 20% energy reduction during periods of low mobility.

The authors of [90], proposed an algorithm using positive orthogonal codes and a semi-extended Kalman filter. In this algorithm, the GPS measurement is treated as the linear part and neighbourhood distance part as a nonlinear part in the same Kalman filter. This algorithm uses ranging, road map and GPS information in order to refine the relative position of the neighbourhood nodes in an energy-rich environment with vehicle grade IMU information.

The authors of [91] proposed an algorithm to correct the DR-based position estimate

using Bluetooth and IMU data shared by neighbouring nodes. In this algorithm, all the data is loaded into a server for relative distance estimation among nodes. The authors assume a scenario where a group of nodes moves in the same direction and uses the average of all readings to deal with the sensor noise. The authors reported 28% error reduction by using the data from neighbouring nodes for position estimate correction.

The authors of [92] improve Wi-Fi positioning in an indoor environment by using the RSSI-based distance among the neighbouring nodes. They calculate a confidence score as a weight to decide the position of the neighbouring node. The confidence of the Wi-Fi-based position is calculated using the standard deviation of the multiple Wi-Fi scans for the same point. Less standard deviation means higher confidence in position and vice versa. The confidence score of Bluetooth is calculated by RSSI modeling in the different settings of the indoor environment. Lastly, the authors use game theory to determine the final position of the nodes. The algorithm yields up to 32% improvement compared to an existing algorithm only using Wi-Fi for positioning.

The reviewed works are summarized in Table 2.2. It shows the performance (energy or accuracy) gain in localization/tracking (both indoor and outdoor) by cooperation among a group of mobile nodes. Sharing the measurements such as distance, self-position estimate, and IMU can improve the position accuracy up to 30%. In terms of energy, cooperation among neighbouring nodes can reduce the consumption up to 80%. Cooperation between GPS and inertial sensors can also help in reducing the energy consumption. The movement pattern, communication range, and maximum tolerable position uncertainty are identified as important parameters affecting the cooperative localization.

2.5 Literature Review: Localization using Multilateration

As described earlier in section 2.3.6, this section covers the literature related to the multilateration-based localization problem in which both anchor nodes and distance information have errors. The error in the anchor's position is assumed to follow a zero-mean normal distribution and errors in distance estimates are assumed to follow a log-normal distribution due to the underlying RSSI-based ranging technique.

In the literature, two main classes of approaches deal with the adverse effects of RSSI and

Table 2.2: Summary: GPS duty-cycling categories

Category	**Basic Concepts/ Directions**	**Energy & Accuracy Improvement Range compared to Individual algorithm or standard GPS sampling**	**Remarks**
Standalone	focused on duty-cycling the locally available GPS; periodic sampling; movement-based sampling; inertial-sensors for movement prediction; modeling the movement behaviour	energy savings up to 60%; position uncertainty limit 50m to 500m	achievable maximum energy and accuracy is limited compared to cooperative
Computation Offloading	shifting computational intensive task involved in GPS-based positioning to central facility; shifting whole raw positioning data to central facility; using existing telecommunication infrastructure for faster access of almanac data	energy saving up to 70%; accuracy up to 5m to 15m	connectivity to the central server may not be available in remote areas; energy cost of raw data upload may suppress the benefits of computation shifting
Multisensor Data Fusion	use of inertial sensors such as accelerometer, magnetometer, compass and barometer; fusion of Wi-Fi- or Bluetooth-based positioning information	energy savings up to 50%; position accuracy up to 1m	additional requirements of inertial sensors; primarily focused on accuracy improvement;limited energy gains
Cooperative GPS Duty-Cycling	position sharing among neighbouring nodes; inertial sensors data sharing	energy-saving 50% to 80% (note: this saving should be multiplied by the group size to get a comparison with standalone category); position uncertainty limit 50m to 500m	potential of high energy gains; energy gains depends on grouping nature; limited position accuracy

anchor position errors on localization performance. The first approach is based on optimization techniques such as semidefinite programming (SDP) or second order cone programming (SOCP). The second class covers closed form solutions based on the linearized system of equations using WLS, total least-squares (TLS) and element-wise total least-squares (EWTLS). The former (iterative solutions) have better positioning performance over the latter (closed form solution) but incur a higher computational cost. The major works in both categories are given next.

2.5.1 Iterative Solutions Using Complex Optimization Techniques

The authors of [93] present a convex position estimation technique in WSN, based exclusively on connectivity-induced constraints processed in a centralized resource centre. They model the known peer-to-peer communication constraints as a set of geometric constraints on the node position and solve the problem using SDP. An iterative multilateration technique in which three or more nodes compute their positions and then act as anchors in the subsequent iterations is given in [94]. In [95], a multidimensional scaling (MDS) technique that uses node connectivity information for localization is proposed. It presents two methods: one builds a global map directly and the other builds local maps then stitches them together to build a global map. The MDS-based algorithms outperform the convex optimization algorithm of [94] when the number of available anchors is low (around 50% lower position error when the number of anchors is less than 5% of total nodes) and only connectivity information is available. In addition, the MDS-based algorithms show better performance than Hop-TERRAIN [96], especially when the number of anchors is small. Hop-TERRAIN is a two-phase sensor network position algorithm consisting of the start-up phase and the refinement phase. The start-up phase ends up providing a rough position estimate to the nodes and the refinement phase uses a weighted least square solution to improve that position estimate. In an evaluation with four anchors (2 percent of the network) and a connectivity level 12 (average number of neighbors), the average error of the MDS-based algorithm is 27% of the radio communication range compared to 90% of Hop-TERRAIN.

In [61], the authors derived a CRLB for the localization problem assuming perturbation in the RSSI measurements and perfect knowledge of anchor positions. In [97], the authors proposed an SDP relaxation-based method for the localization in ad-hoc WSNs assuming the availability of accurate anchor positions. The approach is to convert the non-convex

quadratic distance constraints into linear constraints by introducing a relaxation to remove the quadratic term from the constraint. Similarly, there are other RSSI-based node localization methods such as [98–100]. However, none of the above works consider the presence of errors in both RSSI and anchor position information.

A distributed multidimensional scaling approach for localization in WSNs is proposed in [101]. It weights the range measurements based on their accuracy to account for the communication constraints in a sensor network. A robust joint localization and time synchronization algorithm for WSN with bounded anchor position uncertainties is given [102]. The algorithm implements a robust joint-estimator based on minimizing the worst-case mean square error and the solution is obtained by solving an SDP problem. In [103, 104], the authors propose a three-step distributed sensor network localization approach using SCOP. In the first step, the blind nodes compute their locations using available anchor node position information. In the second step, anchor nodes refine their position estimates using relative distance information exchanged with their neighbors followed by final refinement in position by blind nodes in the third step.

Node localization for underwater and underground networks is considered in [105]. The authors propose an SDP-based localization algorithm in the presence of anchor position error and uncertainties in the signal propagation speed affecting the TOA-based distance measurement. They also derive the CRLB for the corresponding problem. An SOCP-based approach for sensor network localization with anchor position uncertainty is given in [106]. It presents a robust localization approach using maximum-likelihood criteria under an unbounded uncertainty model for the anchor position error. All these works consider normally distributed errors in both anchor positions and distance measurements. In practice, perturbation in RSSI-based distance estimates follows a log-normal normal distribution [107].

The authors of [15] considered normally distributed errors in anchor positions and log-normal distribution of errors in distance estimation. They propose an RSSI-based solution for joint location estimation of a source and multiple anchor nodes. Their algorithm is based on a maximum likelihood (ML) estimation and requires multiple RSSI and anchor position measurements. In outdoor localization of mobile nodes where GPS is the main source of anchor position information, GPS is responsible for the majority of energy consumed. Therefore, the requirement of multiple measurements of an anchor position is not suitable for resource-constrained systems.

2.5.2 Closed-form Solutions Using Least-Squares Techniques

In [108], the authors propose a two-step closed-form solution for localizing a mobile node using noisy TDOA measurements. In the first step, they use the WLS to give the initial solution and in the second step, they use the known geometric constraints to improve the solution. Their solution approximates the maximum-likelihood estimator when the TDOA measurement errors are small. The author of [109] proposes two methods to compensate for the bias of the solution given in [108]. The bias can be very large with high measurement noise. The author proposes two solutions namely BiasSub and BiasRed. In BiasSub, the author subtracts the theoretically computed bias from the source location estimate whereas, in BiasRed, the author creates an augmented solution equation and impose a quadratic constraint to reduce the bias. The BiasSub method is efficient when TDOA noise parameters are known exactly. When the TDOA noise parameters are not available, the BiasRed solution turns out to be more useful than BiasSub.

A closed form solution and corresponding CRLB for localizing a stationary source/emitter based on TDOA measurements is presented in [110]. The authors assume a normally-distributed error in both anchor position information and TDOA measurements. In [111], a range-based positioning technique is proposed that has a computational complexity lower than the least-squares method. Their algorithm is based on the linearized range measurement equations and implementation of a WLS criterion in a computationally efficient way. In [16], the authors propose two WLS algorithms, called hyperbolic and circular, to localize a node using RSSI-based distance measurements while assuming the log-normal shadowing path-loss model. The hyperbolic algorithm linearizes the problem and solves it using the WLS method. The circular algorithm minimizes the weighted approximation of the original non-linear sum-square-error cost function using the gradient-descent method. The circular algorithm performs better than the hyperbolic algorithm due to minimization of the original cost function by an iterative approach. The proposed hyperbolic algorithm matches the low computational requirement of our scenarios of interest but does not consider errors in the anchor node positions.

The authors of [112] propose an EWTLS solution to localize a node in the presence of errors in both anchor position and distance measurements. The EWTLS [113],[114] solutions deal with the element-wise variance but assume the same type of error distribution. In case

of the RSSI-based localization, the distance measurements follow a log-normal distribution whereas anchor position information has normally-distributed noise. In [115], a closed-form solution for node localization using noisy TDOA measurements and anchor position information is presented. The authors assume the scenario of a large equal radius and develop the estimator based on a geometric approach removing the need for introducing an auxiliary variable. The authors of [116] propose a TLS-based solution for location estimation of a stationary source using noisy TDOA measurements and perturbed anchor positions. In [117], the authors present three different solutions based on Taylor series, WLS and constrained total least-squares (CTLS) for localization in the presence of additive zero-mean Gaussian noise in both distance and anchor position information. The Taylor series and WLS-based solutions are proposed for the scenario where errors are only present in distance measurements. In the CTLS-based algorithm, the authors assume perturbation in anchor position information as well. The authors of [118] also consider the presence of independent additive zero-mean Gaussian noise in both distance and anchor position information. They present another CTLS-based localization algorithm for the case where distance measurement errors are negligible compared to anchor position errors.

The authors in [119],[120], propose a WLS-based closed-form solution to determine the position of a mobile target in the presence of multiple transmitters and receivers using TDOA measurements. The algorithm is based on the intersection of the ellipsoids defined by bistatic range measurements from a number of transmitters and receivers. These works are based on the TDOA measurements and assume perfect knowledge of the anchor positions.

Unfortunately, many of the solutions presented here are not suitable for the problem of different anchor and range error distributions. As will be shown in detail later in section 6.1, the overdetermined system of linear equations represented by $\tilde{\mathbf{A}}\mathbf{w} \approx \tilde{\mathbf{b}}$ has components of both distance and anchor position errors in $\tilde{\mathbf{b}}$. The presence of the distance errors in $\tilde{\mathbf{b}}$ leads to an error distribution different from that for $\tilde{\mathbf{A}}$. This violates the basic assumption of identical error distribution in TLS and EWTLS techniques [114, 121], so these techniques cannot be directly used.

2.6 Literature Summary and Research Gaps

This section summaries the literature reviewed in section 2.4 and section 2.5 along with the identified research gaps.

Section 2.4 reviews the literature on localization and tracking algorithms dealing with the relatively high-energy consumption of the GPS which is a poor match to energy-constrained systems. The literature investigate several questions. First, "when to localize?", meaning when GPS should be sampled? Among the various approaches, inertial sensor-based sampling decision gives better position accuracy and energy consumption. However, as noted in the literature as well, this approach may lead to early depletion of the battery for frequent movement behaviour. In addition, long-term and continuous use of inertial sensors is observed to be energy expensive. Second, "how to keep track of the position uncertainty?", in order to delay the GPS activation until position uncertainty reaches a limit. Again, inertial sensors are found useful for tracking position uncertainty.

Third, "how to exploit the multiple sources of position information such as GPS, inertial, map, mobile network, Bluetooth and Wi-fi for accurate localization and tracking?". Investigations of this question reveal that fusing the multiple sources of position information may result in errors as low as 1m. Fourth, "what benefits in term of energy and accuracy can be achieved by sharing position and inertial information among neighbouring nodes?". Investigation reveals an energy saving around 30% *to* 40% and error reduction up to 30% from such cooperation. However, these savings strongly depend on parameters such as the radio communication range of nodes, maximum tolerable position uncertainty, and inertial sensors sampling frequency.

The algorithms reporting cooperation benefits use inertial movement-based position sampling intervals. The movement-based sampling interval is reported to perform better than periodic sampling but the difference is significant only for infrequent movements otherwise the former leads to battery drainage. In addition, the movement-based approach requires continuous sampling of inertial sensors which may be unavailable. The tracking life and available resources are important factors where nodes are uncontrolled, movements are unpredictable, and resources are limited such as the tracking nodes and applications considered in this thesis. For such cases, periodic sampling can guarantee a minimum tracking period. Thus, for such cases, periodic sampling remains a valid choice. However, the literature does

not provide any insights into cooperation benefits for the periodic sampling.

Next, the existing cooperative algorithms follow dynamic sampling intervals based on inertial sensors. Therefore, it is natural to investigate opportunistic cooperation. However, given reasonably stable groups and periodic sampling, planned cooperation seems a viable alternative option. In planned cooperation, participating nodes use cooperative localization as their primary source of positioning and follow a predefined set of operational rules. In contrast, opportunistic cooperation considers cooperative localization as an occasional alternative and primarily relies on the locally available positioning resources. Planned cooperation may avoid redundant GPS activation by different neighbouring nodes at the same time. It may result in better control over the resource pool available in the group. The resource control may allow us to implement simple and effective techniques such as multilateration for localization in a group of mobile nodes, which require simultaneous position measurement from several nodes. The literature does not shed any light on the benefits of planned cooperation. To fill this research gap, this thesis investigates the unexplored benefits of planned cooperation using periodic sampling.

The first part of section 2.5 reviews complex optimization-based solutions to the blind node localization problem given errors in both anchor positions and distance measurements. Most works assume perfect knowledge of anchor positions and consider errors only in distance measurements. There is a significant literature which considers normally distributed errors in both RSSI-based distance measurements and anchor positions. This is not realistic given that the RSSI-based distance measurements follow a log-normal distribution [57]. The work [15], is the only one to my knowledge which considers normally distributed errors in anchor positions and log-normal distributed errors in distance estimation. However, their ML-based joint localization framework requires multiple measurements of anchor positions and RSSI measurements. The applications considered in this thesis assume energy-expensive GPS as the main source of anchor position information. Therefore, the requirement of multiple measurements of an anchor position is not in line with thesis goal of resource-efficient localization.

Most of the closed form solutions discussed in the second part of the section 2.5 also assume perfect knowledge of anchor positions or additive zero-mean Gaussian errors in distance estimates. To solve the localization problem, the algorithms use one or another form of the least-squares solution. From an algebraic point of view, in a system of linear equation

representation $\tilde{\mathbf{A}}\mathbf{w} \approx \tilde{\mathbf{b}}$ of the considered localization problem, perturbation in distance estimates only affects the elements of $\mathbf{b}$. The LS and WLS techniques in general, are designed to take such errors into account. The works considering the error in both anchor position and distance measurement assume a similar type of error distribution and present solutions based on TLS, EWTLS or CTLS. These techniques are able to take into account errors in both $\mathbf{A}$ and $\mathbf{b}$. They require that the noise components in both $\tilde{\mathbf{A}}$ and $\tilde{\mathbf{b}}$ to be independent and identically distributed. In the considered multilateration localization, however, it can be shown that the noise components in the formulated equations are algebraically related. The CTLS-based technique [122] can account for the linear correlation of errors in $\mathbf{A}$ and $\mathbf{b}$ but, in the considered multilateration localization problem, the dependence is not linear.

In summary, the literature of blind-node localization clearly lacks a self-localization solution for resource-constrained nodes given realistic assumptions on errors where distance estimates follow log-normal and anchor position follows a normal distribution. The error distribution assumption for distance is due to the underlying shadowing path-loss radio propagation model [14, 57, 107]. The normal distribution of anchor positions is empirically supported in [13]. This gap also includes theoretical bounds on localization performance under such realistic assumptions on errors. To fill these gaps, this thesis provides the theoretical bound and the self-localization solution.

2.7 Research Questions and Methodology

Based on the research gaps identified in the literature review, the following are the research questions addressed in this thesis.

1. How can GPS sampling load and position readings be shared among a group of mobile nodes to improve individual tracking accuracy given a limited energy budget?

2. What is the theoretical minimum bound on localization performance of a blind node in the presence of normally distributed errors in anchor positions and log-normally distributed errors in RSSI-based distance estimation?

3. How can the theoretical minimum bound on localization be approach or achieved in the assumed scenario of resource-constrained mobile nodes?

4. How can additional information of error characteristics be used to improve the tracking accuracy of such groups of mobile nodes?

In general, the methodology to answer these research questions involves formulation and derivation of a suitable mathematical framework and then validating the results using extensive simulations. All the simulations are performed using Python. The details of each of the experiments are given in the respective chapters answering the research questions. The real-world evaluations of the proposed algorithms require high-resolution group movement dataset. The choice is between running real-world simulations in one very specific scenario, or running multiple trials with consistent parameters. Given the probabilistic nature of the radio propagation model, many tens or hundreds of runs are needed, therefore the proposed algorithms are evaluated using extensive simulations only similar to other established works in this area [15, 37, 40, 90, 105, 106]. However, it will be useful to run real-world trials in future.

Chapter 3

Cluster-Based Tracking

This chapter explores answers to the first research question (RQ1) which is "How can GPS sampling load and position readings be shared among a group of mobile nodes to improve individual tracking accuracy given a limited energy budget?".

This chapter proposes a CBT algorithm and investigates its usefulness to be an answer the RQ1. The algorithm distributes the GPS sampling load among the neighbouring nodes in a planned manner using a CH. Three variants of CBT are evaluated, namely, "CBT-Standard", "CBT-CKF" and "CBT-CKF with Accelerometer and Magnetometer". For the usefulness assessment, this chapter investigates the following fundamental questions regarding the proposed CBT algorithm:

1. What is the individual nodes' energy–accuracy trade-off when distributing the GPS sampling load among the group of mobile nodes. How this trade-off varies with the GPS sampling interval?

2. Can the energy–accuracy trade-off the tracking be further improved through time-series analysis and modeling, such as using the KF?

3. What is the effect on the energy-accuracy trade-off of using the individual nodes' accelerometer (acc.) & magnetometer (mag.) sensor information in the proposed CBT algorithm?

The rest of the chapter first presents the proposed algorithm along with its variants. Next, the chapter covers the dataset, energy model and experiment performed to evaluate the performance of the proposed algorithm. Lastly, the chapter presents results followed by the conclusions drawn.

3.1 Proposed CBT Algorithm

This section describes the proposed CBT algorithm and its variants. The performance of these algorithms is studied later in the chapter, to better understand the key trade-offs that the different variants offer.

3.1.1 CBT-Standard

Initially, all nodes get a GPS lock, form clusters based on their location (e.g., cluster radius is less than 50m) and start the CH election process. The CH is selected in an ad-hoc fashion. Nodes independently run random timers and the node whose timer fires first becomes the CH, where a tie is resolved by lowest node ID. Multiple clusters may occur at a particular time depending on the positions of the nodes. A cluster formed in this process will be partially connected with assured connectivity to the CH. One node can be a member of one cluster only and selection among multiple clusters is made on the basis of the distance to the CH. The CH is responsible for scheduling GPS sampling for all of the cluster's members. The schedule is randomized and takes into consideration the available battery status of individual nodes. The CH is also responsible for receiving the position updates and distributing these to the member nodes. If a node misses three consecutive position updates, it leaves the current cluster and looks for a new cluster if any are available. The decision to consider three misses is based on the amount of position uncertainty limit of an application, nodes velocity and GPS sampling interval. For example, position uncertainty/error limit of a node with average velocity of 6 m/s and a sampling interval of 10s touches to 180m (6*10*3), when misses misses three consecutive updates. A departing node initiates a new cluster formation process if no other cluster is in range. In the absence of new GPS position updates either from the local GPS or from neighbors, the node uses its last position as the current position estimate.

3.1.2 CBT-Cooperative Kalman Filter(CKF)

The basic algorithm of this variant is inherited from the CBT-standard defined above. The differences are as given below:

1. Each node runs its own KF. Whenever there is a requirement of GPS sampling for a KF measurement update, rather than sampling its own GPS, a request to the CH is

submitted to provide the GPS update, leading to a our decision of naming this variant of CBT as cooperative KF.

2. Upon the receipt of a GPS update request from a group member, the CH randomly assigns the GPS sampling task among its members having sufficient energy. Similarly to standard CBT, the CH is responsible for the distribution of new position and velocity values among its members. Note that GPS receivers typically output position and velocity during on-board signal decoding. These velocities can be calculated in a number of ways such as Doppler shift measurement, position difference or differencing carrier phase measurements at consecutive epochs [123]. In this thesis, the exact calculation method is not important, but it is assumed that the GPS output velocity is used from the GPS receiver, rather than calculating the velocity separately from other information.

3. An individual node uses the new position and velocity update as the measurement and control input update in its KF and estimates its current position.

The details of the KF are as given below.

System Model

$$\mathbf{x}_t = \mathbf{A}_t\mathbf{x}_{t-1} + \mathbf{B}_t\mathbf{u}_t + \mathbf{w}_t \tag{3.1}$$

$$\mathbf{z}_t = \mathbf{H}_t\mathbf{x}_t + \mathbf{v}_t \tag{3.2}$$

where, $\mathbf{x}_t$ is the state vector containing node 3D position at time t, $\mathbf{u}_t$ is a control input vector containing 3D velocity values reported in the cooperative GPS update, $\mathbf{A}_t$ is the state transition matrix and $\mathbf{B}_t$ is the control input matrix given as

$$\mathbf{x}_t = \begin{bmatrix} x \\ y \\ z \end{bmatrix}, \ \mathbf{u}_t = \begin{bmatrix} v_x \\ v_y \\ v_z \end{bmatrix}, \ \mathbf{A}_t = \begin{bmatrix} 1 & 0 & 0 \\ 0 & 1 & 0 \\ 0 & 0 & 1 \end{bmatrix}, \ \mathbf{B}_t = \begin{bmatrix} \tau & 0 & 0 \\ 0 & \tau & 0 \\ 0 & 0 & \tau \end{bmatrix}.$$

The symbol τ represents the time interval for KF update. The $\mathbf{w}_t$ in (3.1) is the vector containing the process noise terms for each parameter in the state vector. The process noise is assumed to be drawn from a zero mean normal distribution with covariance given by the

Algorithm 1: CBT-Standard

```
   /* initialization of variables                                                    */
1  number_of_nodes; maximum_battery_capacity ; CM_current_battery_level (initialization with
     maximum_battery_capacity ); minimum_battery (required for tracking activity) ; sampling_interval ;
     total_tracking_period ; radio_range ;
2  Initially all nodes get GPS_lock          // Use of own GPS to get position update ;
   /* cluster formation and cluster head (CH) selection process                      */
3  while every node is either becomes a CH or a cluster member (CM) do
4      check clustering_eligible_nodes        // (the nodes which are neither a CH nor a CM and
         CM_current_battery_level ≥ minimum_battery) ;
5      if count of clustering_eligible_nodes ≤ 0 then
6          exit ;
7      else
8          All clustering_eligible_nodes exchange their position with nodes in radio_range ;
9          clustering_eligible_nodes run a random timer and node with lowest timer_value wins the CH
             race, a tie on timer_value is resolved using lowest_node_ID ;
10         a node joins the nearest CH if multiple CH in radio_range and changes own status to CM ;
11     end
12 end
   /* position updates based on sampling_interval                                    */
13 while CM_current_battery_level ≥ minimum_battery ∧ trajectory_tracked ≤ total_tracking_period do
14     for every CH do
15         count_active_CM ( number of CM with battery level ≥ minimum battery);
16         if count_active_CM ≤ 0 then
17             CM_current_position to CM_last_position (update all CM including CH) ;
18             break the current clsuter;
19             all CM and the CH search for an active CH within radio_range;
20         end
21         if count_active_CM > 0 then
22             random selection of a CM from active_CM list to get GPS lock by the CH ;
23             GPS_lock by the selected CM and GPS position received stored as position_update ;
24             energy_used = GPS_energy + MCU_energy + radio_energy ;
25             update CM_current_battery_level −= energy_used;
               /* distribution of position_update to all the CM by the CH            */
26             if distance_to_CH ≤ radio_range then
27                 update CM_current_position = position_update;
28                 energy_used = MCU_energy + radio_energy ;
29                 update CM_current_battery_level −= energy_used;
30             else
31                 if position_update_not_received ≤ 3        // (number of scheduled updates not
                     received from the CH) then
32                     update CM_current_position = CM_last_position;
33                     energy_used = MCU_energy + radio_energy ;
34                     update CM_current_battery_level −= energy_used;
35                     position_update_not_received += 1;
36                 else
37                     update CM_current_position = GPS_lock ;
38                     energy_used = GPS_energy + MCU_energy + radio_energy ;
39                     update CM_current_battery_level −= energy_used;
40                     position_update_not_received = 0 ;
41                     leave current CH and search for new CH or initiate a new clustering process;
42                 end
43             end
44         end
45     end
46 end
```

covariance matrix

$$\mathbf{Q}_t = \begin{bmatrix} \sigma_{v_x}^2 \tau^2 & 0 & 0 \\ 0 & \sigma_{v_y}^2 \tau^2 & 0 \\ 0 & 0 & \sigma_{v_z}^2 \tau^2 \end{bmatrix},$$

where, σ_{v_x}, σ_{v_y} and σ_{v_z} are the standard deviations in the control input velocity measurements. In practice, the speed accuracy parameter (S_{acc}) of GPS can provide an estimate of standard deviations in the velocity measurements.

In (3.2), $\mathbf{z}_t$ is the measurement vector at time t, which contains the 3D position received in the cooperative GPS update given as

$$\mathbf{z}_t = \begin{bmatrix} c_x \\ c_y \\ c_z \end{bmatrix}$$

and $\mathbf{H}_t$ is the transformation matrix that maps the state vector parameters into the measurement domain given by

$$\mathbf{H} = \begin{bmatrix} 1 & 0 & 0 \\ 0 & 1 & 0 \\ 0 & 0 & 1 \end{bmatrix}.$$

In (3.2), $\mathbf{v}_t$ is the is the vector containing the measurement noise terms for each observation in the measurement vector $\mathbf{z}_t$. Like the process noise, the measurement noise is assumed to be zero mean Gaussian noise with covariance matrix

$$\mathbf{R}_t = \begin{bmatrix} \sigma_{c_x}^2 & 0 & 0 \\ 0 & \sigma_{c_y}^2 & 0 \\ 0 & 0 & \sigma_{c_z}^2 \end{bmatrix}$$

where, σ_{c_x}, σ_{c_y}, and σ_{c_z} are the standard deviations in position updated received through cooperative positioning. As the node who sampled GPS to provide cooperative position update has better estimate of its position therefore σ_{c_x}, σ_{c_y}, and σ_{c_z} used in KF will be same as (P _acc) value. However, the position accuracy value (P_{acc}) provided by the GPS, group size and sampling interval are used as an indicator for estimation of standard deviations in position received in cooperative updates.

Prediction Stage

The KF equations used for the prediction stage are

$$\hat{\mathbf{x}}_{t|t-1} = \mathbf{A}_{t-1}\hat{\mathbf{x}}_{t-1|t-1} + \mathbf{B}_t\mathbf{u}_t \tag{3.3}$$

$$\hat{\mathbf{P}}_{t|t-1} = \mathbf{A}_t\mathbf{P}_{t-1|t-1}\mathbf{A}_t^T + \mathbf{Q}_t. \tag{3.4}$$

Update Stage

The KF update equations used are given by

$$\hat{\mathbf{x}}_{t|t} = \hat{\mathbf{x}}_{t|t-1} + \mathbf{K}_t\left(\mathbf{z}_t - \mathbf{H}_t\hat{\mathbf{x}}_{t|t-1}\right) \tag{3.5}$$

$$\mathbf{P}_{t|t} = \mathbf{P}_{t|t-1} + \mathbf{K}_t\mathbf{H}_t\mathbf{P}_{t|t-1} \tag{3.6}$$

where,

$$\mathbf{K}_t = \mathbf{P}_{t|t-1}\mathbf{H}_t^T\left(\mathbf{H}_t\mathbf{P}_{t|t-1}\mathbf{H}_t^T + \mathbf{R}_t\right)^{-1}.$$

Algorithm 2: CBT-CKF

```
/* The pseudo code for CBT-CKF is same as CBT-Standard except it requires some extra
   variables initialization and changes in pseudo code lines of CBT from 26 to 29.
   */
/* Additional initialization of variables required compared to CBT. For symbol
   descriptions please refer to the text description of the algorithm.          */
1  x_t; u_t; A_t; B_t; Q_t; z_t; H; R_t;
   /* The if-block in pseudo code of CBT which starts from line number 26 is replaced
   by following lines of code in pseudo code of CBT-KF. */;
2  if distance_to_CH ≤ radio_change then
                                                  // prediction stage;
3      x̂_{t|t-1} = A_{t-1} x̂_{t-1|t-1} + B_t u_t;
4      P̂_{t|t-1} = A_t P_{t-1|t-1} A_t^T + Q_t;
                                                    // update stage;
5      x̂_{t|t} = x̂_{t|t-1} + K_t (z_t − H_t x̂_{t|t-1});
6      K_t = P_{t|t-1} H_t^T (H_t P_{t|t-1} H_t^T + R_t)^{-1};
7      P_{t|t} = P_{t|t-1} + K_t H_t P_{t|t-1};
8      position_update = x̂_{t|t};
9      update CM_current_position = position_update;
10     energy_used = MCU_energy (including KF energy processing cost) + radio_energy;
11     update CM_current_battery_level −= energy_used
12 end
```

Algorithm 3: CBT-CKF (Acc.& Mag.)

```
/* The pseudo code for CBT-KF(Acc.& Mag.) is same as CBT-CKF except it updates the
   nodes current velocity estimation based on accelerometer and magnetometer data.
   */
/* Additional initialization of variables required compared to CBT-KF. For symbol
   descriptions please refer to the text description of the algorithm.          */
1 a_t    // velocity correction calculated after processing raw acc. and mag. data;
2 u_t = a_t // the updating frequency of velocity estimation depends on sampling frequency
   of acc. and mag. sensors;
```

3.1.3 CBT-CKF with Acc. &, Mag.

The basic algorithm is the same as CBT-CKF. In CBT-CKF, the velocity estimate is based on the values reported by the GPS and is assumed to be constant between two consecutive GPS sampling intervals. However, in this variant, each node uses its acc. & mag. sensors to update the velocity estimation required by KF in between two GPS sampling intervals. To avoid any algorithm dependencies by raw data processing of acc. and mag., it's assumed that IMU as black-box is available which gives us observations in real-world frame.

3.2 Experimental Setup

3.2.1 Movement Data Insights

The group movement data used in the evaluation is generated using a simulation framework designed in python. The movement generation module of the framework is based on the Reynolds flocking algorithm [12]. The flocking algorithm gives the flexibility to define grouping parameters such as number of nodes, grouping tendency, grouping distance and maximum speed. The evaluation dataset contains 3D position traces of 20 nodes at the resolution of 1s in the movement area of 50×50×1 km for one day. Considering that birds/animals are active only 50% of the time (either at night or during the day), the static position time intervals are ignored to avoid potential bias in the results towards the proposed algorithm. Therefore, movements are only generated for 12 hours (43200s). Nodes from two randomly allocated base camps start towards a common foraging area. Nodes follow the flocking model and a random motion model during journey and feeding activities, respectively. Furthermore, nodes maintain a speed of approximately 6m/s with an inter-node distance of around 20m. In Fig. 3.2 (c), the velocity jumps between different values as the Reynolds flocking model

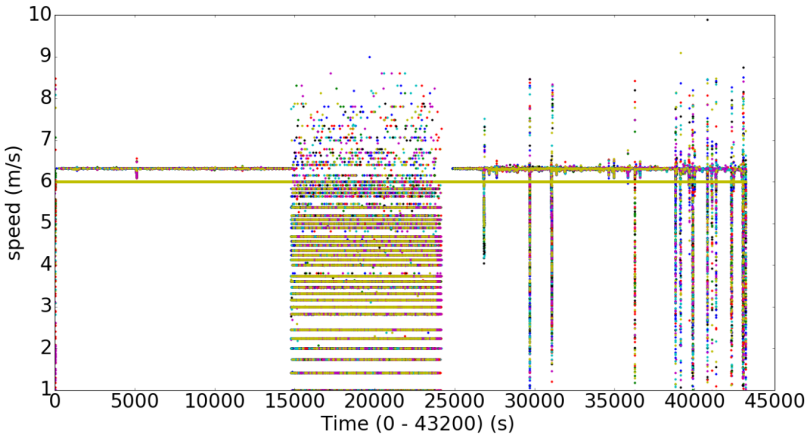

(a)

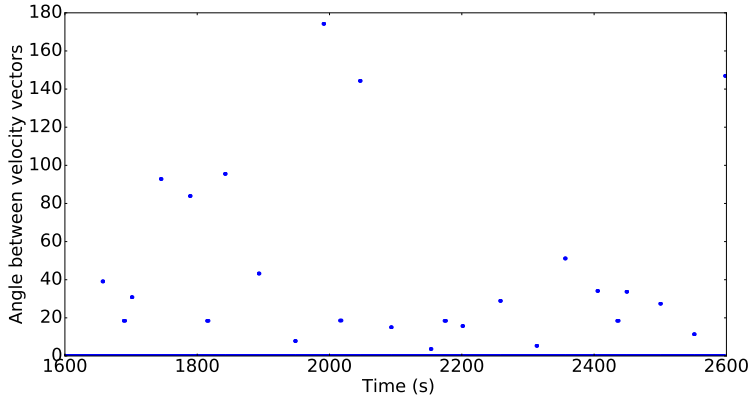

(b)

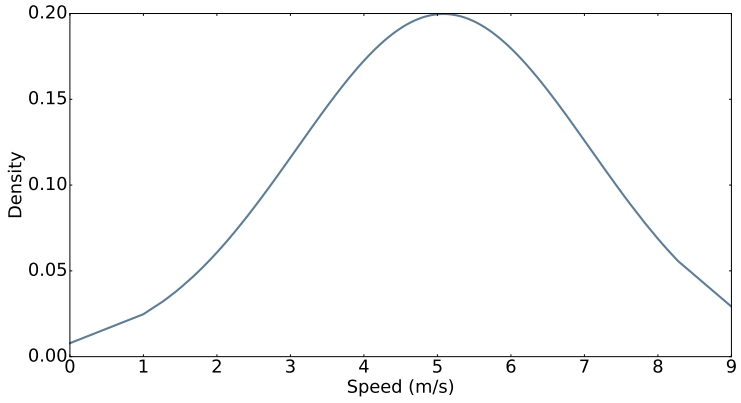

(c)

Figure 3.1: Movement data insights part -I (a) speed of the simulated mobile nodes. Nodes follow random walk model during feeding activity (15000s to 25000s) and flocking model otherwise with maximum speed of 6m/s; (b) time-slice view of the angle between two consecutive velocity vectors of a node. Variation in the angle implies that track followed by node is not a straight line; (c) Speed distribution of a single node.

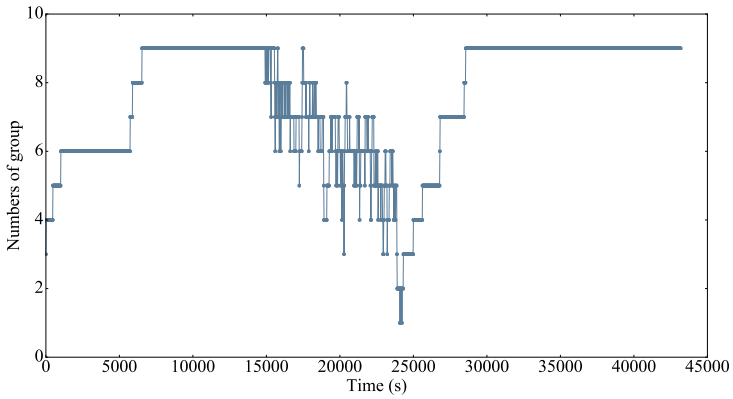

(a)

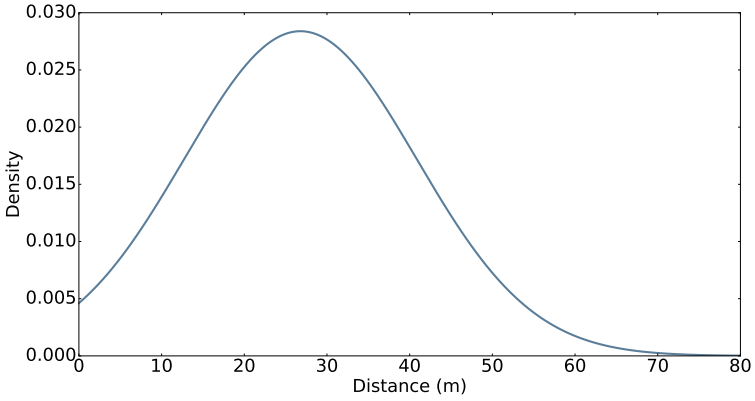

(b)

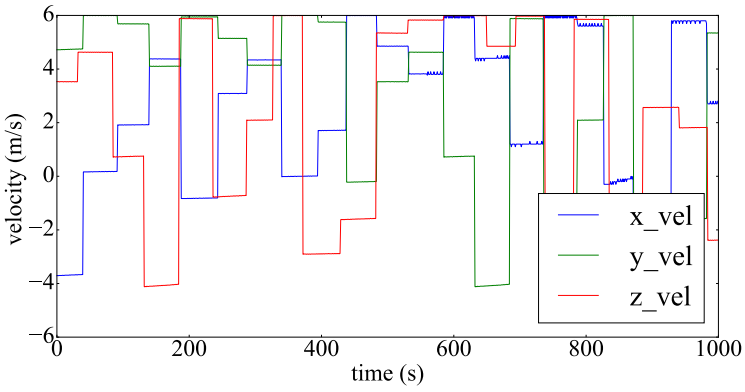

(c)

Figure 3.2: Movement data insights part -II (a) numbers of the clusters formed for a particular position sampling interval over the entire simulation period in which cluster count variation shows the dynamic clustering nature of the simulated data; (b) distribution of distances between CH and cluster members for a particular position sampling interval over the entire simulation period; (c) time slice view of variation in 3D velocity components of a node.

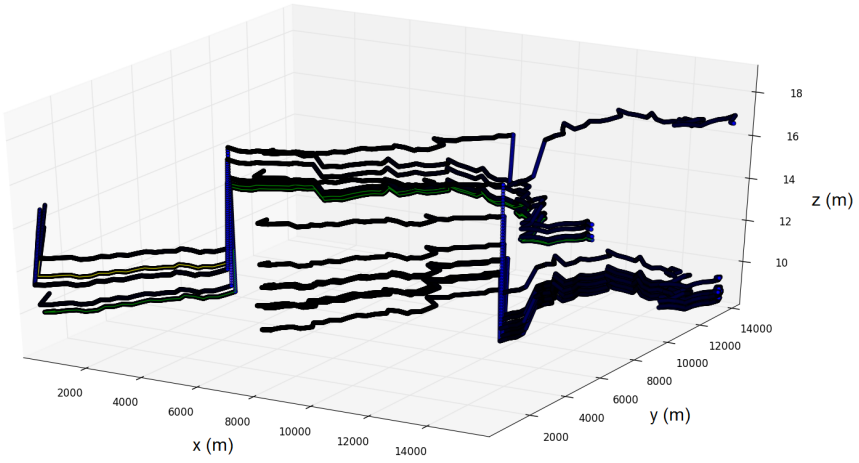

(a)

Figure 3.3: Movement data insights part -III; time slice view of representative trajectories of nodes generated using flocking algorithm.

updates velocity at regular sampling intervals. Typically, velocity is relatively constant until the flocking model finds two nodes too close or too far apart and then takes action to correct this. Figs. 3.1, 3.2 and 3.3 provide more insights into various aspects of the simulated movement data characteristics.

3.2.2 Energy Model

Energy parameters in the experiments are based upon a CSIRO multimodal mobile sensing platform called Camazotz [9]. Camazotz uses a CC430 system on chip with GPS, inertial, acoustic, air pressure and temperature sensors, two solar panels, 300mAh Li-Ion battery operating at 3.7V(3996J), with a total weight just under 30g targeted at tracking small wildlife such as flying foxes.

The calculation of individual activity (e.g. GPS, radio, and MCU) energy consumption of Camazotz is based upon the energy usage reported in [9] and corresponding data sheets of components. A simplified energy model is used in the simulations: it's assumed that GPS does not require a cold start (Section 2.2.3) considering the sampling interval varies only from 10s to 100s. The energy consumption of radio transmission and reception is assumed to be same. The MCU energy used to collect and process acc. and mag. samples is negligible given the low sensor sampling rates. As the KF update for 3D positioning only involves multiplications

and inversions of only 3X3 matrices, therefore, the MCU energy required for processing is also negligible compared to the energy required for a GPS fix. These assumptions helps in avoiding the cycle-accurate estimation of energy consumed by MCU and sensors. Instead, the total energy nodes require for data processing and standby is estimated as miscellaneous energy. The focus of our analysis is on the activities that dominate energy usage: GPS sensor sampling and radio communications. The energy cost of each activity is shown in Table 3.1 and (3.7)-(3.9) are summarized in Table 3.2.

$$E_g = T_g \left(P_g + P_m\right) \tag{3.7}$$

$$E_r = T_r \left(P_r + P_m\right) \tag{3.8}$$

$$E_a = T_d P_n (1 - T_d) P_s \tag{3.9}$$

Table 3.1: Details of energy model

Activity / Component	**Value**
Total simulation period (T)	43200s
GPS power consumption (P_g)	74mW
GPS activity time hot-start mode (T_g)	5s
MCU power consumption (P_m)	13.2mW
Radio power consumption (P_r)	13.2mW
Packet size (S)	80bits
Channel bit rate (C)	256Kbps
Packet transmission/receiving time (S/C) (T_t)	0.31ms
Current drawn by acc.& mag. in normal mode (I_n)	$110\mu A$
Current drawn by acc.& mag. in sleep mode (I_s)	$1\mu A$
Power by acc.& mag. in normal mode (P_n) (2.5v)	$275\mu W$
Power by acc.& mag. in sleep mode (P_a) (2.5v)	$2.5\mu W$
Time taken for 1 sample, considering maximum sampling rate supported by acc.& mag. is 200Hz (minimum of two)	5ms
Sampling Rate (Acc.)	50Hz.
acc.& mag. duty-cycling time (T_d)	0.25s
Standby power drawn by platform (P_s)	1.2 μW
Miscellaneous energy consumption (E_l) = TP_s	54 J

Table 3.2: Activity-wise energy consumption

Activity	**Energy/activity**
GPS (E_g)	0.436J
Radio (E_r)	34.78 μJ
Acc.& Mag. activity (E_a)	70.62μJ

3.2.3 Experiment Details

The experiments are divided into two different categories based on how the GPS sampling is triggered. The first category is "Periodic Sampling", in which GPS sampling is triggered at a fixed time interval. The sampling interval in the experiments varies from 10s to 100s. In the first experiment, the nodes are tracked using the proposed CBT to get the range of benefits using planned cooperation. Next, the nodes are tracked using CBT-CKF, to know the relevance of KF in a situation of where exact velocity measurements may not be available for quite a long period. In the third experiment, the nodes are tracked using CBT-CKF with acc.& mag. This experiment investigates the use of a noisy but continuous estimate of movements of the nodes in the KF. To the best of my knowledge, there is no existing work in this category, therefore, the performance of the proposed CBT-Standard algorithm and its variants are compared with the Individual tracking algorithm. In the Individual algorithm, each node independently samples and records its GPS position.

In the second category, "Dynamic Sampling", GPS sampling is triggered dynamically based on a predefined application specific position error uncertainty tolerance limit. A range of uncertainty limits ranging from 50 m to 450 m are considered in the experiments. The position uncertainty is assumed to have a linear relationship with velocity and time. For CBT and its variants, cluster position uncertainty limit is computed as the average of uncertainty limit of the cluster members. In this category, the performance of the CBT algorithms is compared with an existing cooperative algorithm proposed in [27]. The experiments similar to the periodic category are performed here as well.

For the purpose of evaluation, a zero-mean Gaussian noise with standard deviation of 10m, $\mathcal{N}(0, 10)$, is added to the original GPS position dataset, which is similar to the GPS performance in low-performance GPS areas such as dense forest, city or cloudy sky. based upon the GPS accuracy results presented in [72]. A group size of 50m is considered in all the experiments assuming a one-hop communication model. The node's acceleration estimates are assumed to be received from a black box (e.g. IMU ouput) which processes all the raw

acc. and mag. signals and gives an acceleration estimate corrupted with zero-mean Gaussian noise. The noise parameters in the acceleration estimate (n_a) is calculated using (3.10) and the parameters given in data-sheet, (n_a) is

$$n_a = n_d * \sqrt{(b_d * 1.6)}. \tag{3.10}$$

Where, accelerometer bandwidth b_d equals to (50Hz) and noise density (n_d) ($200\mu g/\sqrt{Hz}$) is the square root of the power spectral density. In simulations, the σ_{c_x}, σ_{c_y}, and σ_{c_z} value used for the node who sampled the GPS is 10m whereas for the rest of the nodes in group the value varies from 20m to 40m.

3.3 Results

The performance of algorithms is measured in term of mean energy consumed and mean position accuracy achieved. Each experiment is repeated 20 times to avoid the effects of random variations in a single experiment. The simulation stops either when all the nodes' batteries are exhausted or the track is completed. The results for each category are given below.

3.3.1 Periodic Sampling

Fig. 3.4a shows the energy consumption by all the nodes for all the algorithms. The GPS energy consumption is relatively high compared to the other components (Table 3.2), leading to a similar energy consumption by all the CBT algorithms. As expected, the proposed CBT algorithms outperform the Individual algorithm in terms of energy consumption. The savings can be as high as 30% over the Individual algorithm for nearly all sampling intervals. This gain comes at the expense of accuracy, as shown next.

Fig. 3.4b compares the mean and standard deviation of the position error of all the nodes for all the algorithms. CBT algorithms have higher errors (42% to 8% in the sampling interval of 10s to 100s) compared to the Individual algorithm. The use of the KF in CBT-CKF increases the position error performance gap between Individual and CBT-standard to 35% from 8% for the higher sampling intervals. This gap increase using KF can be explained by the node velocity fluctuation on the individual axes between two consecutive sampling

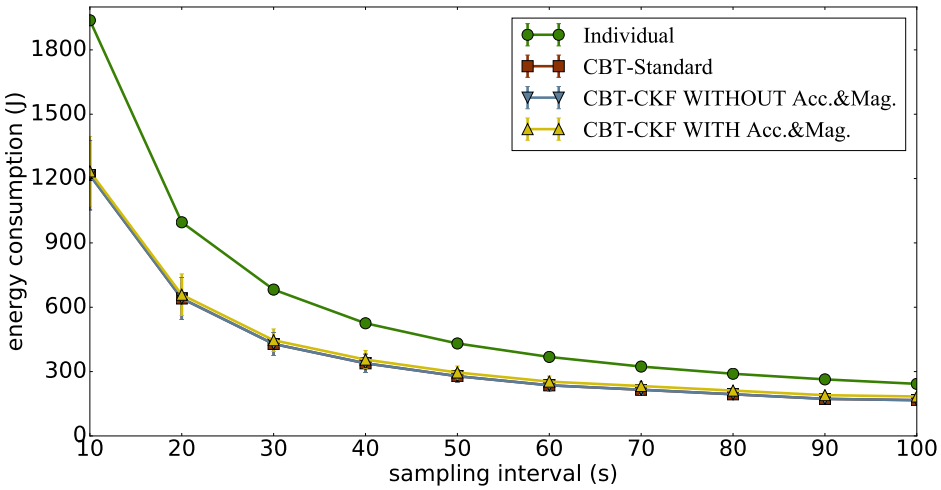

(a)

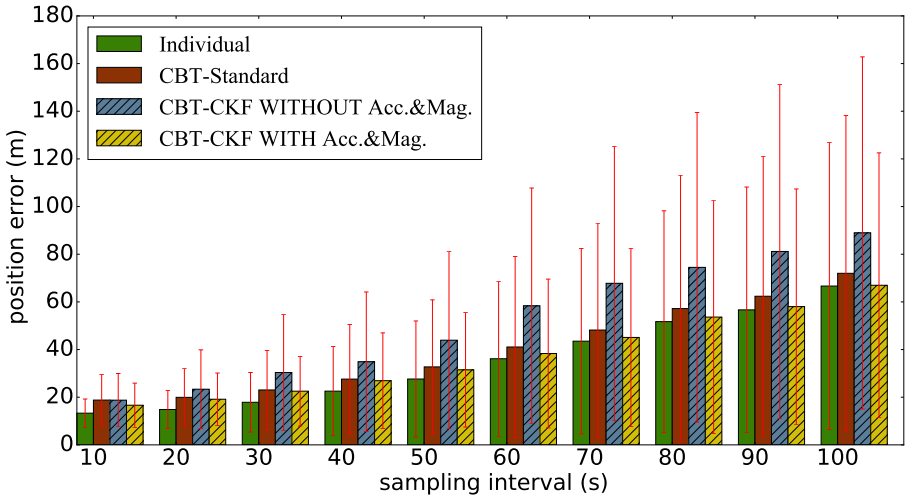

(b)

Figure 3.4: Results (a) mean and standard deviation of energy consumed by different algorithms over various sampling intervals;(b) mean and standard deviation of localization error of different algorithms over various sampling intervals.

points shown in Fig. 3.2c. The KF requires a good estimate of nodes velocity to give a reasonable position estimate which is unavailable without the use of the accelerometer and magnetometer sensors.

The addition of accelerometer and magnetometer information to the KF (CKF with Acc.&Mag.) improves the position error performance. The variant CKF with Acc&Mag. shrinks the position error gap range between Individual and CBT-standard from 42% – 8% to 22% - 1% over various sampling intervals. It is noticeable in Fig. 3.4b that, at the sampling interval of 100s, the variant CKF with Acc.&Mag. has the same mean error and a slight reduction in variability in comparison to the Individual algorithm.

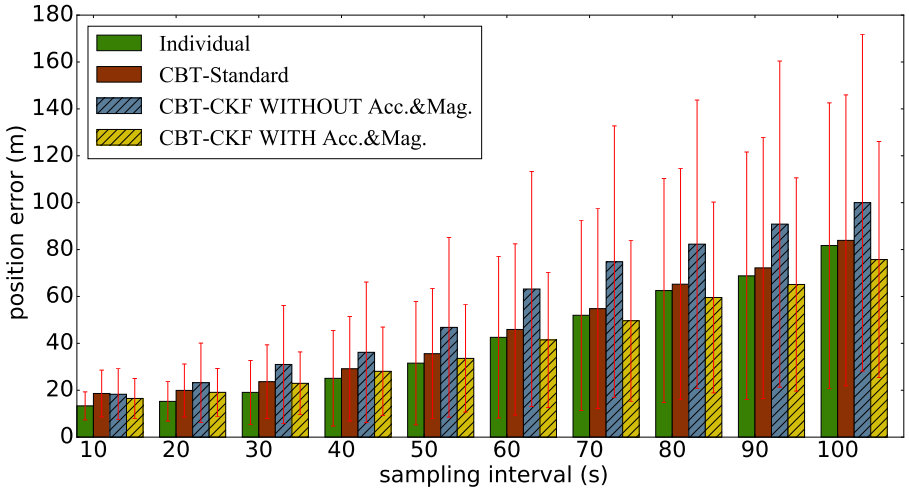

(a)

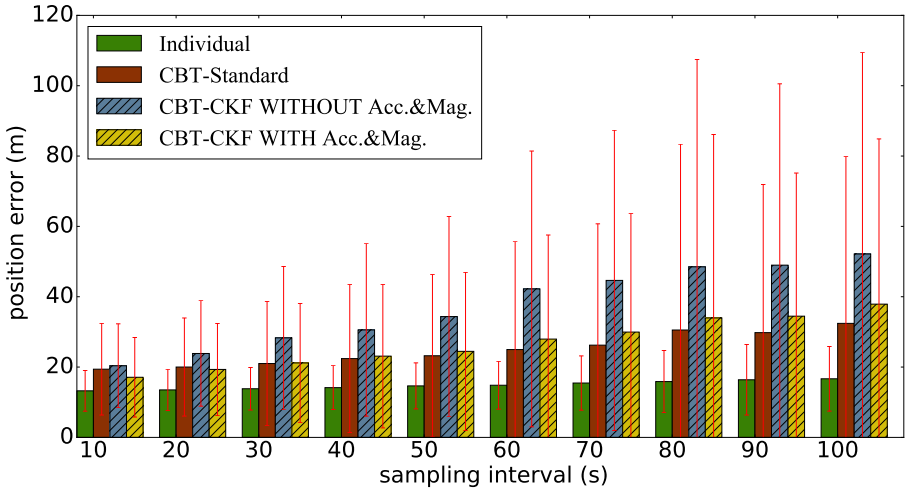

(b)

Figure 3.5: Segment-wise (Flocking vs. Random movement model) localization error of various algorithms (a) flocking movement segment (0s-15000s and 25001s-43200s) ;(b) random movement segment (15001s to 25000s)

Fig. 3.5 presents the segment-wise localization error of various algorithms. The localization error in the segment (0s-15000s and 25001s-43200s) where nodes follow flocking movement model is given in Fig. 3.5a. The error pattern is similar to the pattern in the complete segment (Fig. 3.4b). However, the error pattern differs for the segment (15001s - 25000s) where nodes follow random movement model. As expected, CKF with Acc.&Mag. does not bring any advantage in the random movement segment Fig. 3.5b.

Shifting the focus to the consolidated view of position and energy performance of Individual versus CBT algorithms presented in Fig. 3.6, the benefits can be clearly observed as follows. For an energy budget of 250J, the proposed CBT algorithm and its variants perform

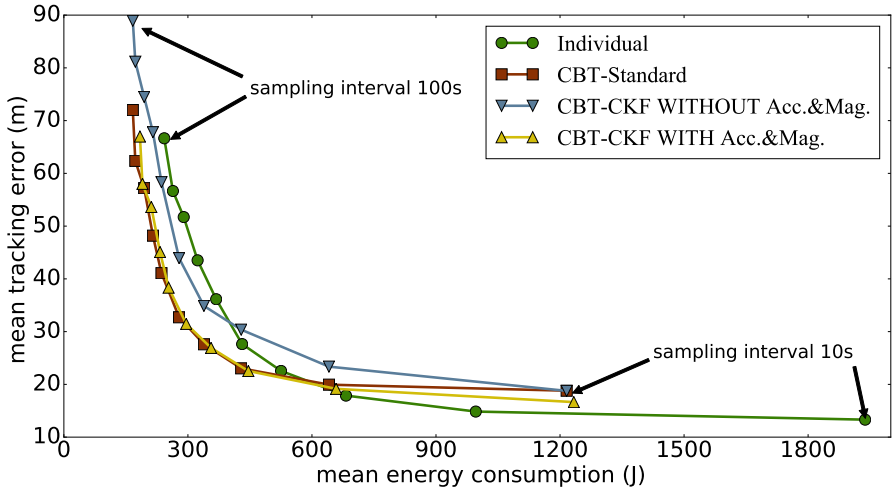

Figure 3.6: Energy-accuracy comparison of periodic sampling for interval 10s (right most point on curves) to 100s.

best with 43% reduction in position error compared to the Individual algorithm. Alternatively, for a fixed error range of 67m the variant CKF with Acc.& Mag. performs better, yielding 27% energy saving compared to the Individual algorithm.

3.3.2 Dynamic Sampling

The results for position uncertainty limit ranging from 50m to 450m are summarized in Fig. 3.7. The results for CBT-CKF are excluded given the bad performance for the similar reasons explained in periodic sampling category. For the initial uncertainty limit of 50m, the existing cooperative algorithm (the algorithm of [27]) performs better in energy usage with comparable position accuracy performance than the proposed CBT algorithm. The poor performance of the proposed CBT algorithm can be seen as a result of the low position uncertainty limit for a group size of 50m. As described earlier, group position uncertainty limit is computed as the average of position uncertainties of all group members.

For a group radius of 50m, the group position uncertainty limit of 50m can be reached easily, leading to a higher GPS sampling rate, causing more energy usage. Overall in this category, the existing co-operative algorithm performs well or comparable to the CBT algorithm. However, there are some points like a given error range of 22m, where the proposed CBT algorithm can save energy up to 40% compared to existing cooperative scheme.

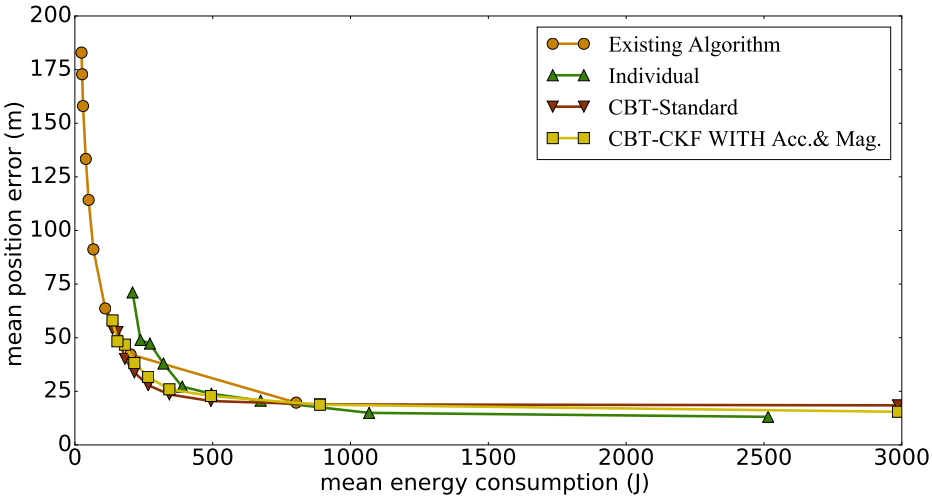

(a)

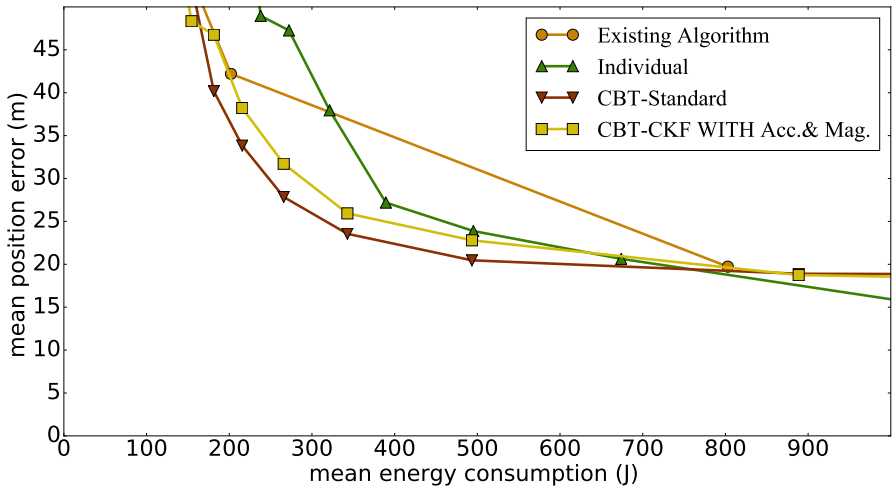

(b)

Figure 3.7: Energy-accuracy comparison of dynamic sampling; (a) position uncertainty limit 50m (right most point on curves) to 450m; (b) Zoom into a portion of sub-figure (a).

3.4 Conclusions

This chapter presents a cluster-based tracking algorithm for resource-constrained mobile nodes. It provides insights into three proposed variants of CBT, without any KF, with KF, and with KF and inertial sensors. The results show that the proposed CBT algorithms (CBT-Standard, CBT-CKF with Acc. and Mag.) improves energy and accuracy by around one-third over the Individual tracking algorithm in periodic GPS sampling scheme. In dynamic sampling, existing cooperative algorithm performs better or comparable to CBT-standard with only few exception points where it performs better.

The experiments show that the proposed CBT-Standard can give us position error reduc-

tion up to 43% for a given energy budget in comparison to the Individual algorithm. On the other side the variant CKF with Acc.&Mag can also save energy up to 27% while staying within the position error performance range of Individual algorithm. For the dynamically triggered GPS sampling category CBT algorithms sometimes can save up to 40% of energy while staying within the same error bound.

In summary, the proposed CBT-Standard algorithm and its variant CBT-CKF with Acc.&Mag are shown to answer RQ1. These algorithms can provide a range of energy-accuracy benefits in tracking resource-constrained mobile nodes.

Chapter 4

Theoretical Bounds on Localization Performance

This chapter considers the second research question (RQ2) "What is the theoretical minimum bound on localization performance of a blind node in the presence of normally distributed errors in anchor positions and log-normally distributed errors in RSSI-based distances estimations?"

This question is answered by deriving the Cramer-Rao lower bound (CRLB) for the self-localization problem given errors in both anchor positions and RSSI measurements.

The CRLB gives the minimal achievable variance for any unbiased estimator. Given an observation vector $\mathbf{x}$ with a known distribution that is related to an unknown parameter vector $\boldsymbol{\theta}$, the CRLB sets a lower bound on the covariance of any unbiased non-Bayesian estimator $\hat{\boldsymbol{\theta}}$ of $\boldsymbol{\theta}$. The CRLB is the inverse of the Fisher information matrix (FIM), denoted by $\mathbf{F}(\boldsymbol{\theta})$. Therefore,

$$\mathrm{Cov}(\hat{\boldsymbol{\theta}}) \geq \mathbf{F}^{-1}(\boldsymbol{\theta}). \tag{4.1}$$

The FIM represents the information provided by the observation $\mathbf{x}$ about the unobserved parameter vector $\boldsymbol{\theta}$ and, when certain regularity conditions are satisfied, is calculated as

$$\mathbf{F}(\boldsymbol{\theta}) = -\,\mathbb{E}\left[\frac{\partial^2 l(\boldsymbol{\theta} \mid \mathbf{x})}{\partial^2 \boldsymbol{\theta}}\right] \tag{4.2}$$

where $l(\boldsymbol{\theta} \mid \mathbf{x})$ is the log-likelihood function of $\boldsymbol{\theta}$ given $\mathbf{x}$.

In the remainder of this chapter, first, a formal problem definition is given followed by the derivation of CRLB. Then, the chapter is concluded with experimental insights given into

the relationship of CRLB with the number of nodes and errors levels in measurements.

4.1 Problem Statement

This chapter considers a self-localization problem for a single node, referred to as the blind node, on the two-dimensional Cartesian plane, as the application such as Bat positioning is about geographical location, so height is not an important issue. The blind node obtains an estimate of its true position, denoted by (x_b, y_b). There are $M \geq 3$ nodes, referred to as the anchor nodes, arbitrarily distributed within the communication range of the blind node at locations (x_i, y_i), $i = 1, ..., M$. The locations of the anchor nodes are known only approximately as their position estimates (e.g., from GPS) are corrupted by random errors. The blind node estimates its distance from the anchor nodes using the available RSSI measurements that are also subject to error. The knowledge of the noisy anchor node positions at the blind node is denoted by $(\tilde{x}_i, \tilde{y}_i)$, $i = 1, ..., M$. The corresponding noisy RSSI measurements are denoted by $\tilde{p}_i$, $i = 1, ..., M$, in the linear (mW) domain and by $\tilde{p}_{i(\text{dBm})}$, $i = 1, ..., M$, in the logarithmic (dBm) domain.

The following common assumptions are adopted:

A1: The available position information of the ith anchor node on the x and y axes are corrupted by independent additive zero-mean Gaussian errors with standard deviation σ_{a_i} (experimentally validated in [13]). The errors in the knowledge of different anchor node positions are independent of each other and the values of σ_{a_i} do not need to be the same for different anchor nodes. Therefore,

$$\tilde{x}_i = x_i + n_{x_i} \tag{4.3}$$

and

$$\tilde{y}_i = y_i + n_{y_i} \tag{4.4}$$

where

$$n_{x_i}, n_{y_i} \sim \mathcal{N}(0, \sigma_{a_i}). \tag{4.5}$$

A2: The path-loss model for the radio signal propagation is the log-normal shadowing model [14]. Therefore, the RSSI measurement of the signal transmitted from the ith anchor node and received at the blind node has a nominal value of $\bar{p}_{i(\text{dBm})}$ in the logarithmic (dBm) domain. However, the actual measured value is a realization of the nominal value corrupted

by a zero-mean Gaussian error with standard deviation σ_{p_i}, i.e.,

$$\tilde{p}_{i(\mathrm{dBm})} = \bar{p}_{i(\mathrm{dBm})} + n_{p_i} \tag{4.6}$$

where

$$n_{p_i} \sim \mathcal{N}\left(0, \sigma_{p_i}\right). \tag{4.7}$$

According to the shadowing path-loss model, it holds that

$$\tilde{p}_{i(\mathrm{dBm})} = p_{0(\mathrm{dBm})} + 10\eta \log_{10} \frac{d_i}{d_0} + n_{p_i} \tag{4.8}$$

where

$$d_i = \sqrt{\left(x_i - x_b\right)^2 + \left(y_i - y_b\right)^2} \tag{4.9}$$

is the distance between the blind node and the ith anchor node. In addition, d_0, $p_{0(\mathrm{dBm})}$, and η are the reference distance, the received power at the reference distance, and the path-loss exponent, respectively. Therefore, given the noisy value $\tilde{p}_{i(\mathrm{dBm})}$, the RSSI-induced estimate for the distance between the blind node and the ith anchor node, denoted by $\tilde{d}_i$, is given by

$$\tilde{d}_i = d_0 10^{\frac{\tilde{p}_{i(\mathrm{dBm})} - p_{0(\mathrm{dBm})}}{10\eta}}. \tag{4.10}$$

Furthermore, it is assumed that the blind node and the anchor nodes have limited computational and energy resources. Hence, at any particular instance of localization, only one RSSI measurement and position estimate from each anchor node is available to the blind node.

4.2 Cramer-Rao Lower Bound

In the considered self-localization problem, the observation vector $\mathbf{x}$ contains the noisy anchor positions $(\tilde{x}_i, \tilde{y}_i)$, $i = 1, ..., M$, as well as the noisy RSSI measurements $\tilde{p}_i$, $i = 1, ..., M$, i.e., it can be written as

$$\mathbf{x} = \left[\tilde{p}_1, \tilde{x}_1, \tilde{y}_1, \tilde{p}_2, \tilde{x}_2, \tilde{y}_2, ..., \tilde{p}_M, \tilde{x}_M, \tilde{y}_M\right]^T. \tag{4.11}$$

Given (4.6) and (4.8), the probability density function (pdf) of $\tilde{p}_i$ is expressed as [61]

$$f_{\tilde{p}_i}(\tilde{p}_i) = \frac{10/\ln 10}{\sqrt{2\pi\sigma_{p_i}^2}\tilde{p}_i} \exp\left[-\frac{c_i}{8}\left(\ln\frac{d_i^2}{\tilde{d}_i^2}\right)^2\right] \tag{4.12}$$

where

$$c_i = \left(\frac{10\eta}{\sigma_{p_i}\ln 10}\right)^2. \tag{4.13}$$

In view of the assumption *A1*, the pdfs of the noisy anchor positions $(\tilde{x}_i, \tilde{y}_i)$, $i = 1, ..., M$, are written as

$$f_{\tilde{x}_i}(\tilde{x}_i) = \frac{1}{\sqrt{2\pi\sigma_{a_i}^2}} \exp\left[-\frac{(\tilde{x}_i - x_i)^2}{2\sigma_{a_i}^2}\right] \tag{4.14}$$

and

$$f_{\tilde{y}_i}(\tilde{y}_i) = \frac{1}{\sqrt{2\pi\sigma_{a_i}^2}} \exp\left[-\frac{(\tilde{y}_i - y_i)^2}{2\sigma_{a_i}^2}\right]. \tag{4.15}$$

Here, unknown parameters of interest are the position coordinates of the blind node (x_b, y_b). However, the RSSI measurements are functions of the unknown original (non-noisy) anchor positions, (x_i, y_i), $i = 1, ..., M$. Therefore, the correct anchor positions are included as the nuisance parameters. Hence, the unknown parameter vector $\boldsymbol{\theta}$ is

$$\boldsymbol{\theta} = [x_b, y_b, x_1, y_1, x_2, y_2, ..., x_M, y_M]^T. \tag{4.16}$$

The noisy anchor node positions $(\tilde{x}_i, \tilde{y}_i)$, $i = 1, ..., M$, are statistically independent of each other as well as the RSSI measurements. Therefore, the log-likelihood function of the joint probability distribution of all the observations is written as

$$\begin{aligned} l(\boldsymbol{\theta} \mid \mathbf{x}) &= \sum_{i=1}^{M} \ln f_{\tilde{p}_i}(\tilde{p}_i \mid \boldsymbol{\theta}) + \sum_{i=1}^{M} \ln f_{\tilde{x}_i}(\tilde{x}_i \mid \boldsymbol{\theta}) \\ &\quad + \sum_{i=1}^{M} \ln f_{\tilde{y}_i}(\tilde{y}_i \mid \boldsymbol{\theta}) \\ &= \sum_{i=1}^{M} \ln f_{\tilde{p}_i}(\tilde{p}_i \mid x_b, y_b, x_i, y_i) \\ &\quad + \sum_{i=1}^{M} \ln f_{\tilde{x}_i}(\tilde{x}_i \mid x_i) + \sum_{i=1}^{M} \ln f_{\tilde{y}_i}(\tilde{y}_i \mid y_i). \end{aligned} \tag{4.17}$$

The second-order partial derivatives of the log-likelihood function $l(\boldsymbol{\theta} \mid \mathbf{x})$ with respect to the entries of its vector argument $\boldsymbol{\theta}$, required for the calculation of the FIM, are computed

as

$$\frac{\partial^2 l\left(\boldsymbol{\theta} \mid \mathbf{x}\right)}{\partial {x_b}^2} = \sum_{i=1}^{M} \left\{ -\frac{c_i (x_i - x_b)^2}{d_i^4} + c_i \ln\left(\frac{d_i^2}{\tilde{d}_i^2}\right) \left[\frac{(x_i - x_b)^2}{d_i^4} - \frac{1}{2d_i^2}\right] \right\} \tag{4.18}$$

$$\frac{\partial^2 l\left(\boldsymbol{\theta} \mid \mathbf{x}\right)}{\partial {y_b}^2} = \sum_{i=1}^{M} \left\{ -\frac{c_i (y_i - y_b)^2}{d_i^4} + c_i \ln\left(\frac{d_i^2}{\tilde{d}_i^2}\right) \left[\frac{(y_i - y_b)^2}{d_i^4} - \frac{1}{2d_i^2}\right] \right\} \tag{4.19}$$

$$\frac{\partial^2 l\left(\boldsymbol{\theta} \mid \mathbf{x}\right)}{\partial x_b \partial y_b} = \sum_{i=1}^{M} \left\{ \frac{c_i (x_i - x_b)(y_i - y_b)}{d_i^4} \left[\ln\left(\frac{d_i^2}{\tilde{d}_i^2}\right) - 1\right] \right\} \tag{4.20}$$

$$\frac{\partial^2 l\left(\boldsymbol{\theta} \mid \mathbf{x}\right)}{\partial x_b \partial x_i} = \frac{c_i (x_i - x_b)^2}{d_i^4} - c_i \ln\left(\frac{d_i^2}{\tilde{d}_i^2}\right) \left[\frac{(x_i - x_b)^2}{d_i^4} - \frac{1}{2d_i^2}\right] \tag{4.21}$$

$$\frac{\partial^2 l\left(\boldsymbol{\theta} \mid \mathbf{x}\right)}{\partial x_b \partial y_i} = \frac{c_i (x_i - x_b)(y_i - y_b)}{d_i^4} \left[1 - \ln\left(\frac{d_i^2}{\tilde{d}_i^2}\right)\right] \tag{4.22}$$

$$\frac{\partial^2 l\left(\boldsymbol{\theta} \mid \mathbf{x}\right)}{\partial y_b \partial x_i} = \frac{c_i (x_i - x_b)(y_i - y_b)}{d_i^4} \left[1 - \ln\left(\frac{d_i^2}{\tilde{d}_i^2}\right)\right] \tag{4.23}$$

$$\frac{\partial^2 l\left(\boldsymbol{\theta} \mid \mathbf{x}\right)}{\partial y_b \partial y_i} = \frac{c_i (y_i - y_b)^2}{d_i^4} - c_i \ln\left(\frac{d_i^2}{\tilde{d}_i^2}\right) \left[\frac{(y_i - y_b)^2}{d_i^4} - \frac{1}{2d_i^2}\right] \tag{4.24}$$

$$\frac{\partial^2 l\left(\boldsymbol{\theta} \mid \mathbf{x}\right)}{\partial x_i \partial x_j} = \begin{cases} -\frac{c_i (x_i - x_b)^2}{d_i^4} - \frac{1}{\sigma_{a_i}^2} + c_i \ln\left(\frac{d_i^2}{\tilde{d}_i^2}\right) \left[\frac{(x_i - x_b)^2}{d_i^4} - \frac{1}{2d_i^2}\right] & i = j \\ 0 & i \neq j \end{cases} \tag{4.25}$$

$$\frac{\partial^2 l\left(\boldsymbol{\theta} \mid \mathbf{x}\right)}{\partial y_i \partial y_j} = \begin{cases} -\frac{c_i (y_i - y_b)^2}{d_i^4} - \frac{1}{\sigma_{a_i}^2} + c_i \ln\left(\frac{d_i^2}{\tilde{d}_i^2}\right) \left[\frac{(y_i - y_b)^2}{d_i^4} - \frac{1}{2d_i^2}\right] & i = j \\ 0 & i \neq j \end{cases} \tag{4.26}$$

$$\frac{\partial^2 l\left(\boldsymbol{\theta} \mid \mathbf{x}\right)}{\partial x_i \partial y_j} = \begin{cases} \frac{c_i}{d_i^4} (x_i - x_b)(y_i - y_b) \left[\ln\left(\frac{d_i^2}{\tilde{d}_i^2}\right) - 1\right] & i = j \\ 0 & i \neq j. \end{cases} \tag{4.27}$$

Considering [61]

$$\mathbb{E}\left[\ln\left(\frac{d_i^2}{\tilde{d}_i^2}\right)\right] = 0, \tag{4.28}$$

the expectations of the above second-order derivative terms are given as

$$\mathbb{E}\left[\frac{\partial^2 l\left(\boldsymbol{\theta} \mid \mathbf{x}\right)}{\partial {x_b}^2}\right] = \sum_{i=1}^{M}\left\{ - \frac{c_i(x_i - x_b)^2}{d_i^4}\right\} \tag{4.29}$$

$$\mathbb{E}\left[\frac{\partial^2 l\left(\boldsymbol{\theta} \mid \mathbf{x}\right)}{\partial {y_b}^2}\right] = \sum_{i=1}^{M}\left\{ - \frac{c_i(y_i - y_b)^2}{d_i^4}\right\} \tag{4.30}$$

$$\mathbb{E}\left[\frac{\partial^2 l\left(\boldsymbol{\theta} \mid \mathbf{x}\right)}{\partial x_b \partial y_b}\right] = \sum_{i=1}^{M}\left\{ - \frac{c_i(x_i - x_b)(y_i - y_b)}{d_i^4}\right\} \tag{4.31}$$

$$\mathbb{E}\left[\frac{\partial^2 l\left(\boldsymbol{\theta} \mid \mathbf{x}\right)}{\partial x_b \partial x_i}\right] = \frac{c_i(x_i - x_b)^2}{d_i^4} \tag{4.32}$$

$$\mathbb{E}\left[\frac{\partial^2 l\left(\boldsymbol{\theta} \mid \mathbf{x}\right)}{\partial x_b \partial y_i}\right] = \frac{c_i(x_i - x_b)(y_i - y_b)}{d_i^4} \tag{4.33}$$

$$\mathbb{E}\left[\frac{\partial^2 l\left(\boldsymbol{\theta} \mid \mathbf{x}\right)}{\partial y_b \partial x_i}\right] = \frac{c_i(x_i - x_b)(y_i - y_b)}{d_i^4} \tag{4.34}$$

$$\mathbb{E}\left[\frac{\partial^2 l\left(\boldsymbol{\theta} \mid \mathbf{x}\right)}{\partial y_b \partial y_i}\right] = \frac{c_i(y_i - y_b)^2}{d_i^4} \tag{4.35}$$

$$\mathbb{E}\left[\frac{\partial^2 l\left(\boldsymbol{\theta} \mid \mathbf{x}\right)}{\partial x_i \partial x_j}\right] = \begin{cases} -\frac{c_i(x_i - x_b)^2}{d_i^4} - \frac{1}{\sigma_{a_i}^2} & i = j \\ 0 & i \neq j \end{cases} \tag{4.36}$$

$$\mathbb{E}\left[\frac{\partial^2 l\left(\boldsymbol{\theta} \mid \mathbf{x}\right)}{\partial y_i \partial y_j}\right] = \begin{cases} -\frac{c_i(y_i - y_b)^2}{d_i^4} - \frac{1}{\sigma_{a_i}^2} & i = j \\ 0 & i \neq j \end{cases} \tag{4.37}$$

$$\mathbb{E}\left[\frac{\partial^2 l\left(\boldsymbol{\theta} \mid \mathbf{x}\right)}{\partial x_i \partial y_j}\right] = \begin{cases} \frac{-c_i}{d_i^4}(x_i - x_b)(y_i - y_b) & i = j \\ 0 & i \neq j. \end{cases} \tag{4.38}$$

Using, (4.29) to (4.38), the FIM can be expressed as

$$\mathbf{F}(\boldsymbol{\theta}) = \begin{bmatrix} \mathbf{F}_{11} & \mathbf{F}_{12} \\ \mathbf{F}_{12}^T & \mathbf{F}_{22} \end{bmatrix} \tag{4.39}$$

where

$$\mathbf{F}_{11} = \sum_{i=1}^{M} \frac{c_i}{d_i^4} \mathbf{Q}_i, \tag{4.40}$$

$$\mathbf{F}_{12} = -\left[\frac{c_1}{d_1^4} \mathbf{Q}_1, \cdots, \frac{c_M}{d_M^4} \mathbf{Q}_M \right], \tag{4.41}$$

$$\mathbf{F}_{22} = \text{blockdiag} \left\{ \frac{c_1}{d_1^4} \mathbf{Q}_1 + \frac{1}{\sigma_{a_1}^2} \mathbf{I}_2, \cdots, \frac{c_M}{d_M^4} \mathbf{Q}_M + \frac{1}{\sigma_{a_M}^2} \mathbf{I}_2 \right\}, \tag{4.42}$$

$$\mathbf{Q}_i = \begin{bmatrix} (x_i - x_b)^2 & (x_i - x_b)(y_i - y_b) \\ (x_i - x_b)(y_i - y_b) & (y_i - y_b)^2 \end{bmatrix}, \tag{4.43}$$

and $\mathbf{I}_2$ is the 2×2 identity matrix. Consequently, a lower bound is obtained on the root-mean-square error (RMSE) of any unbiased estimator of the blind node location as

$$\sqrt{\mathbb{E}\left[(\hat{x}_b - x_b)^2 + (\hat{y}_b - y_b)^2 \right]} \geq \sqrt{\text{Tr}\left\{ \left(\mathbf{F}_{11} - \mathbf{F}_{12} \mathbf{F}_{22}^{-1} \mathbf{F}_{12}^T \right)^{-1} \right\}}. \tag{4.44}$$

4.3 Experimental Insights

This section describes some experiments performed to validate the lower bound on the RMSE of the localization error given by (4.44) as well as to obtain more insights into its relationship with the number of anchors and their physical arrangement.

To experimentally validate the CRLB results given in (4.44), it is noted that the authors of [61] have calculated the CRLB for a similar localization problem. They assume perfect knowledge of anchor positions and consider errors only in the RSSI measurements following a log-normal shadowing path-loss model. The additional errors in anchor positions is expected to increase the CRLB values relative to these previously published results.

The results for three arbitrarily selected network topologies of anchors for a fixed blind node are given in Fig. 4.1. The evaluation is performed for three stages, differentiated based on the number of available anchor nodes, of every network topology . The first stage considers the availability of only three anchors followed by the addition of another three anchors in the second stage and finally adding six more anchors in the third stage. The anchors of the first, second, and third stages are labeled as "anchors 1-3","anchors 4-6" and

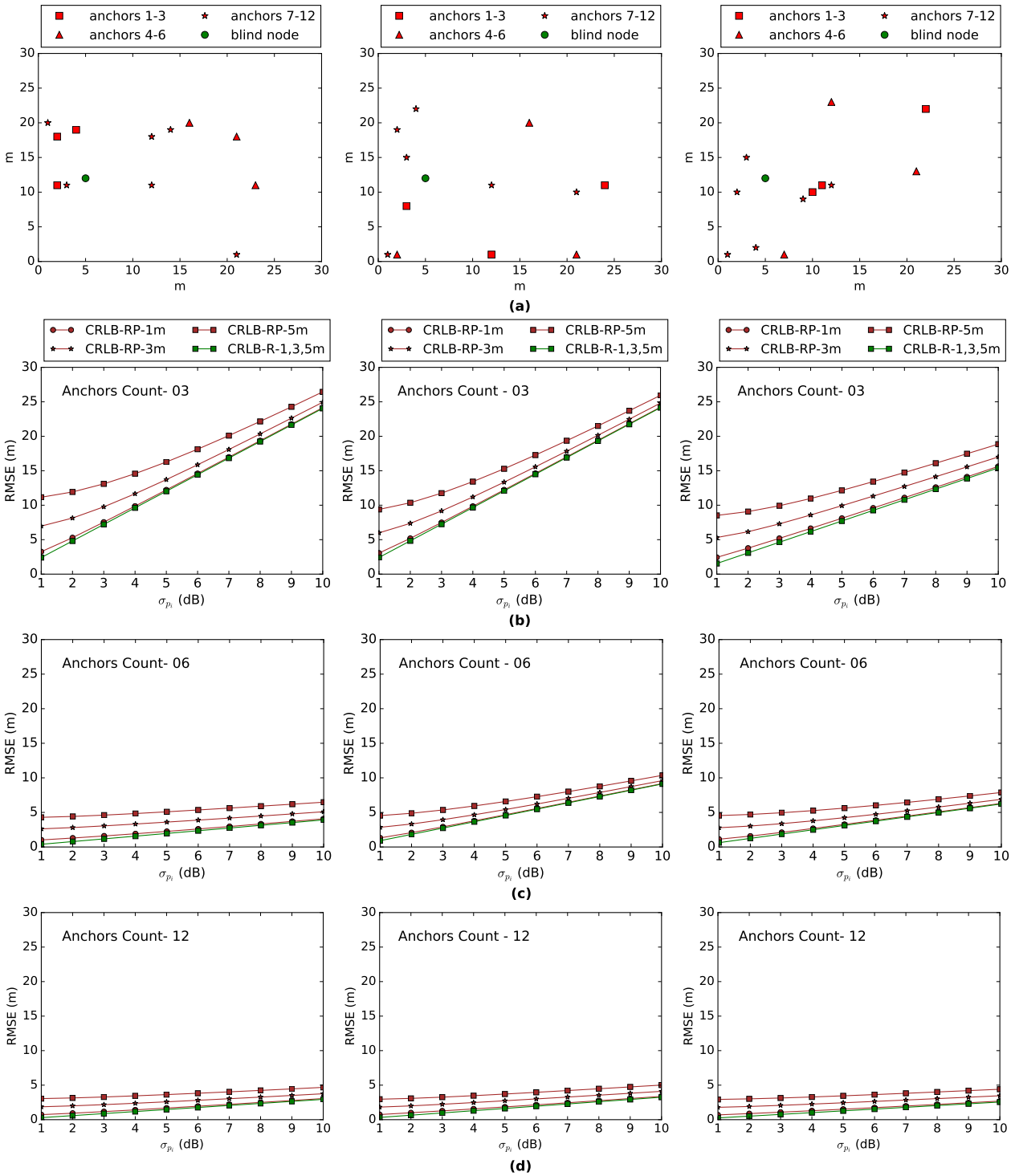

Figure 4.1: (a) Three stages of three different networks with a fixed blind node position (the green dot). The first stage consists of three anchors represented by squares, the triangles represent the added three anchors in the second stage, and the stars represent the six anchors added in the third stage of the network; (b) the CRLB of localization RMSE given the first stage of the network; (c) the CRLB of localization RMSE for second stage of the network; (d) the CRLB of localization RMSE for third stage of the network.

"anchors 7-12", respectively in Fig. 4.1a. The experiments are performed for anchor position errors with standard deviations equal to 1m, 3m, and 5m over a range of RSSI errors with standard deviations between 1dB and 10dB. The results obtained using (4.44) are labeled as "CRLB-RP-1m", "CRLB-RP-3m", and "CRLB-RP-5m", respectively. The CRLB given in [61] consider errors only in RSSI which means the CRLB values will be same for anchor position error 1m, 3m and 5m. Therefore, the CRLB values calculated using [61] are labeled as "CRLB-R-1,3,5m".

The following observations are made from Fig. 4.1:

- For a fixed blind node, CRLB varies with the number as well as the arrangement of the available anchor nodes.
- In all topologies, CRLB-RP is larger than CRLB-R, which shows that errors in the anchor positions have a significant impact on CRLB.
- With three anchor nodes, the minimum number of anchors required for 2D localization, the CRLB is very high for all the evaluated topologies. Therefore, it takes more than three anchor nodes to attain a reasonable estimate of the blind node position in the assumed scenario of errors.
- The CRLB using twelve nodes is considerably smaller compared to using three anchor nodes. The CRLB gap between six and twelve anchor nodes has a maximum value around 20% in all the cases, whereas from an energy consumption perspective, the latter case requires twice the energy. A similar observation of the non-significant performance improvement by adding anchor nodes beyond six has also been made in [95]. Based on this observation, the experiments given in the next chapters assume the availability of a minimum six anchor nodes to perform multilateration.

4.4 Conclusions

This chapter presented the theoretical lower bound on the RMSE of self-localization by a blind node, which can be achieved by any unbiased estimator in the presence of normally distributed errors in the anchor positions and log-normally distributed errors in the RSSI-based distance estimations. Evaluations under different topologies and varying error scenarios revealed the CRLB depends on topologies as well as the number of anchor nodes.

Chapter 5

Heuristic Non-Linear Algorithm

This chapter explores the third research question which is " How can the theoretical minimum bound on localization be approached or achieved in the assumed scenario" of resource-constrained mobile nodes?

As discussed in the literature review, Chapter 2, the authors of [15] addressed a similar problem. Their algorithm is based on the ML estimation and requires multiple RSSI and anchor position measurements. This thesis focuses on energy-efficient outdoor localization of mobile nodes where the GPS is the main source of anchor position information while being responsible for the majority of energy consumed; hence, multiple GPS measurements are not practically desirable.

This chapter presents a resource-efficient algorithm, referred to as the heuristic nonlinear (HNL) algorithm, for the self-localization problem formally defined in Section 4.1 given only single RSSI and anchor node position measurements. HNL is heuristic in nature and is based on the weighted least-squares (WLS) estimation method. It is based on minimizing a non-linear weighted sum-square-error cost function. Each term in the cost function is the weighted square of the difference between the distance inferred from an RSSI measurement and the Euclidean distance between the blind node and the anchor node to which the RSSI measurement corresponds. The square-error terms are weighted by their variances, which are estimated by taking into account errors in both RSSI measurements and anchor node position information.

A number of numerical simulations are carried out with various geometrical arrangements of the blind node and the anchor nodes in arbitrary network topologies to evaluate the performance of the proposed algorithm in comparison with an existing ML-based algorithm [15].

The simulation results show that the proposed HNL algorithm offers significant improvement in the localization performance over the algorithm of [15].

5.1 Proposed Algorithm - HNL

If the original values x_i, y_i, and d_i are available, one can estimate the position of the blind node by minimizing the following sum-square-error objective function over its arguments x and y:

$$c(x,y) = \sum_{i=1}^{M} {e_i}^2(x,y) \tag{5.1}$$

where the ith error (loss) term of the objective function is defined as

$$e_i(x,y) = \delta_i(x,y) - d_i \tag{5.2}$$

with

$$\delta_i(x,y) = \sqrt{(x_i - x)^2 + (y_i - y)^2}. \tag{5.3}$$

Since, in practice, the original values x_i, y_i, and d_i are not known, they are replaced with their corresponding noisy observations $\tilde{x}_i$, $\tilde{y}_i$, and $\tilde{d}_i$ and the ith error term is approximated as

$$\bar{e}_i(x,y) = \tilde{\delta}_i(x,y) - \tilde{d}_i \tag{5.4}$$

where

$$\tilde{\delta}_i(x,y) = \sqrt{(\tilde{x}_i - x)^2 + (\tilde{y}_i - y)^2}. \tag{5.5}$$

Additionally, in order to factor in the variations in the scale and statistical properties of the values associated with different anchor nodes, each error term is weighted with the inverse of its standard deviation. Therefore, the following objective function* is minimized:

$$\bar{c}(x,y) = \sum_{i=1}^{M} \frac{{\bar{e}_i}^2}{\mathrm{Var}(\bar{e}_i)}. \tag{5.6}$$

*the arguments x and y are dropped from $\bar{e}_i(x,y)$ and $\tilde{\delta}_i(x,y)$ on the right-hand side of (5.6) and afterwards to simplify the notation.

As the errors are independent of each other, we have

$$\mathrm{Var}(\bar{e}_i) = \mathrm{Var}(\tilde{\delta}_i) + \mathrm{Var}(\tilde{d}_i). \tag{5.7}$$

The first term on the right-hand side of (5.7) is calculated as

$$\mathrm{Var}(\tilde{\delta}_i) = \mathbb{E}[\tilde{\delta}_i^2] - (\mathbb{E}[\tilde{\delta}_i])^2. \tag{5.8}$$

Given (5.5), $\mathbb{E}[\tilde{\delta}_i^2]$ in (5.8) is computed as

$$\begin{aligned} \mathbb{E}[\tilde{\delta}_i^2] &= \mathbb{E}[(\tilde{x}_i - x)^2] + \mathbb{E}[(\tilde{y}_i - y)^2] \\ &= \mathbb{E}[(x_i + n_{x_i} - x)^2] + \mathbb{E}[(y_i + n_{y_i} - y)^2] \\ &= \delta_i^2 + 2\sigma_{a_i}^2. \end{aligned} \tag{5.9}$$

To calculate $(\mathbb{E}[\tilde{\delta}_i])^2$ in (5.8), it is noted that $\tilde{\delta}_i$ is the Euclidean distance between the points (x, y) and $(\tilde{x}_i, \tilde{y}_i)$ where x and y are deterministic variables and $\tilde{x}_i$ and $\tilde{y}_i$ are independent stochastic variables that have Gaussian distributions with means x_i and y_i, respectively, and the same variance $\sigma_{a_i}^2$. Therefore, $\tilde{\delta}_i$ has a Rice distribution [124] with the expectation

$$\mathbb{E}[\tilde{\delta}_i] = \sqrt{\frac{\pi}{2}}\sigma_{a_i} L_{1/2}\left(-\frac{\delta_i^2}{2\sigma_{a_i}^2}\right) \tag{5.10}$$

where $L_{1/2}(.)$ is a Laguerre polynomial expressed as

$$L_{1/2}(z) = \exp(z/2)\left[(1-z)\, I_0\left(-\frac{z}{2}\right) - z I_1\left(-\frac{z}{2}\right)\right] \tag{5.11}$$

with $I_0(.)$ and $I_1(.)$ being the modified Bessel functions of the first kind with orders zero and one, respectively. Bessel functions are not particularly cheap on an embedded platform, however, one can approximate these functions as a simple sum of scaled exponential functions [125]. For (5.8), this approximation works well when the argument to the Bessel functions is small (less than 25).

The second term on the right-hand side of (5.7) is calculated as

$$\mathrm{Var}(\tilde{d}_i) = \mathbb{E}[\tilde{d}_i^2] - (\mathbb{E}[\tilde{d}_i])^2. \tag{5.12}$$

To calculate the entries of (5.12), it is noted that $\tilde{d}_i$ using (4.6) - (4.10) is equal to

$$\begin{aligned}\tilde{d}_i &= d_i \exp\left(\frac{\ln 10}{10\eta} n_{p_i}\right) \\ &= \exp(\ln d_i) \exp\left(\frac{\ln 10}{10\eta} n_{p_i}\right) \\ &= \exp\left(\ln d_i + \frac{\ln 10}{10\eta} n_{p_i}\right).\end{aligned} \tag{5.13}$$

Hence, as per the assumption *A2*, $n_{p_i} \sim \mathcal{N}(0, \sigma_{p_i})$, $\tilde{d}_i$ has a log-normal distributed with mean $\mu_{d_i} = \ln d_i$ and standard deviation $\sigma_{d_i} = \frac{\ln 10}{10\eta}\sigma_{p_i}$. Therefore, it holds that

$$\begin{aligned}(\mathbb{E}[\tilde{d}_i])^2 &= \exp\left(2\ln d_i + \sigma_{d_i}^2\right) \\ &= d_i^2 \exp\left(\sigma_{d_i}^2\right)\end{aligned} \tag{5.14}$$

and

$$\begin{aligned}\mathbb{E}[\tilde{d}_i^2] &= \exp\left(2\ln d_i + 2\sigma_{d_i}^2\right) \\ &= d_i^2 \exp\left(2\sigma_{d_i}^2\right)\end{aligned} \tag{5.15}$$

and consequently $\mathrm{Var}(\tilde{d}_i)$ in (5.12) is calculated as

$$\mathrm{Var}(\tilde{d}_i) = d_i^2 \left[\exp\left(2\sigma_{d_i}^2\right) - \exp\left(\sigma_{d_i}^2\right)\right]. \tag{5.16}$$

Given an initial estimate $\left(\hat{x}_b^{(0)}, \hat{y}_b^{(0)}\right)$ and having calculated (5.7), the position of the blind node can be estimated by minimizing (5.6) in an iterative manner using any suitable optimization technique. Since the original anchor positions (x_i, y_i), $i = 1, ..., M$, are unknown, hence δ_i in (5.9) and (5.10) is replaced by its approximate value of

$$\bar{\delta}_i^{(k)} = \sqrt{\left(\tilde{x}_i - \hat{x}_b^{(k)}\right)^2 + \left(\tilde{y}_i - \hat{y}_b^{(k)}\right)^2} \tag{5.17}$$

where $\left(\hat{x}_b^{(k)}, \hat{y}_b^{(k)}\right)$ is the blind node's position estimate at the kth iteration. In addition, the unknown values of d_i, $i = 1, ..., M$ in (5.16) are replaced by their available approximate values $\tilde{d}_i$, $i = 1, ..., M$.

5.2 Experimental Setup and Results

5.2.1 Setup and Scenario

The proposed HNL algorithm is evaluated by simulating a group of seven nodes in a $30\text{m} \times 30\text{m}$ wide area. It is assumed that all the nodes have limited energy and computational resources. All the nodes are assumed to have a GPS receiver for independent positioning and a low-power radio for communication. GPS is widely accepted for the purpose of outdoor localization but suffers from high energy consumption. Therefore, to balance life-time and localization accuracy, all the nodes are considered to operate in a cooperative manner. For the purposes of this experiment, only one node is used as a blind node and there are six anchor nodes.

The errors on the position information of all anchor nodes are assumed to have Gaussian distribution with zero mean and known standard deviations. The radio propagation environment is represented by a log-normal shadowing path-loss model with known parameters. The values of the path-loss model parameters used in our experiments are $d_0 = 1\text{m}$, $p_{0(\text{dBm})} = -33.44$, and $\eta = 3.567$. These values are based on the results reported in [63], which uses same hardware for experiments as the one assumed in this thesis.

Both homogeneous and heterogeneous GPS noise scenarios in the region are considered for the performance evaluation. The homogeneous scenario refers to the case where the standard deviation of the GPS noise is the same all over the region. In the heterogeneous scenario, the standard deviation of the GPS noise varies within the region. In practice, if the GPS operational context, e.g., surroundings, hardware, etc., is the same for all the nodes, then the scenario is homogeneous. Otherwise, it is a heterogeneous scenario. As an example, the GPS localization performance is a function of the length of time during which the GPS receiver is active [89]. Therefore, variations in the GPS activity time may lead to a heterogeneous scenario. The heterogeneous scenario may also arise with cooperative or group/cluster-based energy-efficient localization schemes [88, 90, 126, 127] where the GPS activation time is decided based on the available energy budget of the individual nodes. In the experiments, the standard deviations of the errors on the anchor node position information, σ_{a_i}, $i = 1, ..., M$, are the same for all the anchor nodes when the GPS noise scenario is homogeneous. However, in the heterogeneous scenario, these standard deviations may differ

depending on the position of the anchor nodes within the region.

The performance of the RSSI-based localization highly depends on the network geometry [128]. Therefore, the performance of HNL is evaluated with different arbitrarily selected anchor and blind node positions. The GPS noise standard deviation varies from 1m to 10m. The RSSI measurement errors range from 1dB to 10dB in all the experiments. An arbitrary point in the region is selected as the initial estimate for the blind node. The initialization point is kept considerably far from the true position of the blind node while being fixed in all trials of each experiment.

5.2.2 Algorithm comparison

The performance of HNL is compared with the algorithm given in [15] referred to as "SPEAR". As discussed earlier, SPEAR makes similar assumptions on the errors as assumed in this thesis and solves a joint localization problem for the anchor nodes and the blind nodes using ML estimation. SPEAR requires multiple measurements of RSSI and anchor positions. However, the problem considered in this thesis is a self-localization problem in a resource-constrained scenario where the blind node as well the anchor nodes have limited energy. Therefore, only a single measurement of RSSI and anchor positions is provided to the proposed algorithm as well SPEAR. Both algorithms use a sequential least squares programming (SLSQP) solver available in the SciPy package for Python. For an unconstrained problem, SLSQP is similar to Newton's method.

5.2.3 Results

The RMSE and the bias norm are selected as the performance measures in the evaluations. To compare the complexities of the evaluated algorithms, the average number of iterations and convergence time of a single localization instance are measured. The algorithms are executed on a machine with a 2.9GHz processor and 8GB of RAM and the time stamping is done using Python's cProfile module. The results are calculated by averaging over 1000 independent trials for each experiment. The corresponding values of the theoretical lower bound on the RMSE given by CRLB are also plotted for reference, wherever applicable. The results for HNL are labeled as "proposed". The results of the SPEAR algorithm are denoted as "SPEAR-S" for source position estimation for anchor position uncertainty reduction with

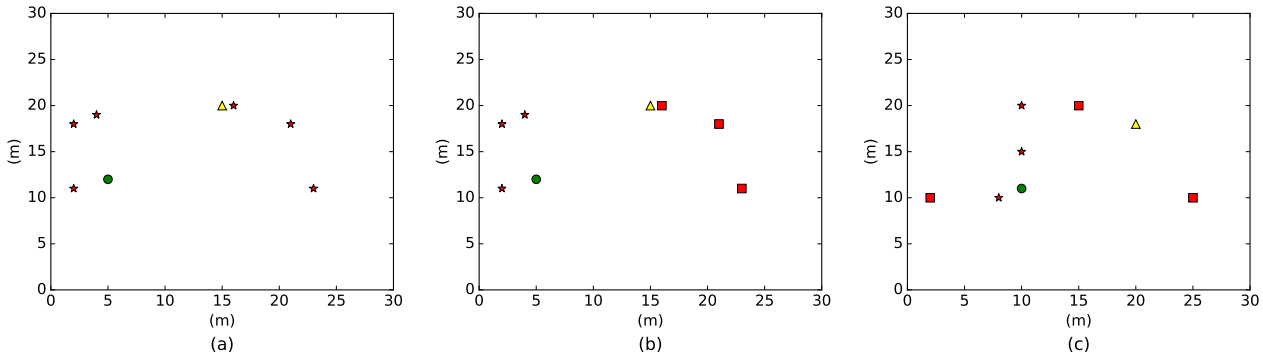

Figure 5.1: Considered network topologies. (a) The network topology in which the stars are the anchor nodes with homogeneous GPS error (σ_{a_i}): the σ_{a_i} values are 1m, 3m, and 5m; the circle is the true position of the blind node; the triangle is the initial estimate for the blind node position. (b) The network topology with heterogeneous GPS error: the stars are the anchor nodes with $\sigma_{a_i} = 6$m; the squares are the anchor nodes with $\sigma_{a_i} = 3$m; the circle is the true position of the blind node; the triangle is the initial estimate for the blind node position. (c) The network topology with heterogeneous GPS error: the stars are the anchor nodes with $\sigma_{a_i} = 4$m; the squares are the anchor nodes with $\sigma_{a_i} = 2$m; the circle is the true position of the blind node; the triangle is the initial estimate for the blind node position.

single measurement (SPEAR-S). The iteration count reported is based on an output parameter "nit" reported by the SLSQP method under the default convergence criteria. The convergence time reported for SPEAR-S is the time spent by the algorithm in the "SLSQP" method only. However, the convergence time reported for the proposed algorithm is the sum of the time spent in "SLSQP" method and the time spent to evaluate Bessel functions required to compute weights in the proposed algorithm.

Homogeneous GPS error

Fig. 5.2 presents the results for the homogeneous GPS error scenario in an arrangement given in Fig. 5.1a. From Figs. 5.2a - 5.2c, it is clear that HNL outperforms SPEAR-S in term of RMSE and the performance gap increases with the increase of errors in the RSSI measurements. For example, the RMSE improvement for error combination $\sigma_{a_i} = 3$m and $\sigma_{p_i} = 5$dB is only 10% but increased to 35% when σ_{p_i} is 10dB. Note that CRLB sets the theoretical lower bound for any unbiased estimator. The proposed estimator/algorithm is biased therefore, the RMSE may sometime be lower than CRLB as visible in Fig. 5.2c. The bias of both algorithms is comparable as evident from Figs. 5.2d - 5.2f. However, Figs. 5.2g - 5.2l revel that HNL requires significantly fewer iterations and time for convergence compared to SPEAR-S.

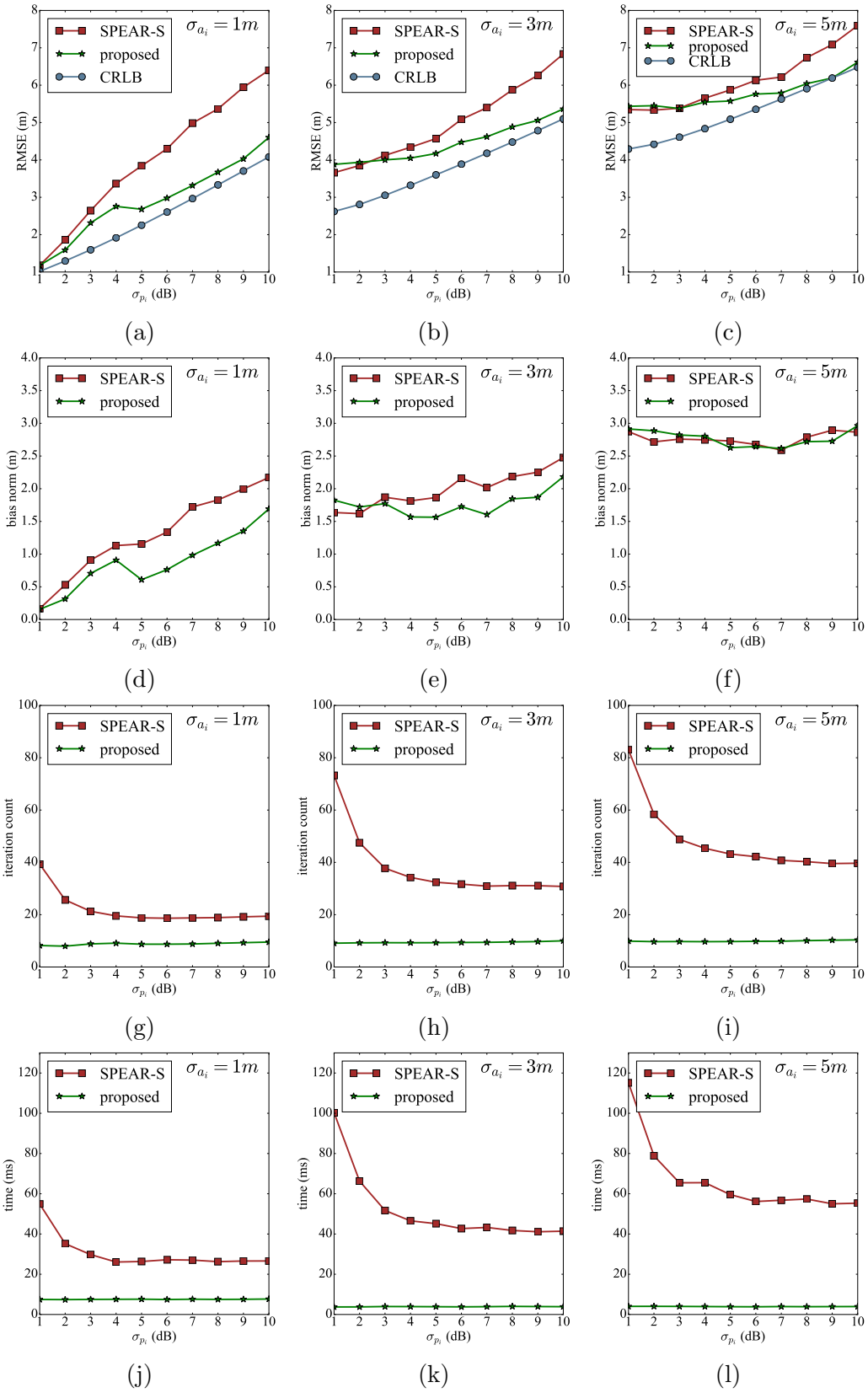

Figure 5.2: Localization performance for the network topology given in Fig. 5.1a and different homogeneous GPS error scenarios of $\sigma_{a_i} = 1$m, 3m, and 5m and different values of σ_{p_i}. (a)-(c) The RMSE of the algorithms as well as the corresponding CRLB. (d)-(f) The bias norm of the algorithms. (g)-(i) The iteration counts. (j)-(l) The convergence times of the algorithms for a single localization instance.

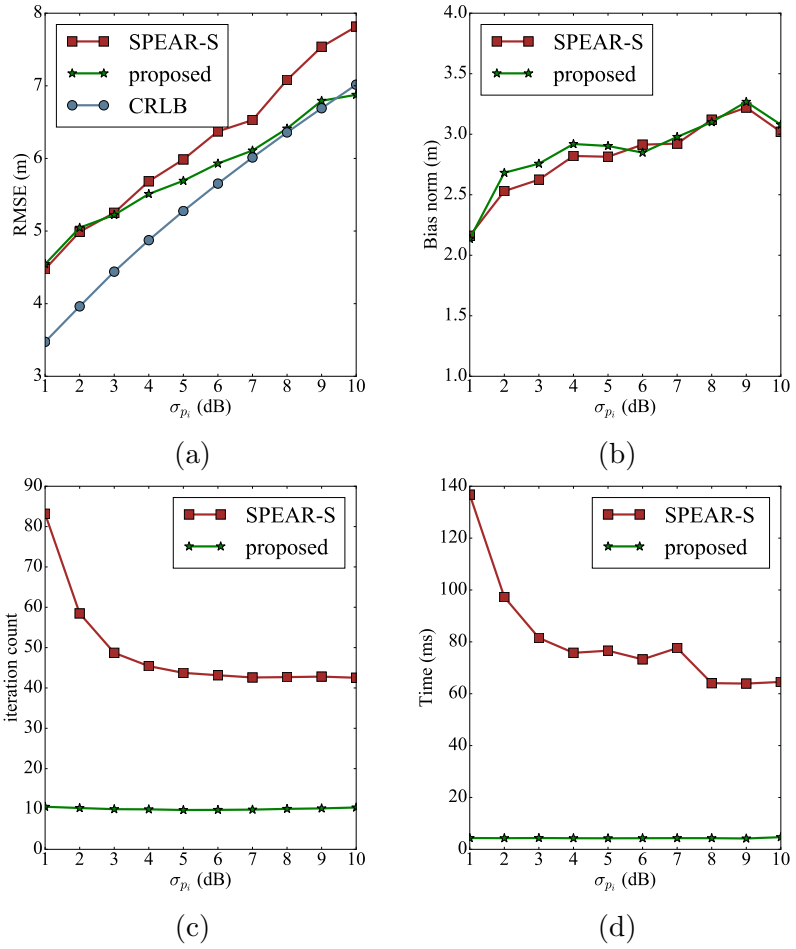

Figure 5.3: Localization performance for the network topology given in fig 5.1b for heterogeneous GPS error and different values of σ_{p_i}. (a) The RMSE of the algorithms as well as the corresponding CRLB. (b) The bias norm of the algorithms. (c) The iteration counts. (d) The convergence times of the algorithms for a single localization instance.

Heterogeneous GPS error

Fig. 5.3 shows the results for heterogeneous GPS scenario for the node placement given in Fig. 5.1b. There are three anchor nodes with $\sigma_{a_i} = 6$m and three anchor nodes with $\sigma_{a_i} = 3$m. Similar to the homogeneous scenario, HNL outperforms SPEAR-S in terms of RMSE and computational time requirement. The performance trend is also verifiable by the results given in Fig. 5.4 for another heterogeneous topology shown in Fig. 5.1c.

In summary, HNL significantly outperforms SPEAR-S in both RMSE and convergence time. The significantly low and almost constant convergence time for all the combinations of errors makes HNL more suitable for the resource constrained battery-operated mobile nodes considered in this thesis.

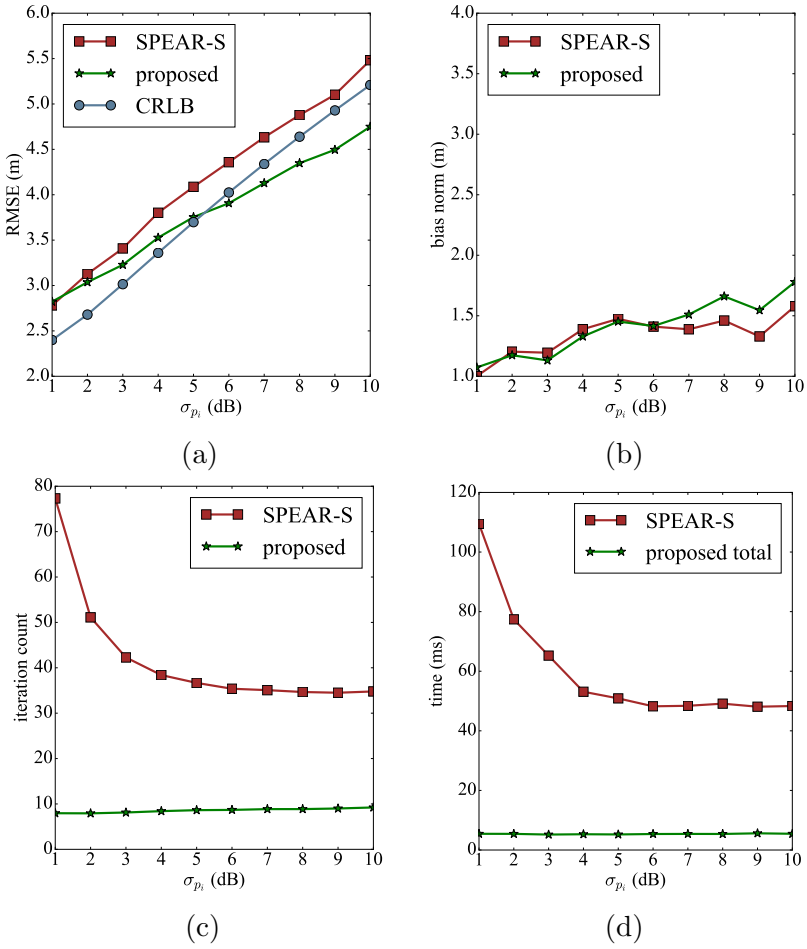

Figure 5.4: Localization performance for the network topology given in fig 5.1c for heterogeneous GPS error and different values of σ_{p_i}. (a) The RMSE of the algorithms as well as the corresponding CRLB. (b) The bias norm of the algorithms. (c) The iteration counts. (d) The convergence times of the algorithms for a single localization instance.

5.2.4 Performance for Imperfect Knowledge of the Model Parameters

The error distributions in real scenarios are usually not perfectly known. These experiments investigate what happens when incorrect distribution parameters are used. The results for overestimation of σ_{a_i}, σ_{p_i}, and path-loss exponent (η) are given in Fig. 5.5. HNL shows robust behaviour in overestimation of the different parameters for high errors in measurements and sensitive behaviour for low measurement errors. For example, there was no performance change for high errors in measurements ($\sigma_{p_i} = 8\text{dB} - 10\text{dB}$) even 50% overestimation of parameters. However, for low measurement errors an increase in the RMSE and bias was noticed even for 25% of overestimation.

The underestimation results are given in Fig. 5.6. Here, HNL performs better than

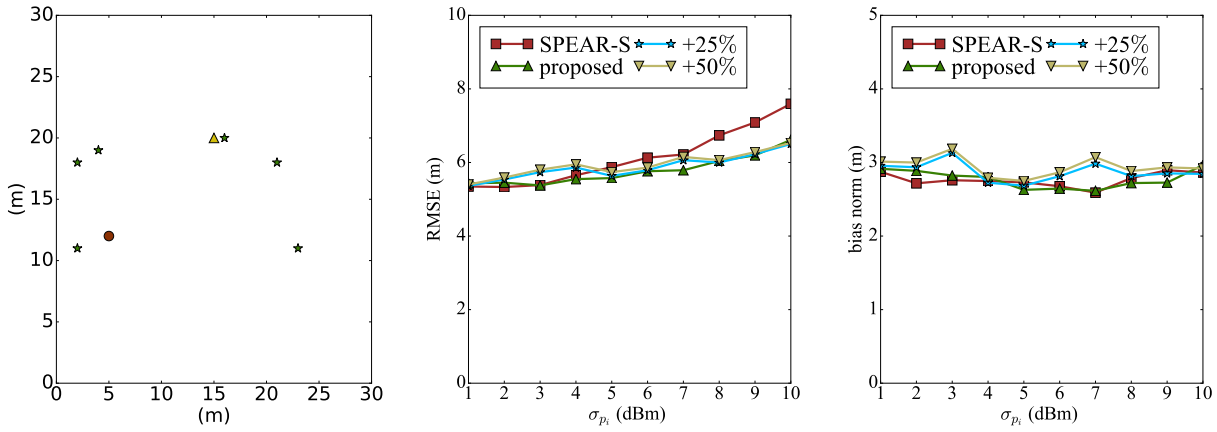

(a) (b) (c)

Figure 5.5: Localization performance with the overestimated parameters: $\sigma_{a_i}, \sigma_{p_i}$, and η. (a) The network topology with homogeneous GPS error: the stars are the anchor nodes with $\sigma_{a_i} = 5$m, the circle is the true position of the blind node, the triangle is the initial estimate for the blind node position. (b) The RMSE results with overestimated parameters. (c) The bias results with overestimated parameters.

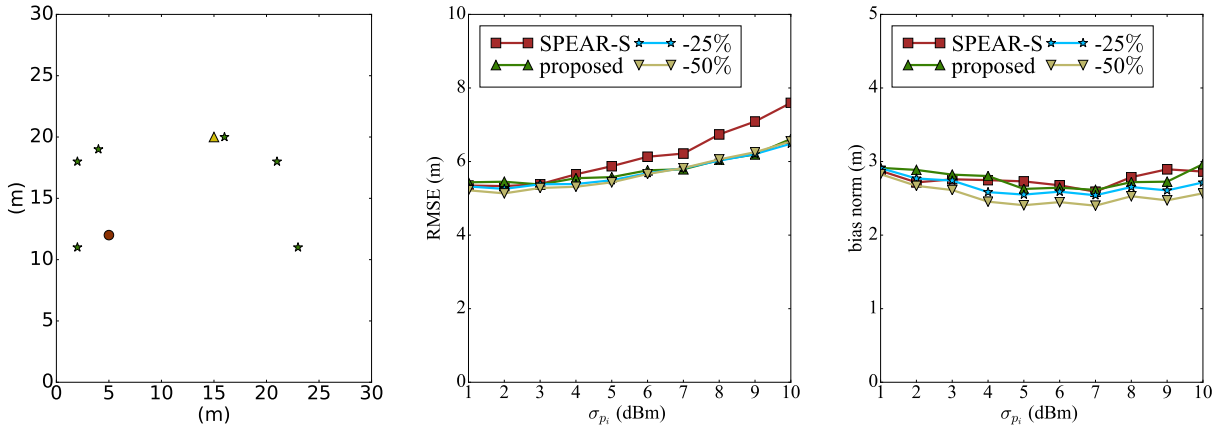

(a) (b) (c)

Figure 5.6: Localization performance with the underestimated parameters: $\sigma_{a_i}, \sigma_{p_i}$, and η. (a) The network topology with homogeneous GPS error: the stars are the anchor nodes with $\sigma_{a_i} = 5$m, the circle is the true position of the blind node, the triangle is the initial estimate for the blind node position. (b) The RMSE results with underestimated parameters. (c) The bias results with underestimated parameters.

SPEAR-S even when the different parameters are underestimated by 50%. In summary, HNL shows moderate robustness against imperfect knowledge of model parameters.

5.3 Conclusions

This chapter presented a localization algorithm in the presence of errors in the RSSI-based distance measurements as well as the anchor node position information. The performance of the proposed HNL algorithm was compared with a previously-proposed algorithm, called

SPEAR, that solves a joint localization problem of the blind node position and the anchor node positions using the ML estimation. Simulation results showed that the proposed algorithm can significantly reduce the localization RMSE and computational time compared with the SPEAR algorithm making it more suitable for localization in resource constrained environments. The robust behaviour of HNL given imperfect knowledge of various model parameters also makes it suitable for real-life implementation.

Chapter 6

Heuristic Pseudo-Linear Algorithm

This chapter presents a heuristic pseudo-linear (HPL) algorithm to solve the self-localization problem. This is another approach to the research question 3, which removes the limitations of iterative optimization and 2D applicability of the algorithm proposed in chapter 5.

The proposed HPL algorithm delivers a closed-form solution and approximates the original system of nonlinear equations with a system of linear equations given by $\tilde{\mathbf{A}}\mathbf{w} \approx \tilde{\mathbf{b}}$. As shown in the next section, the resulting linearised system of equations contains errors on both sides of the equations due to errors in distance and anchor position measurements. Notably, the errors in $\tilde{\mathbf{b}}$ and $\tilde{\mathbf{A}}$ are non-linearly correlated. In addition, the probability distributions of errors in distance and anchor position measurements are different. This violates the pre-requisites of existing techniques such as TLS, EWTLS, and CTLS.

To deal with this error scenario, HPL uses a weighted least-squares approach. The weights are estimated by taking into account the statistical properties of errors in both RSSI and anchor position information. In addition, the algorithm compensates for the bias caused by anchor position and RSSI measurements errors. The evaluation is performed using numerical simulations with various arrangements of the blind node and anchor nodes within arbitrary network topologies. Due to similar computational requirements, the performance of the proposed algorithm is compared with an existing WLS-based hyperbolic algorithm [16] that only takes into account the errors in the RSSI measurements. The simulation results show that the proposed algorithm offers significant improvement in the localization performance over the hyperbolic algorithm of [16].

The remainder of this chapter presents the proposed HPL algorithm followed by experiments and results.

6.1 Proposed Algorithm - HPL

Given the anchor positions (x_i, y_i) and the corresponding distances d_i, $i = 1, \cdots, M$, the blind node position can be estimated by intersecting the circles defined by

$$(x - x_i)^2 + (y - y_i)^2 = d_i^2, \quad i = 1, \cdots, M. \tag{6.1}$$

To solve the system of non-linear equations (6.1), subtracting the equation corresponding to $i = 1$ from the others results in a system of linear equations expressed as

$$2\mathbf{A}\mathbf{w} = \mathbf{b} \tag{6.2}$$

where

$$\begin{aligned} \mathbf{A} &= \begin{bmatrix} x_2 - x_1 & y_2 - y_1 \\ x_3 - x_1 & y_3 - y_1 \\ \cdots & \cdots \\ x_i - x_1 & y_i - y_1 \end{bmatrix}, \\ \mathbf{b} &= \begin{bmatrix} d_1^2 - d_2^2 + k_2 - k_1 \\ d_1^2 - d_3^2 + k_3 - k_1 \\ \cdots \\ d_1^2 - d_i^2 + k_i - k_1 \end{bmatrix}, \end{aligned} \tag{6.3}$$

$$\mathbf{w} = \begin{bmatrix} x \\ y \end{bmatrix}, \tag{6.4}$$

and

$$k_i = x_i^2 + y_i^2. \tag{6.5}$$

The ordinary least-squares solution of (6.2) is

$$\mathbf{w} = \frac{1}{2} \left(\mathbf{A}^T \mathbf{A} \right)^{-1} \mathbf{A}^T \mathbf{b}. \tag{6.6}$$

Because the original values x_i, y_i, and d_i are not available, they are replaced with their corresponding noisy observations $\tilde{x}_i$, $\tilde{y}_i$ and $\tilde{d}_i$. Both $\mathbf{A}$ and $\mathbf{b}$ are noisy and (6.2) becomes

$$2\tilde{\mathbf{A}}\hat{\mathbf{w}} \approx \tilde{\mathbf{b}} \tag{6.7}$$

where

$$\tilde{\mathbf{A}} = \begin{bmatrix} \tilde{x}_2 - \tilde{x}_1 & \tilde{y}_2 - \tilde{y}_1 \\ \tilde{x}_3 - \tilde{x}_1 & \tilde{y}_3 - \tilde{y}_1 \\ \cdots & \cdots \\ \tilde{x}_M - \tilde{x}_1 & \tilde{y}_M - \tilde{y}_1 \end{bmatrix}, \tag{6.8}$$

$$\tilde{\mathbf{b}} = \begin{bmatrix} \tilde{d}_1^2 - \tilde{d}_2^2 + \tilde{k}_2 - \tilde{k}_1 \\ \tilde{d}_1^2 - \tilde{d}_3^2 + \tilde{k}_3 - \tilde{k}_1 \\ \cdots \\ \tilde{d}_1^2 - \tilde{d}_M^2 + \tilde{k}_M - \tilde{k}_1 \end{bmatrix}, \tag{6.9}$$

$$\hat{\mathbf{w}} = \begin{bmatrix} \hat{x} \\ \hat{y} \end{bmatrix}, \tag{6.10}$$

$$\tilde{k}_i = \tilde{x}_i^2 + \tilde{y}_i^2. \tag{6.11}$$

To factor in the difference in the scale and statistical properties of the values associated with different anchor nodes and distance measurements, the WLS solution to (6.7) is given as

$$\hat{\mathbf{w}} = \frac{1}{2}\left(\tilde{\mathbf{A}}^T\mathbf{S}^{-1}\tilde{\mathbf{A}}\right)^{-1}\tilde{\mathbf{A}}^T\mathbf{S}^{-1}\tilde{\mathbf{b}}. \tag{6.12}$$

In (6.12), $\mathbf{S}$ is the covariance matrix of $\tilde{\mathbf{b}}$ with its (i,j)th entry being

$$s_{ij} = \begin{cases} \mathrm{Var}(\tilde{d}_1^2 - \tilde{d}_{i+1}^2 + \tilde{k}_{i+1} - \tilde{k}_1) & \text{if } i = j \\ \mathrm{Var}(\tilde{d}_1^2 - \tilde{k}_1) & \text{if } i \neq j. \end{cases} \tag{6.13}$$

Considering the assumptions *A1* and *A2* in addition to the independent nature of the errors

of the anchor positions and the RSSI-induced distances, (6.13) can be written as

$$s_{ij} = \begin{cases} \mathrm{Var}(\tilde{k}_{i+1}) + \mathrm{Var}(\tilde{k}_1) + \mathrm{Var}(\tilde{d}_1^2) + \mathrm{Var}(\tilde{d}_{i+1}^2) & \text{if } i = j \\ \mathrm{Var}(\tilde{k}_1) + \mathrm{Var}(\tilde{d}_1^2) & \text{if } i \neq j. \end{cases} \tag{6.14}$$

To calculate $\mathrm{Var}(\tilde{k}_i)$, it's noted that $\tilde{k}_i$ is the sum of squares of independent normally distributed random variables $\tilde{x}_i$ and $\tilde{y}_i$ with non-zero mean. Therefore, $\tilde{k}_i/\sigma_{a_i}^2$ has a non-central chi-squared distribution with the variance

$$\mathrm{Var}\left(\frac{\tilde{k}_i}{\sigma_{a_i}^2}\right) = 2\left(2 + 2\frac{x_i^2 + y_i^2}{\sigma_{a_i}^2}\right) \tag{6.15}$$

and consequently

$$\mathrm{Var}\left(\tilde{k}_i\right) = 4\sigma_{a_i}^2(\sigma_{a_i}^2 + (x_i^2 + y_i^2)). \tag{6.16}$$

Considering the assumption *A2*, $\mathrm{Var}(\tilde{d}_i^2)$ is calculated as [16]

$$\mathrm{Var}(\tilde{d}_i^2) = \exp(4\mu_{d_i})\left[\exp(8\sigma_{d_i}^2) - \exp(4\sigma_{d_i}^2)\right] \tag{6.17}$$

where

$$\mu_{d_i} = \ln d_i \quad \text{and} \quad \sigma_{d_i} = \frac{\ln 10}{10\eta}\sigma_{p_i}. \tag{6.18}$$

As x_i, y_i, and d_i are not available, their corresponding noisy observations $\tilde{x}_i$, $\tilde{y}_i$, and $\tilde{d}_i$ are used in (6.16) and (6.17).

In addition, it is noted that (6.7) has multiple sources of bias. The left-hand side of (6.7) has error, the right-hand side errors are neither additive nor zero-mean and there is a correlation between left-hand and right-hand side errors. To estimate the bias in the algorithm assuming an additive error model, (6.7) can be written as

$$2\left(\mathbf{A} + \mathbf{N}\right)\hat{\mathbf{w}} = \mathbf{b} + \mathbf{e} \tag{6.19}$$

where

$$\mathbf{N} = \underbrace{\begin{bmatrix} n_{x_2} & n_{y_2} \\ n_{x_3} & n_{y_3} \\ \dots & \dots \\ n_{x_M} & n_{y_M} \end{bmatrix}}_{\check{\mathbf{N}}} - \underbrace{\begin{bmatrix} n_{x_1} & n_{y_1} \\ n_{x_1} & n_{y_1} \\ \dots & \dots \\ n_{x_1} & n_{y_1} \end{bmatrix}}_{\mathbf{N}_1}, \tag{6.20}$$

$$\mathbf{e} = \tilde{\mathbf{b}} - \mathbf{b}, \tag{6.21}$$

and

$$\mathbf{N} = \tilde{\mathbf{A}} - \mathbf{A}. \tag{6.22}$$

Using (6.12) and (6.19), $\mathbb{E}[\hat{\mathbf{w}}]$ becomes

$$\begin{aligned} \mathbb{E}[\hat{\mathbf{w}}] = & \underbrace{\mathbb{E}\left[\left(\tilde{\mathbf{A}}^T\mathbf{S}^{-1}\tilde{\mathbf{A}}\right)^{-1}\right]\mathbf{A}^T\mathbf{S}^{-1}\mathbf{b}}_{\mathbf{I}} \\ & + \underbrace{\mathbb{E}\left[\left(\tilde{\mathbf{A}}^T\mathbf{S}^{-1}\tilde{\mathbf{A}}\right)^{-1}\mathbf{N}^T\right]\mathbf{S}^{-1}\mathbf{b}}_{\mathbf{II}} \\ & + \underbrace{\mathbb{E}\left[\left(\tilde{\mathbf{A}}^T\mathbf{S}^{-1}\tilde{\mathbf{A}}\right)^{-1}\mathbf{A}^T\mathbf{S}^{-1}\mathbf{e}\right]}_{\mathbf{III}} \\ & + \underbrace{\mathbb{E}\left[\left(\tilde{\mathbf{A}}^T\mathbf{S}^{-1}\tilde{\mathbf{A}}\right)^{-1}\mathbf{N}^T\mathbf{S}^{-1}\mathbf{e}\right]}_{\mathbf{IV}}. \end{aligned} \tag{6.23}$$

The term I in (6.23) is the approximation of $\hat{\mathbf{w}}$, term II gives the bias due to the noise in $\tilde{\mathbf{A}}$, and terms III and IV exist due to the fact that $\mathbb{E}[\mathbf{e}]$ and $\mathbb{E}[\mathbf{N}^T\mathbf{e}]$ are not equal to zero.

To compensate for the bias terms II and III in (6.23), the expectation of the corresponding noise covariance is subtracted in (6.12) as

$$\begin{aligned} \hat{\mathbf{w}} = & \frac{1}{2}\left(\tilde{\mathbf{A}}^T\mathbf{S}^{-1}\tilde{\mathbf{A}} - \mathbb{E}\left[\mathbf{N}^T\mathbf{S}^{-1}\mathbf{N}\right]\right)^{-1} \\ & \times \left(\tilde{\mathbf{A}}^T\mathbf{S}^{-1}\tilde{\mathbf{b}} - \mathbb{E}\left[\mathbf{N}^T\mathbf{S}^{-1}\tilde{\mathbf{b}}\right]\right). \end{aligned} \tag{6.24}$$

Using (6.19), $\mathbb{E}\left[\mathbf{N}^T\mathbf{S}^{-1}\mathbf{N}\right]$ is equals to

$$\begin{aligned} \mathbb{E}\left[\mathbf{N}^T\mathbf{S}^{-1}\mathbf{N}\right] = & \mathbb{E}\left[\check{\mathbf{N}}^T\mathbf{S}^{-1}\check{\mathbf{N}}\right] + \mathbb{E}\left[\mathbf{N}_1^T\mathbf{S}^{-1}\mathbf{N}_1\right] \\ & - \mathbb{E}\left[\mathbf{N}_1^T\mathbf{S}^{-1}\check{\mathbf{N}}\right] - \mathbb{E}\left[\check{\mathbf{N}}^T\mathbf{S}^{-1}\mathbf{N}_1\right]. \end{aligned} \tag{6.25}$$

The last two terms on the right-hand side of (6.25) are equal to zero, which leads to

$$\mathbb{E}\left[\mathbf{N}^T\mathbf{S}^{-1}\mathbf{N}\right] = \mathbf{L} \tag{6.26}$$

where

$$\mathbf{L} = \begin{bmatrix} l_{11} & l_{12} \\ l_{21} & l_{22} \end{bmatrix} \tag{6.27}$$

with various entries equal to

$$l_{11} = \sum_{k=1}^{M-1} \mathbf{S}_{kk}^{-1}\sigma^2_{n_{x_{k+1}}} + \sigma^2_{n_{x_1}}\left(\mathbf{u}^T\mathbf{S}^{-1}\mathbf{u}\right), \tag{6.28}$$

$$l_{22} = \sum_{k=1}^{M-1} \mathbf{S}_{kk}^{-1}\sigma^2_{n_{y_{k+1}}} + \sigma^2_{n_{y_1}}\left(\mathbf{u}^T\mathbf{S}^{-1}\mathbf{u}\right), \tag{6.29}$$

$$l_{12} = l_{21} = 0, \tag{6.30}$$

and $\mathbf{u} = [1, 1, ..., 1]$. The bias due to the correlation between the noises in $\tilde{\mathbf{A}}$ and $\tilde{\mathbf{b}}$ is

$$\mathbb{E}\left[\mathbf{N}^T\mathbf{S}^{-1}\tilde{\mathbf{b}}\right] = \mathbb{E}\left[\check{\mathbf{N}}^T\mathbf{S}^{-1}\tilde{\mathbf{b}}\right] - \mathbb{E}\left[\mathbf{N}_1^T\mathbf{S}^{-1}\tilde{\mathbf{b}}\right]. \tag{6.31}$$

The independent and uncorrelated nature of RSSI and anchor position noises makes the entries in the first term of (6.31) involving noise in d_i and x_1, y_1 zero *. Hence

$$\mathbb{E}\left[\check{\mathbf{N}}^T\mathbf{S}^{-1}\tilde{\mathbf{b}}\right] = \begin{bmatrix} \sum_{k=1}^{M-1} x_{k+1}\mathbf{s}_{kk}^{-1}\sigma^2_{n_{x_{k+1}}} \\ \sum_{k=1}^{M-1} y_{k+1}\mathbf{s}_{kk}^{-1}\sigma^2_{n_{y_{k+1}}} \end{bmatrix} \tag{6.32}$$

and with the same logic the entries in the second term of (6.31) involving d_i and $(x_i, y_i, i \neq 1)$ are zero. Therefore,

$$\mathbb{E}\left[\mathbf{N}_1^T\mathbf{S}^{-1}\tilde{\mathbf{b}}\right] = -\begin{bmatrix} x_1\sigma^2_{n_{x_1}}\left(\mathbf{u}^T\mathbf{S}^{-1}\mathbf{u}\right) \\ y_1\sigma^2_{n_{y_1}}\left(\mathbf{u}^T\mathbf{S}^{-1}\mathbf{u}\right) \end{bmatrix}. \tag{6.33}$$

To compensate for term IV in (6.23), $\mathbb{E}[\tilde{\mathbf{b}}]$ is calculated with the ith entry of $\tilde{\mathbf{b}}$, $\mathbb{E}[\tilde{b}_i]$

*This assumption of "independent and uncorrelated RSSI measurements" is certainly used in the simulation experiments. Different practical scenarios would require these assumptions to be verified.

equals to

$$\mathbb{E}[\tilde{b}_i] = \mathbb{E}[\tilde{d}_1^2 - \tilde{d}_i^2 + \tilde{k}_i - \tilde{k}_1]\,. \tag{6.34}$$

Considering the independent nature of the noises of the anchor positions and RSSI-induced distances, (6.34) can be rewritten as

$$\mathbb{E}[\tilde{b}_i] = \mathbb{E}[\tilde{d}_1^2] - \mathbb{E}[\tilde{d}_i^2] + \mathbb{E}[\tilde{k}_i] - \mathbb{E}[\tilde{k}_1]\,. \tag{6.35}$$

To calculate $\mathbb{E}[\tilde{d}_i^2]$, note that $\tilde{d}_i^2$ using (4.10) is equal to

$$\tilde{d}_i^2 = d_i^2 \exp\left(\sqrt{2} u n_{p_i}\right) \tag{6.36}$$

where

$$u = \frac{\ln 10}{5\sqrt{2}\eta}. \tag{6.37}$$

Thus,

$$\begin{aligned} \mathbb{E}[\tilde{d}_i^2] &= d_i^2\, \mathbb{E}\left[\exp\left(\sqrt{2} u n_{p_i}\right)\right] \\ &= d_i^2 \exp\left(u^2 \sigma_{n_{p_i}}^2\right). \end{aligned} \tag{6.38}$$

Note that $u^2\sigma_{n_{p_i}}^2$ is small even for high values of $\sigma_{n_{p_i}}$ such as 5dB. Therefore, using the second-order Taylor-series expansion of the function $\exp(u^2\sigma_{n_{p_i}}^2)$ around zero, (6.38) is approximated as

$$\mathbb{E}[\tilde{d}_i^2] = d_i^2 + d_i^2 \left(u^2 \sigma_{n_{p_i}}^2 + \frac{u^4 \sigma_{n_{p_i}}^4}{2}\right). \tag{6.39}$$

The term $\mathbb{E}[\tilde{k}_i]$ in (6.35) is equal to

$$\mathbb{E}[\tilde{k}_i] = x_i^2 + y_i^2 + 2\sigma_{n_{a_i}}^2. \tag{6.40}$$

Using (6.39) and (6.40), $\mathbb{E}[\tilde{\mathbf{b}}]$ can be written as

$$\mathbb{E}\left[\tilde{\mathbf{b}}\right] = \mathbf{b} + \mathbf{t} \tag{6.41}$$

where the ith entry of $\mathbf{t}$ is

$$t_i = \left(u^2\sigma_{n_{p_i}}^2 + \frac{u^4}{2}\sigma_{n_{p_i}}^4\right)\left(d_1^2 - d_i^2\right) + 2\left(\sigma_{n_{a_i}}^2 - \sigma_{n_{a_1}}^2\right). \tag{6.42}$$

As d_i is not accessible, the corresponding noisy values are used in the calculation of $\mathbf{t}$.

Experimental evaluation reveals that the bias due to correlation of noise in $\tilde{\mathbf{A}}$ and $\tilde{\mathbf{b}}$ using (6.31) is close to the real bias for only small values of anchor position error. The dependence of bias on x_i, y_i makes the estimation poor for high values of σ_{a_i}. The estimated position, which is bias compensated (BC), in the proposed algorithm named as HPL-BC, is calculated as a closed form equation:

$$\hat{\mathbf{w}} = \frac{1}{2}\left(\tilde{\mathbf{A}}^T\mathbf{S}^{-1}\tilde{\mathbf{A}} - \mathbf{L}\right)^{-1}\tilde{\mathbf{A}}^T\mathbf{S}^{-1}\left(\tilde{\mathbf{b}} - \mathbf{t}\right). \tag{6.43}$$

6.2 Experimental Setup and Results

6.2.1 Setup and Scenario

The scenario for the evaluation of this algorithm is the same as the one used for the evaluation of the previous algorithm given in Section 5.2.1. There are six anchor nodes and one blind node in a region of 30m by 30m. The distance and anchor position measurement errors follow the log-normal distribution and normal distribution, respectively, as given in the problem statement Section 4.1.

HPL-BC is evaluated for both homogeneous and heterogeneous GPS error scenarios. A variety of node arrangements are considered in addition to a wide range of standard-deviation for the anchor position and distance measurement errors. The algorithm is also evaluated for imperfect knowledge of error parameters and RSSI radio propagation parameter (path-loss exponent). The performance is evaluated for both overestimation and underestimation of these parameters. To assess the suitability of HPL-BC in real-life implementations, the range of overestimation and underestimation is varied from 25% to 50%.

6.2.2 Algorithm in Comparison

The performance of the proposed HPL-BC algorithm is compared with that of the so-called weighted hyperbolic algorithm proposed in [16]. The selection is based on the similarity

in computational requirements for both algorithms. This algorithm is referred to here as "WLSR" and is given below for a quick reference. The WLSR algorithm is also a weighted least-squares type algorithm but based on the assumption that only the RSSI measurements are corrupted by noise and the anchor node positions are known exactly at the blind node. Therefore, HPL-BC can be viewed as an improvement over the algorithm of [16] taking into account the effects of errors in anchor node positions.

WLSR algorithm

The WLSR algorithm considers errors only in RSSI-based distance measurements between a blind node and anchor nodes while assuming perfect knowledge of the anchor node positions. WLSR estimates the position as

$$\hat{\mathbf{w}} = \frac{1}{2}\left(\tilde{\mathbf{A}}^T\mathbf{S}^{-1}\tilde{\mathbf{A}}\right)^{-1}\tilde{\mathbf{A}}^T\mathbf{S}^{-1}\tilde{\mathbf{b}} \tag{6.44}$$

where

$$\tilde{\mathbf{A}} = \begin{bmatrix} \tilde{x}_2 - \tilde{x}_1 & \tilde{y}_2 - \tilde{y}_1 \\ \tilde{x}_3 - \tilde{x}_1 & \tilde{y}_3 - \tilde{y}_1 \\ \cdots & \cdots \\ \tilde{x}_M - \tilde{x}_1 & \tilde{y}_M - \tilde{y}_1 \end{bmatrix}, \tag{6.45}$$

$$\tilde{\mathbf{b}} = \begin{bmatrix} \tilde{d}_1^2 - \tilde{d}_2^2 + \tilde{k}_2 - \tilde{k}_1 \\ \tilde{d}_1^2 - \tilde{d}_3^2 + \tilde{k}_3 - \tilde{k}_1 \\ \cdots \\ \tilde{d}_1^2 - \tilde{d}_M^2 + \tilde{k}_M - \tilde{k}_1 \end{bmatrix}, \tag{6.46}$$

$$\hat{\mathbf{w}} = \begin{bmatrix} \hat{x} \\ \hat{y} \end{bmatrix}, \tag{6.47}$$

and

$$\tilde{k}_i = \tilde{x}_i^2 + \tilde{y}_i^2. \tag{6.48}$$

In (6.44), the (i, j)th entry in the covariance matrix $\mathbf{S}$ of $\tilde{\mathbf{b}}$ is given by

$$s_{ij} = \begin{cases} \mathrm{Var}(\tilde{d}_1^2 - \tilde{d}_{i+1}^2) & \text{if } i = j \\ \mathrm{Var}(\tilde{d}_1^2) & \text{if } i \neq j. \end{cases} \tag{6.49}$$

6.2.3 Results

The localization accuracy is assessed in terms of RMSE and bias. The results given are based on averaging over 10,000 independent trials. The true locations of the nodes are the same in every trial; variations exist only in the noise values. The proposed algorithm with bias compensation is presented as "HPL-BC". The results without bias compensation are labeled as "HPL". The results of WLSR are marked as "existing".

In the rest of this section, first, the results for homogeneous GPS error are given followed by heterogeneous GPS error. Then, the performance for imperfect knowledge of error parameters is given. Finally, the performance of both proposed HNL and HPL algorithms are compared given the accurate knowledge of error and radio propagation model parameters used in generating simulated data.

Homogeneous GPS error

The performance of the proposed HPL-BC algorithm is evaluated over two different node arrangements shown in Fig. 6.1. The original position of the anchor nodes and blind node are fixed in all the trials of any experiment. Three values for the anchor position error standard-deviation σ_{a_i} (1m, 3m, 5m) are considered in the experiments. The standard deviation of error in RSSI measurements σ_{p_i} varies in the range of 1dB to 10dB.

Fig. 6.2 shows the performance of different algorithms over the node arrangement given in Fig 6.1(a). HPL-BC shows improvement over the existing algorithm in terms of both RMSE and bias. The performance improvement is significant for high errors in the measurements. For example, HPL-BC reduces the RMSE by up to 30%, along with reduction in bias, for

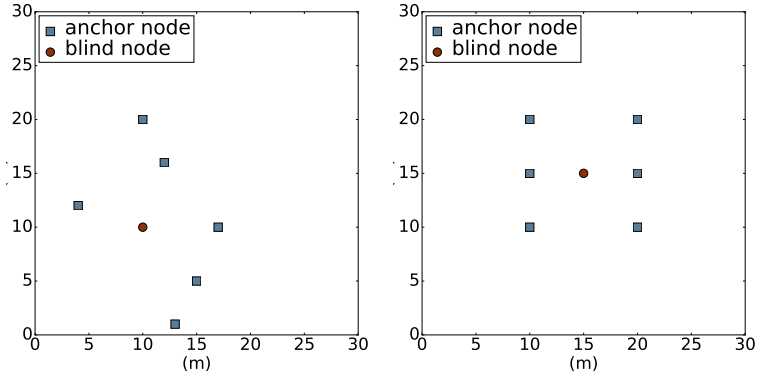

(a) (b)

Figure 6.1: Network node arrangements for homogeneous scenario.

σ_{a_i} = 3m and 5m when σ_{p_i} is in the range of 5dB to 10dB . In addition, the RMSE of HPL-BC is also close to the CRLB. Note that CRLB sets the theoretical lower bound for any unbiased estimator. The proposed estimator/algorithm is biased therefore, the RMSE may sometime be lower than CRLB as visible in Fig. 6.2(a). The performance improvement offered by HPL and HPL-BC is also visible in the cumulative error distribution plots in 6.2(g) - 6.2(i). Similar performance trends are also noticed in the results shown in Fig. 6.3 for the node arrangement shown in Fig 6.1(b).

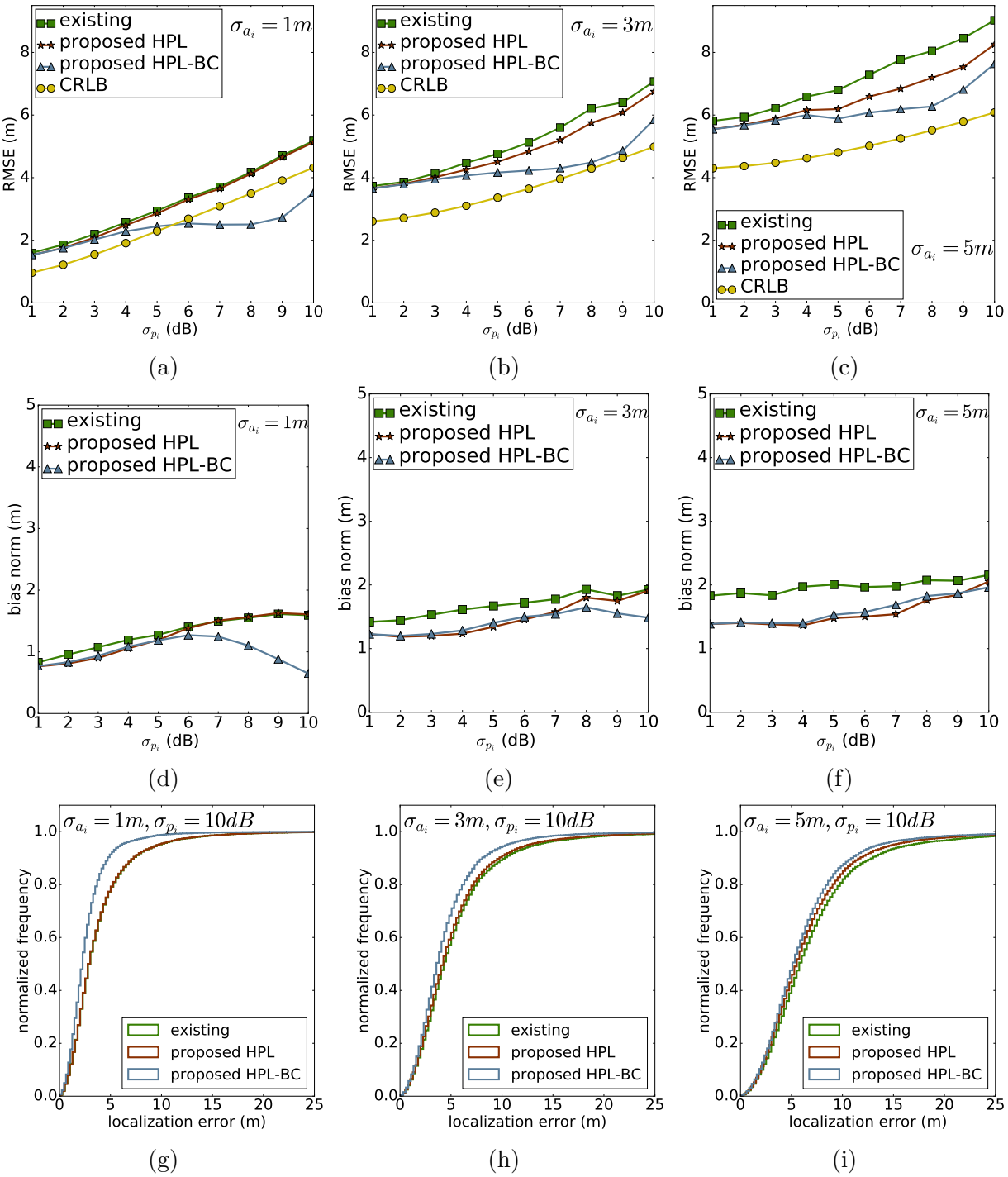

Figure 6.2: Localization performance of various algorithms for homogeneous GPS error node arrangement given in Fig. 6.1a; (a) to (c) show the RMSE and CRLB for σ_{a_i} = 1m, 3m, 5m, respectively, for different values of σ_{p_i}, with their corresponding bias shown in (d) to (f); (g) to (i) present the cumulative distribution of errors for different combinations of σ_{p_i} and σ_{a_i}.

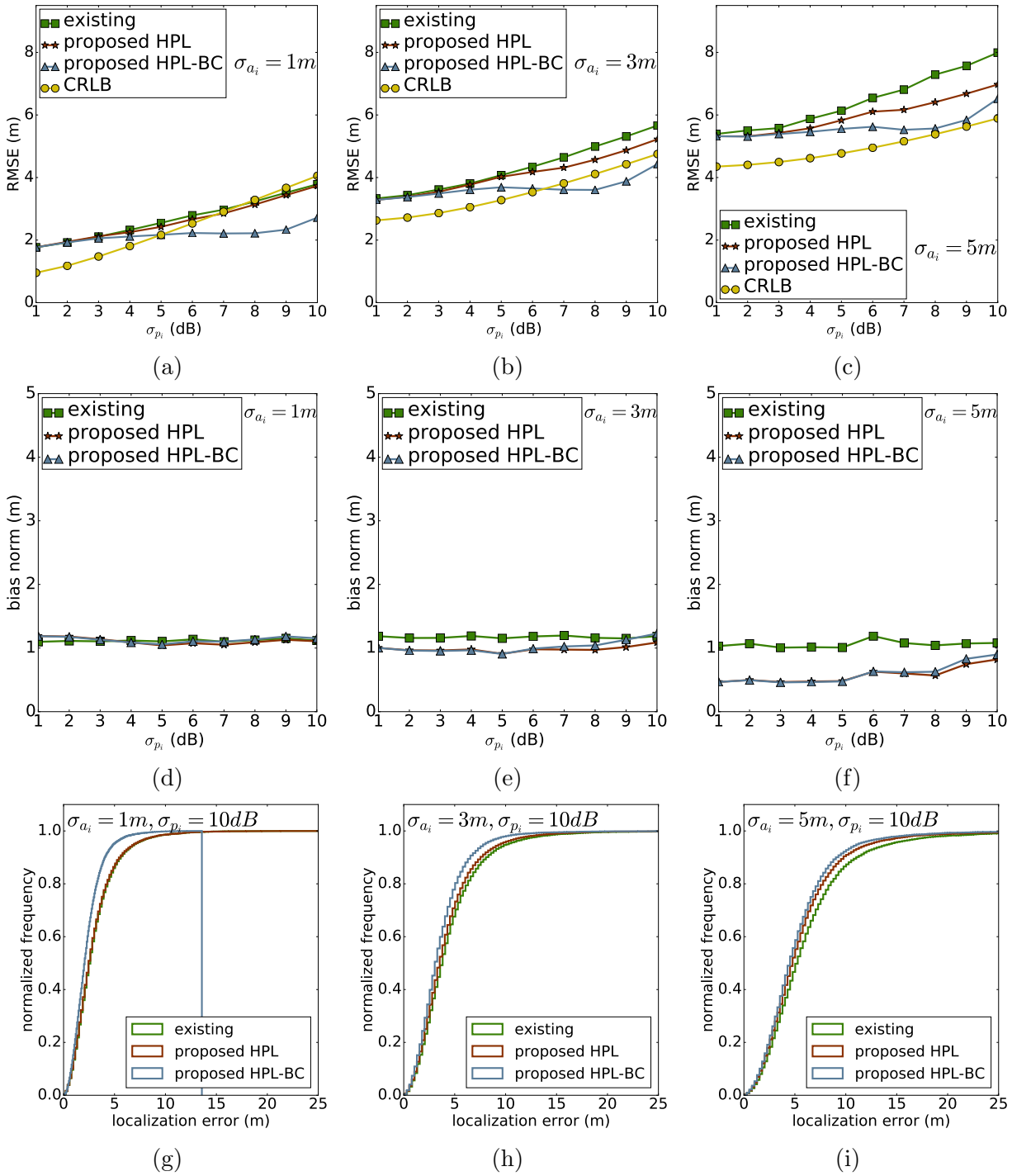

Figure 6.3: Localization performance of various algorithms for homogeneous GPS error node arrangement given in Fig. 6.1b; (a) to (c) show the RMSE and CRLB for σ_{a_i} = 1m, 3m, 5m, respectively, for different values of σ_{p_i}, with their corresponding bias shown in (d) to (f); (g) to (i) present the cumulative distribution of errors for different combinations of σ_{p_i} and σ_{a_i}.

Heterogeneous GPS error

The results for an arbitrarily selected node arrangement with heterogeneous GPS error are given in Fig. 6.4. In this experiment, three nodes have $\sigma_{a_i} = 5$m and the other three have $\sigma_{a_i} = 1$m. HPL-BC significantly outperforms the existing algorithm in terms of both RMSE and bias, especially when RSSI values have large standard deviation. In addition, HPL-BC has a bias less than 0.5m whereas the bias in the existing algorithm is around 2.0m. The plots of cumulative distribution of errors also shows better performance of HPL-BC compare to the existing algorithm. It is worth noting that HPL-BC performs close to the CLRB as well.

The performance of HPL-BC is evaluated in another arbitrarily selected node arrangement

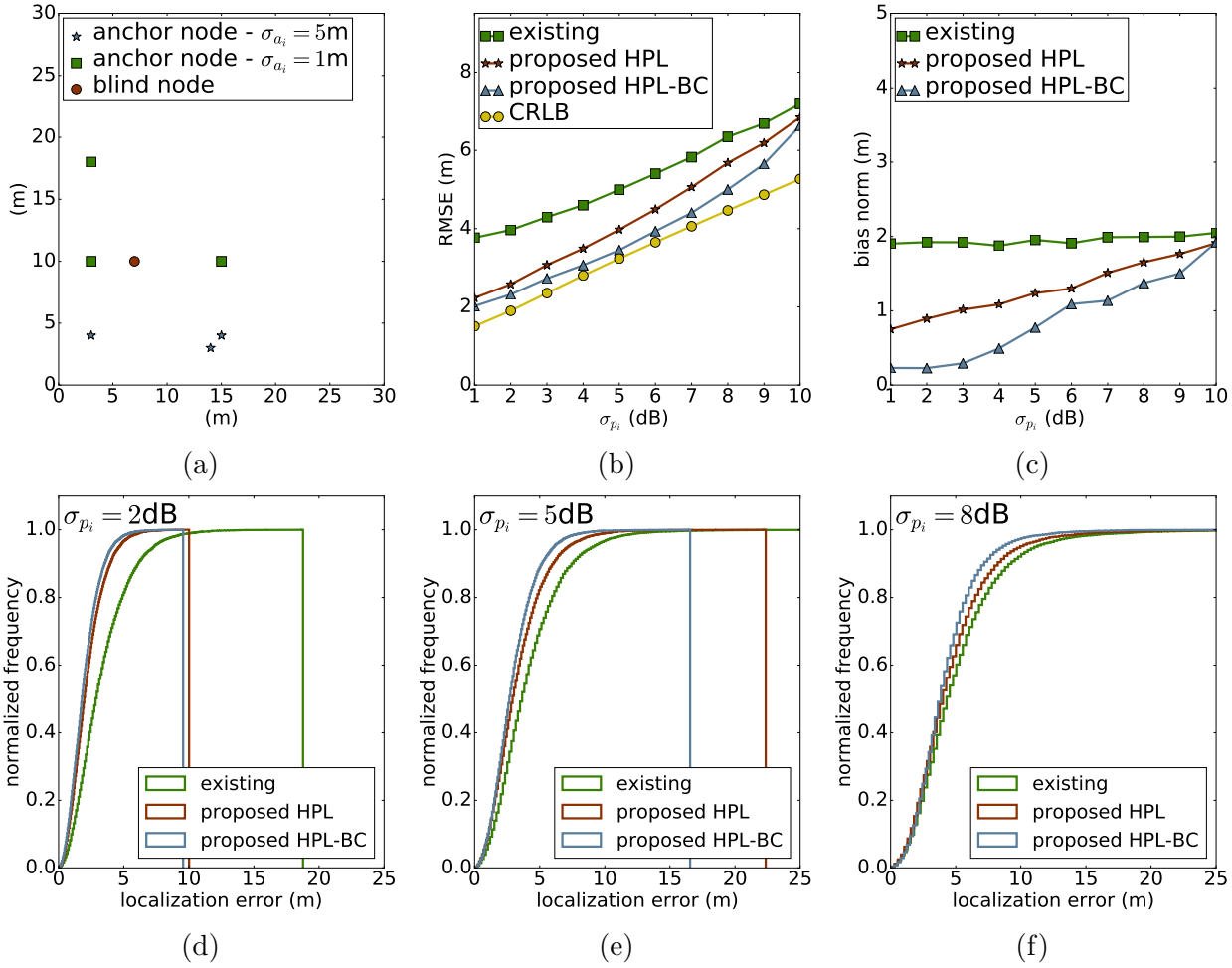

Figure 6.4: Localization performance for heterogeneous GPS error; (a) the network topology; (b) the RMSE of the proposed and existing algorithms as well as the corresponding CRLB for different values of σ_{p_i}; (c) the bias of the proposed and existing algorithms for different values of σ_{p_i}; (d) to (f) the cumulative distribution of errors for values of $\sigma_{p_i} = 2$dB, 5dB and 8dB, respectively.

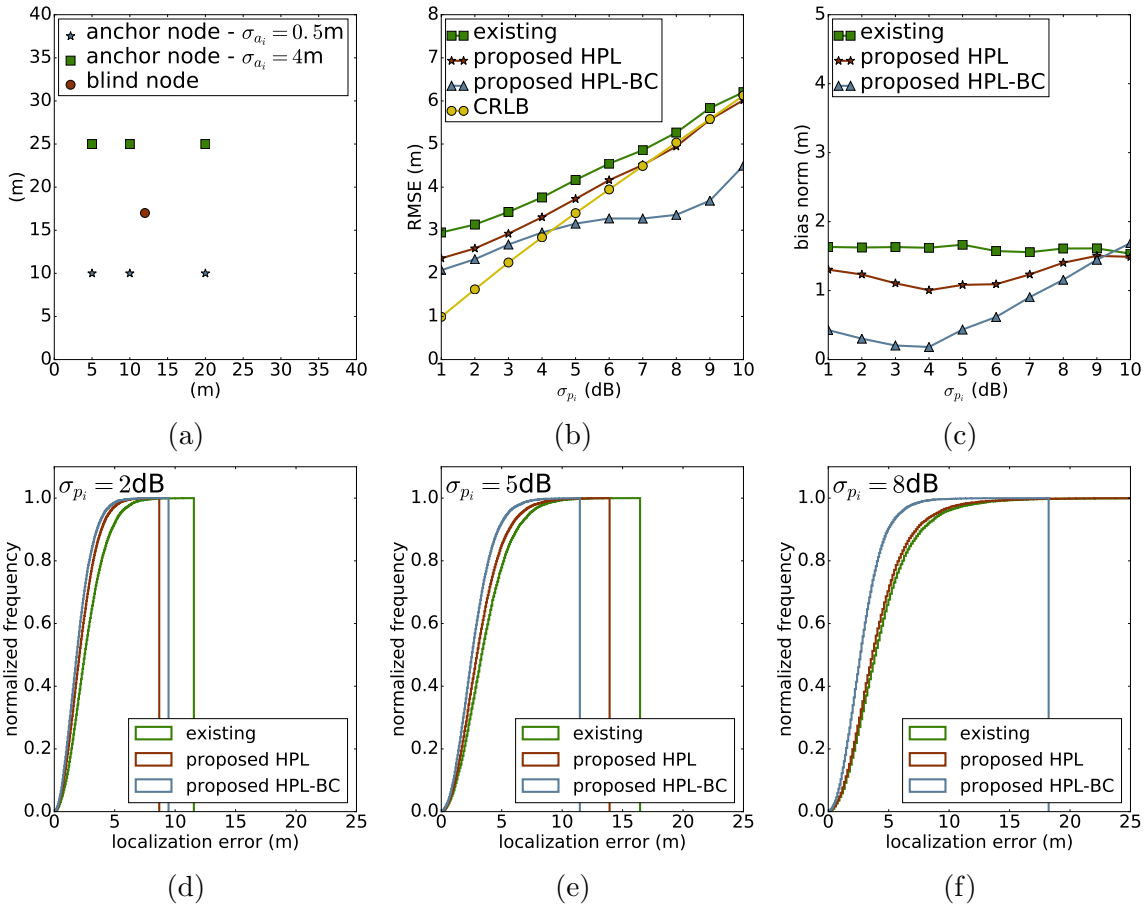

Figure 6.5: Localization performance for heterogeneous GPS error; (a) the network topology; (b) the RMSE of the proposed and existing algorithms as well as the corresponding CRLB for different values of σ_{p_i}; (c) the bias of the proposed and existing algorithms for different values of σ_{p_i}; (d) to (f) the cumulative distribution of errors for values of $\sigma_{p_i} = 2$dB, 5dB and 8dB, respectively.

given in Fig. 6.5. Here, three anchor nodes with $\sigma_{a_i} = 4$m and three with $\sigma_{a_i} = 0.5$m are considered. HPL-BC performs better as compared to the existing algorithm in this node arrangement as well. Overall, HPL-BC reduces the RMSE by more than 1m, in addition to the reduction of bias.

6.2.4 Performance for Imperfect Knowledge of the Model Parameters

The results for overestimation of σ_{a_i}, σ_{p_i}, and path-loss exponent η in both node arrangements shown in Figs. 6.4(a) and 6.5(b) are given in Fig. 6.6. HPL-BC shows robust behaviour with overestimation of the parameters. HPL-BC shows no major change in the RMSE and bias up to 25% of overestimation of the parameters in both node arrangements. However, in comparison to the existing algorithm, HPL-BC still performs better even when

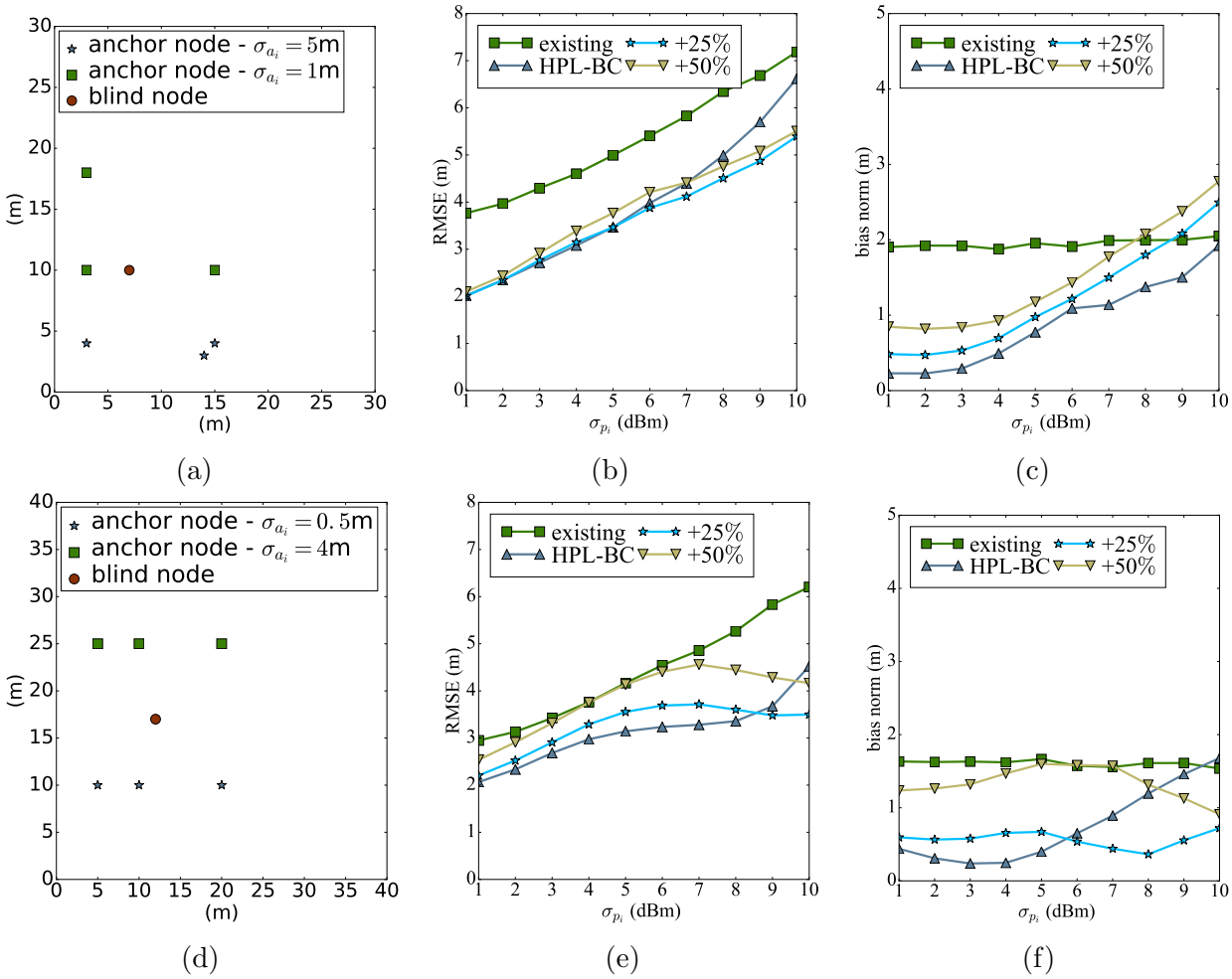

Figure 6.6: Localization performance with overestimation of parameters: $\sigma_{a_i}, \sigma_{p_i}$and η; **scenario1**: (a) node arrangement; (b) the RMSE with overestimated parameters; (c) the bias with overestimated parameters; **scenario2**: (d) node arrangement; (e) the RMSE with overestimated parameters; (f) the bias with overestimated parameters.

the parameters are overestimated by 50%.

The underestimation results for corresponding node arrangements are given in Fig. 6.7. HPL-BC performs better than the existing algorithm for up to 25% underestimation of parameters in both node arrangements.

In summary, the proposed HPL-BC algorithm significantly improves the localization performance compared to the existing WLS algorithm of [16] in terms of RMSE and bias. In addition, HPL-BC is also robust against overestimation and underestimation of the parameters up-to 25%.

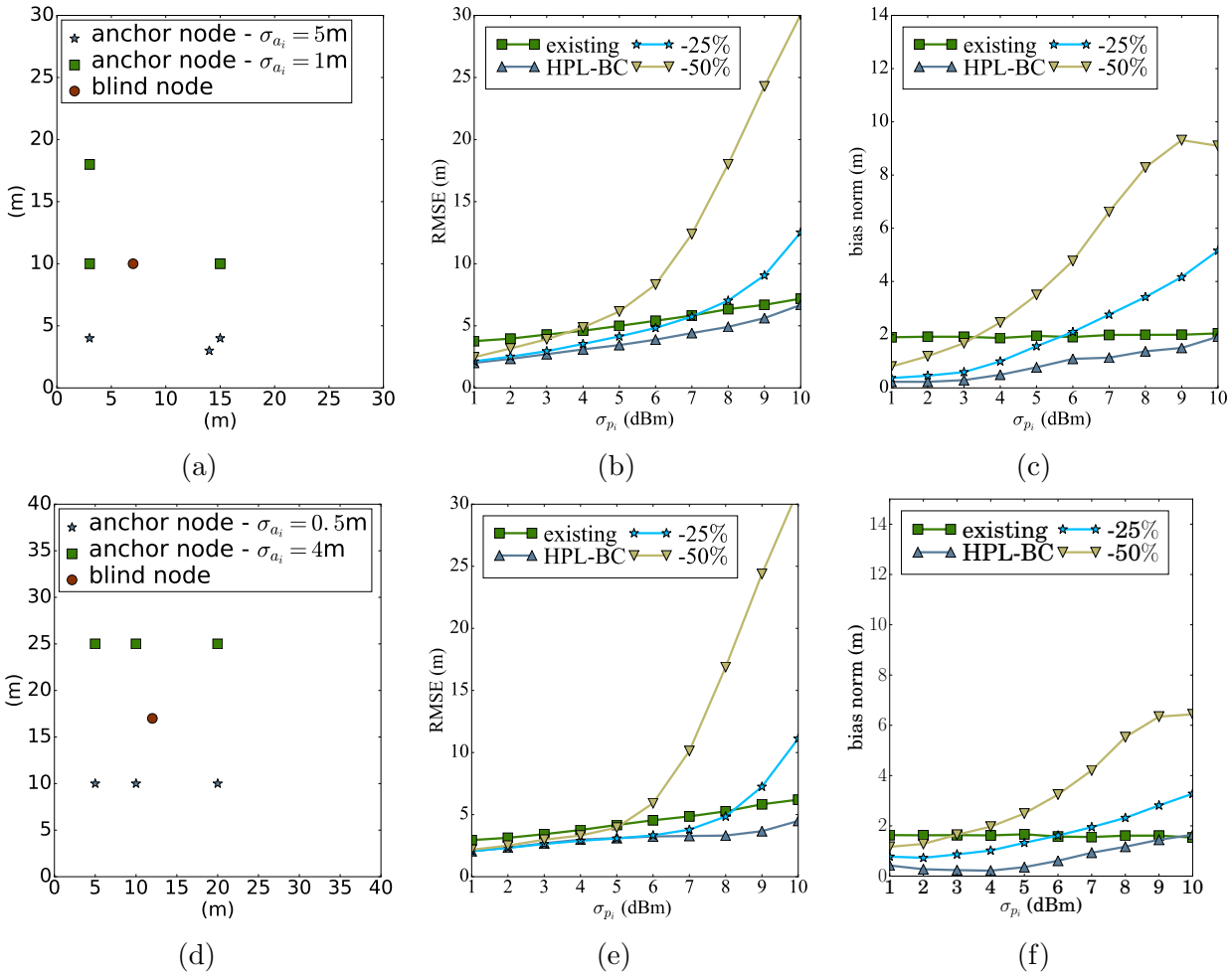

Figure 6.7: Localization performance with underestimation of parameters $\sigma_{a_i}, \sigma_{p_i}$and η; **scenario1** (a) node arrangement;(b) the RMSE with overestimated parameters; (c) the bias with overestimated parameters; **scenario2** (d) node arrangement;(e) the RMSE with overestimated parameters; (f) the bias with overestimated parameters.

6.2.5 Comparison Between HPL-BC and HNL

The performance comparison of both proposed algorithms over an arbitrarily selected node arrangement is given in Fig. 6.8. The experiment assumes the perfect knowledge of various simulation model parameters (σ_{a_i}, σ_{p_i} and η).

As expected, the HNL algorithm performs better than HPL-BC in terms of RMSE with a better cumulative distribution of errors. However, the improved performance of HNL comes at the cost of extra computation time as shown in Fig. 6.8(f). HNL requires roughly five times more processing time than HPL-BC to reduce the RMSE by approximately 20%. As well as the advantage of low-computational time, HPL-BC does not require any initial position estimate.

In summary, both proposed algorithms have their own advantages and disadvantages.

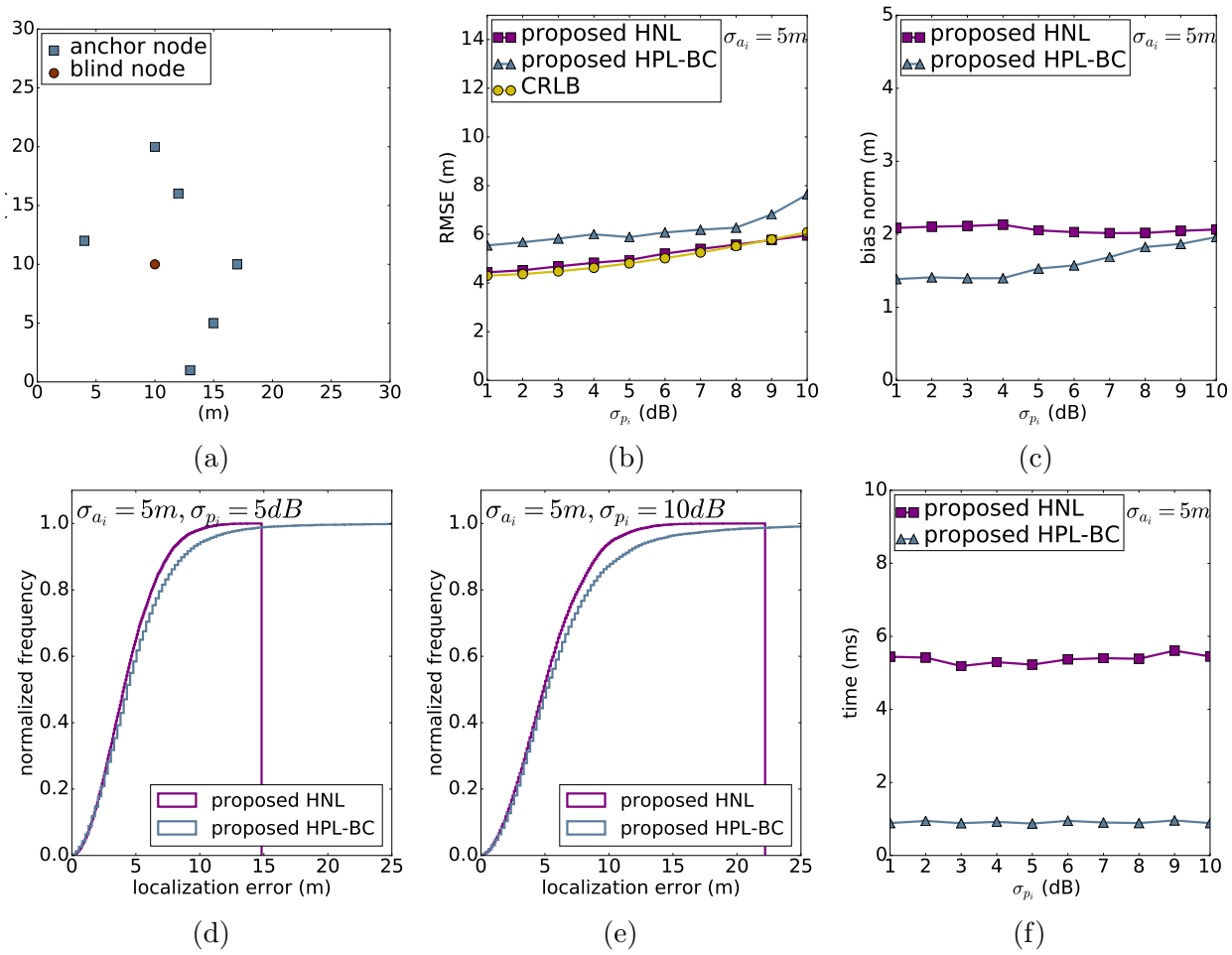

Figure 6.8: Performance comparison between the proposed HPL-BC and HNL algorithms; (a) node arrangement; (b) the RMSE for various values of σ_{p_i}; (c) the bias for various values of σ_{p_i}; (d) cumulative distribution of errors for σ_{a_i} = 5m and σ_{p_i} = 5dB; (e) cumulative distribution of errors for σ_{a_i} = 5m and σ_{p_i} = 10dB; (f) time taken by a single run of each algorithm for different values of σ_{p_i}.

HNL comes with an advantage of low positioning error with the limitation of 2D positioning and the requirement of an initial position estimate. HPL-BC has low computational time compared to HNL (at the cost of higher RMSE) and is applicable to 3D positioning as well.

6.3 Conclusions

This chapter presents a heuristic pseudo-linear solution to the self-localization problem stated in Section 4.1. The proposed algorithm, called HNL-BC, is of WLS type in which weights are calculated using statistical properties of the errors. In addition, various sources of the bias in the proposed algorithms are estimated and accounted for.

The performance of HPL-BC is compared to the WLS-based hyperbolic algorithm presented in [16]. The proposed algorithm significantly outperforms this existing algorithm. To

assess the suitability of HBL-BC in real-life applications, its performance is also evaluated for overestimation and underestimation of various noise parameters and radio propagation model. HPL-BC is robust against up to 25% overestimation and underestimation of error and radio propagation model parameters.

This chapter also presents a comparison between the proposed HNL and HPL-BC algorithms. HNL gives up to 20% low RMSE but requires five times more computational effort compared to HPL-BC. In addition to low computational time, HPL-BC has also the advantage of being applicable to 3D localization. In conclusion, both algorithms have their own merits and demerits and a choice can be made depending on the accuracy requirements of the application and the available computing and energy resources.

Chapter 7

Multi-Mode Tracking

This chapter explores the fourth research question which is "How can additional information of error characteristics be used to improve the tracking accuracy of such groups of mobile nodes?"

For static or slowly-varying sensor networks, a relatively straightforward answer to this research question is to use multilateration-based tracking such as the one proposed in this project (e.g. Chapter 6). However, such solutions are not directly applicable to long-term tracking of dynamic groups of resource-constrained mobile nodes such as humans, animals, and vehicles. The dynamic group structure brings the challenges of frequently changing neighbouring nodes and available resources for localization. In some instances, the number of neighbouring nodes may not be sufficient to run multilateration. To address these challenges, this chapter proposes a group-based multi-mode tracking algorithm. The proposed algorithm has three modes namely multilateration mode, cluster-based mode and standalone mode. At any particular time instance, the proposed algorithm selects the best mode given the group size and available resources. A clustering approach is used where a cluster head (CH) is responsible for position update process and other cluster management related activities. In some scenarios, the statistical properties of the anchor position errors is not known. Therefore, evaluation is performed for two variants of the proposed group-based multi-mode algorithm namely "Multi-mode WLSR" and "Multi-mode HPL" based on the WLSR, the hyperbolic solution proposed in [16], and HPL solutions.

The energy-accuracy trade-off of the proposed algorithm is evaluated for fixed sampling intervals ranging from 5s to 50s. The evaluation is based on the 2D position tracks of 40 nodes generated using Reynolds' flocking model [12]. The proposed multi-mode algorithm

provides significant improvements over the cluster-based tracking algorithm proposed in [127] and over cooperative localization assuming a node's position to be the same as a neighbouring node [87]. The results are also compared with the Individual case when a node only uses its own GPS for a position update and is not involved in any cooperation with other nodes. The proposed multimode algorithm is as accurate as the individual-based tracking while using about half the energy.

The rest of the chapter describes the proposed algorithm followed by experimental evaluations, results and conclusion.

7.1 Proposed Algorithm

The description of the proposed group-based multi-mode tracking algorithm is as follows:

7.1.1 Cluster Formation and CH selection

The first task is to form clusters among a group of nodes based on a pre-defined communication range. For this, all the nodes get their position information using GPS. Then, the position information is shared with the nodes within their communication range. To decide the CH, there are multiple strategies such as deterministic (node ID, node degree), adaptive (energy level etc.) and hybrid metric [129]. Given that the focus of proposed algorithms is to get the range of energy-accuracy benefits which can be achieved under cooperative scenario, therefore, the simplest random timer approach is being used. However, in future one can investigate the effects of various CH selection strategies on the range of energy-accuracy benefits. In random-timer strategy each node runs a random timer and the node with the least value of the timer is selected as the CH. The random timer is exactly a random number generator for each node, plus a communication message to identify the "winner", minimizing the messages to be sent. The ties in the timer value are resolved on the basis of lowest node identifier value. A cluster member may have connectivity to only some of the cluster members but all members have assured connectivity to the CH. Each node can belong to one cluster only and selection among multiple clusters is made on the basis of the distance to the CH.

7.1.2 Cluster Merging and Node Splitting

There can be multiple clusters with varying numbers of nodes in each cluster at any given instant of time. Both the number of clusters and their members change over time. For the situation where two or more CHs come within the communication range, a cluster merging is performed. The cluster merging process follows the rule of "the bigger cluster absorbs the smaller cluster".

A node leaves its current cluster and looks to join a new one if it does not receive three scheduled updates (based on GPS sampling interval) from its current CH. In case there is no nearby CH, the node starts a new cluster formation process.

7.1.3 Position Update Process

The CH is responsible for all the cluster management activities. It is also responsible for providing support in position update activity to the cluster members. Whenever a position update is required, CH checks the number of members in its cluster and their energy levels to choose one of the following modes accounting for the temporary grouping behaviour of the nodes.

Multilateration Mode

The algorithm enters into this mode if the cluster size C_s is more than a predefined threshold C_t and uses A number of nodes as anchor nodes randomly selected by CH. One can perform multilateration as long as A nodes are available. However, it would not be energy-efficient to use for example six anchor nodes ($A = 6$) to get position of one blind node, in case where anchor nodes are also energy and resource constrained as blind nodes. A combination of a large value of C_t and low value of A means higher energy benefit but low position accuracy. The anchor nodes update their position through GPS and share their positions among the cluster members. Then, all the cluster members use an RSSI-based multilateration technique (WLSR or HPL) to estimate their current positions. Here, an assumption is made that change in the cluster-geometry is negligible while taking the GPS and the corresponding RSSI measurements. A cluster member discards a position estimate if the distance between any anchor node and the estimated position is greater than double the communication range. The node then assumes its position to be the same as the nearest

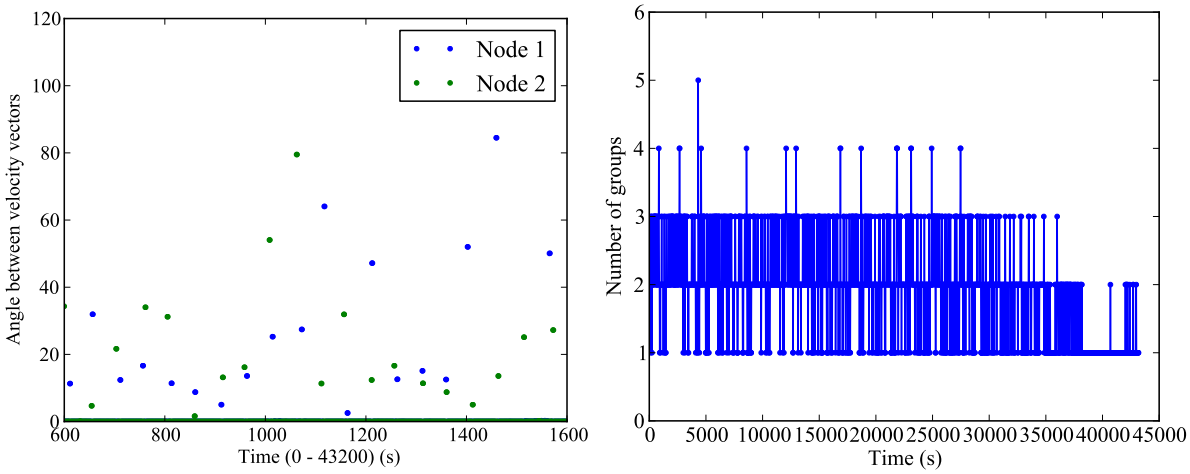

(a) (b)

Figure 7.1: Movement data insights. (a) A time-slice view of the angle between two consecutive velocity vectors of a node. Variation in the angle implies that the track followed by the node is not a straight line. (b) Numbers of the clusters formed for a particular position sampling interval over the entire simulation period. The variation shows the dynamic clustering nature of the simulated data.

anchor node selected based on the RSSI-based distance. This helps the member nodes to filter the bad position estimates given by the RSSI-based multilateration technique.

Cluster-Based Mode

The algorithm enters into this mode, if $1 < C_s \leq C_t$. In this, CH selects the nodes with available minimum energy required for GPS sampling from its member list and randomly selects only one node as the anchor node. Cluster members assume their position is the same as that the anchor node. In the absence of new GPS position updates either from the GPS or from any neighbor, the node uses its last position as the current position estimate.

Standalone Mode

The algorithm enters into this mode if $C_t = 1$ or if a particular node does not receive three consecutive updates from either Cluster-based mode or multilateration mode. In this mode, the node activates its own GPS for current position update and later on searches for an existing cluster. In case of no nearby existing cluster, the node starts the process of forming a new cluster.

Algorithm 4: Multi-mode Tracking (MMT)

```
   /* initialization of variables                                                                    */
1  number_of_nodes; maximum_battery_capacity ; CM_current_battery_level ( initialization with
     maximum_battery_capacity ); minimum_battery (required for tracking activity) ; sampling_interval ;
     total_tracking_period ; radio_range, C_t, A ;
2  Initially all nodes get GPS_lock                    // Use of own GPS to get position update ;
   /* cluster formation and cluster head (CH) selection process                                      */
3  while every node is either becomes a CH or a cluster member (CM) do
4      check clustering_eligible_nodes // (the nodes which are neither a CH nor a CM and CM_current_battery_level
         ≥ minimum_battery) ;
5      if count of clustering_eligible_nodes ≤ 0 then
6          exit ;
7      else
8          All clustering_eligible_nodes exhachage their position with nodes in radio_range ;
9          clustering_eligible_nodes run a random timer and node with lowest timer_value wins the CH race, a tie on
             timer_value is resolved using lowest_node_ID ;
10         a node joins the nearest CH if multiple CH in radio_range and changes own status to CM ;
11     end
12 end
                                                  /* cluster merging */;
13 if distance_between_CH ≤ radio_range (two or more clusters in range) then
14     merge clusters (the bigger cluster absorbs the smaller cluster);
15 end
   /* position updates based on sampling_interval                                                    */
16 while CM_current_battery_level ≥ minimum_battery ∧ trajectory_tracked ≤ total_tracking_period do
17     for every CH do
18         C_s( number of CM with bettery level ≥ minimum battery, also termed as cluster size);
19         if C_s≤ 0 then
20             CM_current_postion to CM_last_position (update all CM icluding CH) ;
21             break the current clsuter;
22             all CM and the CH search for an active CH within radio_range;
23         end
24         if 0 < C_s < C_t then
                                                        // Cluster-Based Mode;
25             random selection of a CM from active_CM list to get GPS lock by the CH ;
26             GPS_lock by the selected CM and GPS position received stored as position_update ;
27             energy_used = GPS_enegy + MCU_energy + radio_energy ;
28             update CM_current_battery_level −= energy_used;
               /* distribution of position_update to all the CM by the CH                            */
29             if distance_to_CH ≤ radio_range then
30                 update CM_current_postion = position_update;
31                 energy_used = MCU_energy + radio_energy ;
32                 update CM_current_battery_level −= energy_used;
33             else
34                 if position_update_not_received ≤ 3    // (number of scheduled updates not received from the
                     CH) then
35                     update CM_current_postion = CM_last_position;
36                     energy_used = MCU_energy + radio_energy ;
37                     update CM_current_battery_level −= energy_used;
38                     position_update_not_received += 1;
39                 else
                                                                  // Standalone mode;
40                     update CM_current_postion = GPS_lock ;
41                     energy_used = GPS_energy + MCU_energy + radio_energy ;
42                     update CM_current_battery_level −= energy_used;
43                     position_update_not_received = 0 ;
44                     leave current CH and search for new CH or initiate a new clustering process;
45                 end
46             end
47         end
48         if C_s ≥ C_t then
                                                      // Multilateration Mode;
49             CH randomly select A number of active nodes (anchor nodes) for GPS_lock;
50             distribution of anchor positions to all blind nodes;
                                            // energy update for all the anchor nodes;
51             energy_used = GPS_energy + MCU_energy + radio_energy ;
52             update CM_current_battery_level −= energy_used;
                                         // energy update for all the blind nodes nodes;
53             energy_used = MCU_energy + radio_energy ;
54             update CM_current_battery_level −= energy_used;
55             if only σ_{p_i} is available then
56                 Blind nodes use WSR solution to calculate their positions;
57             end
58             if both σ_{p_i} and σ_{a_i} is available then
59                 Blind nodes use HPL solution to calculate their positions;
60             end
61         end
62     end
63 end
```

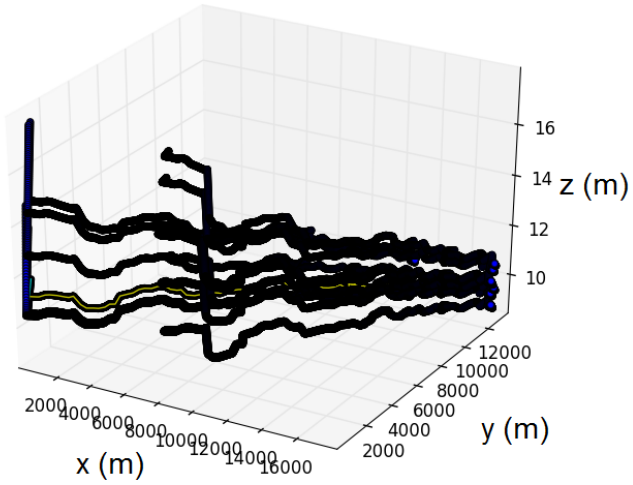

Figure 7.2: Time-slice view of the trajectories of some nodes.

7.2 Experimental Setup

7.2.1 Movement Data Insights

The data generated is quite similar to the data generated in 3.2.1 of chapter 3 with the difference that the positions generated are in 2D only. The dimension reduction from 3D to 2D is to save simulation time for the large number of trials. The Python based simulator is used to generate group movements of 40 mobile nodes (for example, bats) in an area of 50km×50km. This scenario also consists of two living areas and one foraging area. All nodes start their journey from living areas towards the foraging area at a maximum speed of 6m/s while trying to maintain an inter-node distance of around 20m. A total of 43200 positions per node at the time resolution of one second are generated for the experiments. Again Reynolds' flocking model is used to generate the positions during the journey [12] and a random walk movement model is used in the foraging area. During the journey, there are formations of different clusters among the nodes. Both the number of clusters and the number of their respective members vary in time. Some further insight into the data generated through the considered simulation framework are given in Fig. 7.1 and Fig. 7.2.

Table 7.1: Energy consumption summary

Activity	**Energy/activity**
GPS (E_g)	0.436J
Radio (E_r)	34.78 μJ

7.2.2 Energy Model

The energy model used for evaluation is the same as described in section 3.2.2 of chapter 3.

7.2.3 Experiment Details

Four scenarios are simulated which are differentiated based on the amount of error in the GPS-based positions and RSSI measurements. The key simulation parameters for all four scenarios are summarized in Table 7.2. In all four scenarios, 50% of the nodes have a high GPS performance (small values of σ_{a_i} e.g. 1m to 5m) and 50% have a low GPS performance (large values of σ_{a_i} e.g. 6m to 10m). Therefore, at any particular moment, a cluster can have a mixture of devices with low and high GPS performance. The value of σ_{a_i} is kept in the range of 1m to 10m. The clustering performance highly depends on the accuracy of the underlying ranging technique. Hence, the performance of the proposed algorithm is evaluated for values of $\sigma_{p_i} = 1$dBm and $\sigma_{p_i} = 3$dBm. The clustering threshold $C_t = 10$, i.e. clusters on average have 10 members. The number of anchor nodes, N , is set to 6 for all simulations. This value N is based on the results of our preliminary experiments performed in chapter 4 to find the number of anchors required to achieve a reasonable mean localization error with the assumed tracking environment. The value of C_t is based on a trade-off between N and the average cluster size in the simulated data.

7.3 Experiment Results

The mean tracking error and mean energy consumption of all nodes at a given sampling interval are considered as the performance evaluation criteria. To calculate the mean tracking error, first, a linear interpolation is performed between any two consecutive points of the sampled trajectory of a node to match the maximum available resolution of 1s in the original trajectories. Then, the individual tracking error is calculated for each node as the mean of the

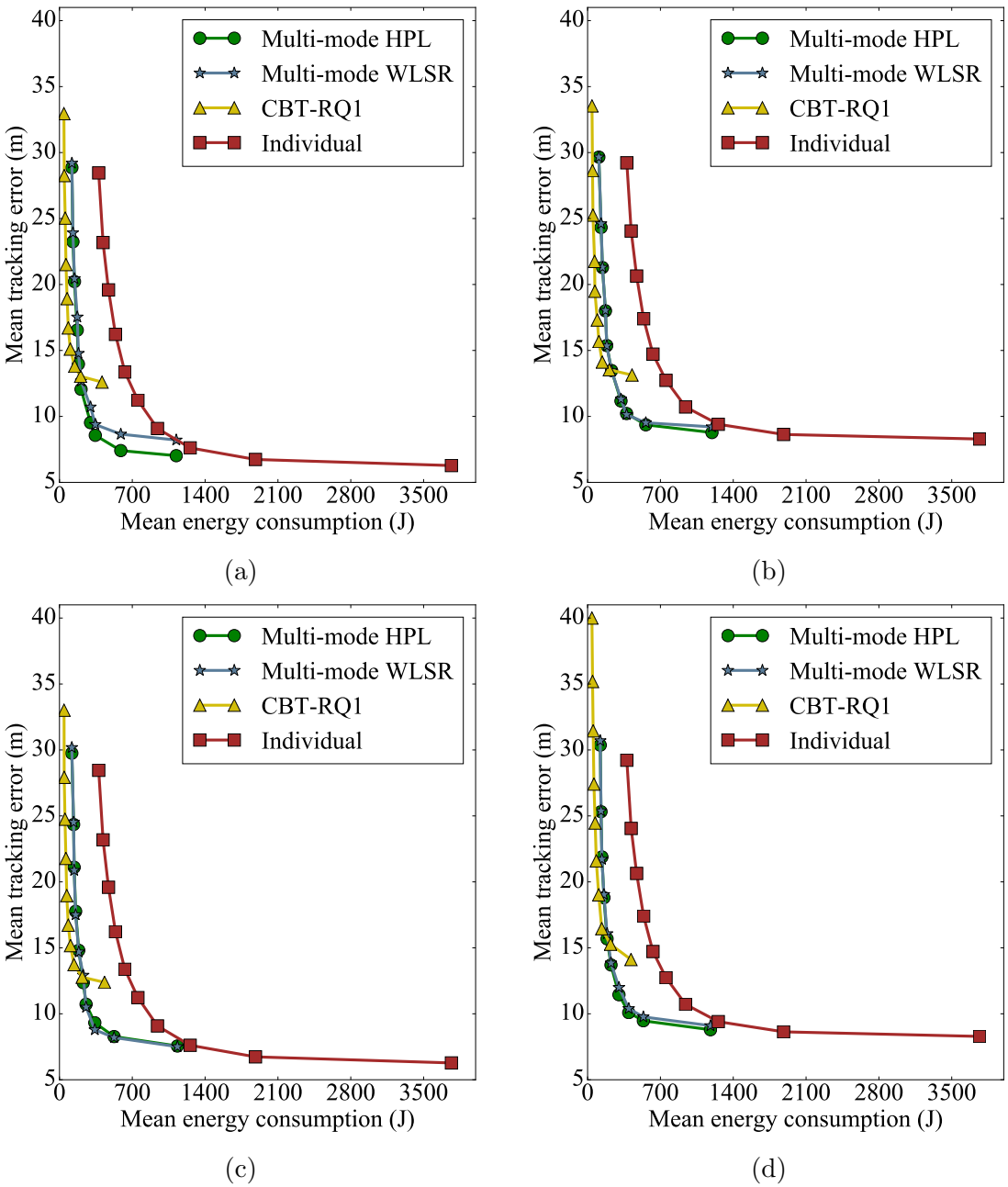

Figure 7.3: Performance of evaluated algorithms in different errors scenarios. The top-left, bottom-right points of curves shows the results for sampling interval of $50s$ and $5s$ respectively, with rest of intervals following the order. (a) $\sigma_{p_i} = 1\text{dB}$ and $\sigma_{a_i} = 1\text{m}, 10\text{m}$; (b) $\sigma_{p_i} = 1\text{dB}$ and $\sigma_{a_i} = 5\text{m}, 10\text{m}$; (c) $\sigma_{p_i} = 3\text{dB}$ and $\sigma_{a_i} = 1\text{m}, 10\text{m}$; (d) $\sigma_{p_i} = 3\text{dB}$ and $\sigma_{a_i} = 5\text{m}, 10\text{m}$.

Note: In all cases sampling Interval goes from 50s top left (high tracking error) to 5s bottom right (low tracking error) in intervals of 5s.

Table 7.2: Simulation parameters

Parameter	**Value**
Clustering threshold (C_t)	10
Number of anchor nodes(N)	6
scenario-1	
σ_{p_i}	1dB
σ_{a_i}	1m or 10m
scenario-2	
σ_{p_i}	1dB
σ_{a_i}	5m or 10m
scenario-3	
σ_{p_i}	3dB
σ_{a_i}	1m or 10m
scenario-4	
σ_{p_i}	3dB
σ_{a_i}	5m or 10m

Euclidean distances between the points of the trajectory obtained after linear interpolation and their corresponding points of the original trajectory. Finally, the mean tracking error is calculated as the mean of all nodes' individual tracking errors. Similarly, the energy consumption of each node is calculated based on its individual activities during tracking through the energy model calculated using (3.7), (3.8) and table 3.1 and summarized in table 7.1 for quick reference. The mean energy consumption is calculated by taking the mean of nodes' individual energy consumption.

The results are presented in Fig. 7.3 for two variants of the proposed algorithm called multi-mode WLSR and multi-mode HPL, which, respectively, use WLSR and HPL solutions for multilateration. The tracking algorithms based on solely multilateration (WLSR or HPL) had large errors due to lack of sufficient number of anchor nodes at some instances of localization; hence, they are not included. "CBT" is the cluster-based tracking used in [27, 87, 127]. In CBT, the blind node assumes its position to be the same as the position estimate of its neighboring node with the latest position information. "Individual" refers to a tracking algorithm based on standalone GPS sampling. The group tracking performance is evaluated over sampling intervals ranging from 5s to 50s. The top-left and bottom-right points of each curve in Fig. 7.3 show the results for a sampling interval of 50s and 5s, respectively. The points in between correspond to the intermediate intervals following the order with equal step size of 5s.

First, let us consider the effects of various combinations of error levels on the performance

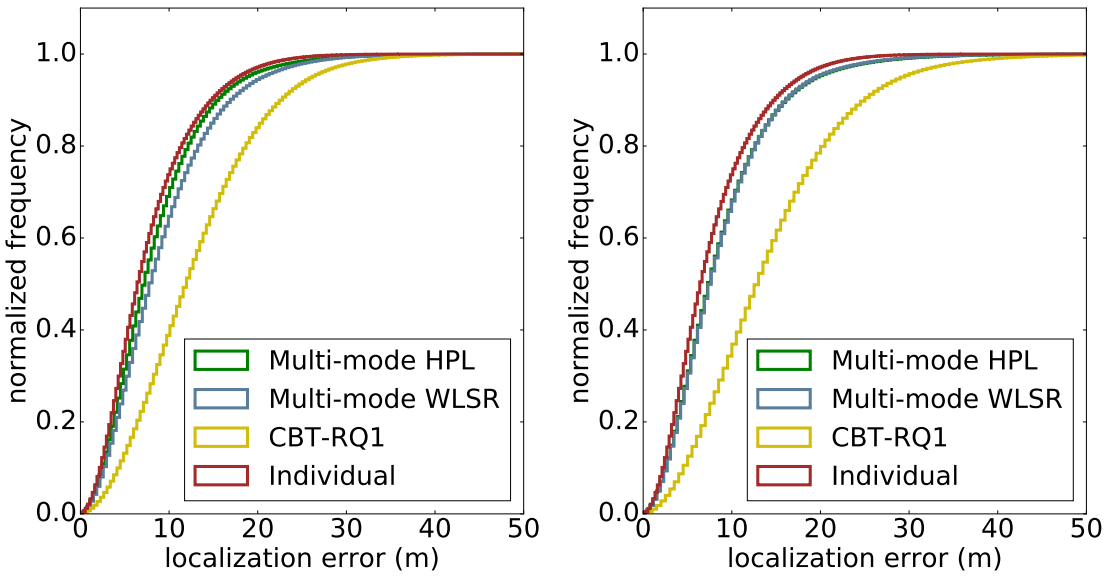

Figure 7.4: Cumulative distribution of mean tracking error of the simulated algorithms with a sampling interval of 5s, $\sigma_{a_i} = 5, 10$m, and (a) $\sigma_{p_i} = 1$dB or (b) $\sigma_{p_i} = 3$dB.

of evaluated group-based tracking algorithms. The individual tracking algorithm has no dependence on the RSSI measurements. Therefore, the performance of individual tracking is the same in Fig. 7.3a and Fig. 7.3c and similarly in Fig. 7.3b and Fig.7.3d. The effect of the increase in the standard deviation of noise in anchor position σ_{a_i} on the performance of individual tracking can be seen as the increase in the error from 6m to 9m for low sampling intervals in Fig. 7.3a and Fig. 7.3b. It appears that linear interpolation errors dominate the localization errors in high-sampling intervals reducing the effect of an increase in the value of σ_{a_i}. All the other algorithms have dependence on the RSSI measurement errors resulting in performance change from one scenario to another. The effect on the performance of various combinations of errors is more noticeable at lower sampling intervals due to the dominance of the linear interpolation errors at the higher sampling intervals.

Both variants of the proposed multi-mode group-based tracking algorithm provide significant energy savings over the individual tracking while performing similarly in terms of mean tracking error. As an example, for the sampling interval of 10s, the proposed algorithm consumes 50% less energy than the individual tracking. In a point-to-point sampling-interval-wise comparison, both variants of the proposed algorithm have lower tracking error than the CBT algorithm but consume more energy with most of the sampling intervals. For low sampling intervals such as 20s, both variants of the proposed algorithm have roughly half the tracking error while consuming similar amount of energy.

The performance of the multi-mode HPL and multi-mode WLSR variants is comparable for higher sampling intervals in all the scenarios. However, multi-mode HPL performs better for low sampling intervals. For example, in Fig. 7.3a, the multi-mode HPL has 20% less tracking error as compared to the multi-mode WLSR with a sampling interval of 10s. In general, taking into account the anchor noise error (by multi-mode HPL) is more beneficial in low sampling intervals.

The cumulative distributions of mean tracking error for two arbitrary scenarios is given in Fig. 7.4. The cumulative distributions of both variants of the proposed algorithm are close to that of the individual-based tracking algorithm and attest to a significantly better performance compared with the CBT algorithm.

In summary, the proposed multi-mode group-based tracking algorithm offers substantial improvements in terms of energy efficiency and tracking accuracy over the individual as well as CBT tracking algorithms. The offered performance benefits are more prominent with high error levels and low sampling intervals.

7.4 Conclusions

This chapter proposes an energy-efficient multi-mode group-based tracking algorithm by combining efficient and accurate multilateration techniques with practical and flexible cluster processing to address the challenges of tracking a dynamic group of mobile agents. The performance of the proposed algorithm is evaluated in comparison with the existing related algorithms using a dataset generated via Reynolds' flocking algorithm and considering various amounts of error in RSSI and anchor position information. The proposed algorithm was shown to preform favorably against the existing cluster-based and individual-based group tracking algorithms. For a given energy budget, the proposed algorithm reduces the mean tracking error by up to 20% in comparison with the existing energy-efficient cooperative algorithms. Moreover, the proposed algorithm is as accurate as the individual-based tracking while using around 50% less energy. The performance improvement afforded by the proposed algorithm was more pronounced when having high error levels and low sampling intervals.

Chapter 8

Conclusions and Future Work

This thesis examined a number of research questions around localization and tracking of mobile nodes constrained in the available energy and computational resources. Specifically, the thesis considers the localization of mobile nodes exhibiting a grouping behaviour.

In general, this thesis first develops the required mathematical framework and then uses extensive simulations to validate the results. The group movement data required for validation is generated using a well-known flocking algorithm due to Reynolds [12]. The energy model used is based on Camazotz, the CSIRO's in-house developed tracking device [9]. The thesis uses the log-normal shadowing path-loss model for radio propagation and model parameters used in the simulations are based on the results reported in [63].

The rest of the chapter first presents, in Sections 8.1 -8.4, the answers to the four research questions posed in chapter 2. Thereafter, Section 8.5 summarizes the key original contributions. Finally, Section 8.6 proposes directions for future work.

8.1 Research Question 1

RQ1: How can GPS sampling load and position readings be shared among a group of mobile nodes to improve individual tracking accuracy given a limited energy budget?

To answer this question, a cluster-based tracking (CBT) algorithm for resource-constrained mobile nodes has been proposed in this thesis. Three variants of CBT, without any KF, with KF, and with KF and inertial sensors were evaluated on the group movement data generated using Reynolds' flocking algorithm.

It is found that significant energy reduction and accuracy improvements can be gained by

distributing the GPS sampling load among a group of nearby mobile nodes. For example, the proposed CBT technique results in 27% energy saving while staying in the error range of individual tracking or 43% less error by consuming the same energy as individual tracking. Hence, the proposed CBT algorithm and its variant CBT-CKF with accelerometer-magnetometer answer this research question.

8.2 Research Question 2

RQ2: What is the theoretical minimum bound on localization performance of a blind node in the presence of normally distributed errors in anchor positions and log-normally distributed errors in RSSI-based distances estimations?

This question is answered by deriving the Cramer-Rao lower bound (CRLB) on the RMSE of self-localization by a blind node, which can be achieved by any unbiased estimator given normally distributed errors in anchor positions and log-normally distributed errors in RSSI-based distance estimations due to the underlying path-loss model.

The evaluation of the CRLB under different topologies and varying noise scenarios revealed its dependence on both node arrangements (topology) and the number of anchor nodes. It is noticed that when there are errors in both anchor positions and distance estimates, a minimum of six anchor nodes are required to obtain a reasonably good estimate of the blind node position.

8.3 Research Question 3

RQ3: How can the theoretical minimum bound on localization be approached or achieved in the assumed scenario of resource-constrained mobile nodes?

To answer this research question, this thesis proposed two different algorithms.

The first algorithm called heuristic non-linear (HNL) solves an appropriately-weighted non-linear least-squares problem. The calculation of the weights is a key component of the proposed algorithm and is done using the statistical properties of the perturbations present in the observations of both anchor positions and RSSI-induced distances. The results of HNL are compared with a previously proposed ML-based algorithm, SPEAR. The experimental evaluations in which only single measurements for both RSSI and anchor positions are provided to both algorithms show that HPL reduces the RMSE up to 30% in comparison to

SPEAR while requiring only 10% to 20% of its computation time.

The second algorithm called heuristic pseudo-linear (HPL) approximates the original system of non-linear equations with a linear set of equations and then solves it using the weighted least-squares method. HPL also estimates various sources of the bias and compensates for them. The performance of HPL is compared with a related existing algorithm called WLSR. HPL improves the performance of WLSR both in terms of RMSE and Bias (up to 30% reduction in RMSE and 50% reduction in bias).

Compared to HNL, HPL is applicable in 3D as well and gives a closed-form solution and only takes 20% of the computation time taken by HNL. However, this time reduction comes at the cost of increased RMSE by up to 20%. Both HNL and HPL algorithms are robust against up to 25% overestimation and underestimation of modeling parameters.

8.4 Research Question 4

RQ4: How can additional information of error characteristics can be used to improve the tracking accuracy of such groups of mobile nodes?

To answer this research question, this thesis proposed a multi-mode tracking algorithm. The proposed algorithm takes the group size and resource availability into consideration and determines the best solution at any particular time. The proposed algorithm has three modes, namely, multilateration, cluster-based, and standalone. The multilateration mode uses the proposed HPL algorithm.

The evaluation is based on the position tracks generated using Reynolds' flocking algorithm. The proposed algorithm achieves the same accuracy as individual-based tracking while using 50% less energy.

8.5 Original Contributions

This thesis makes the following original contributions:

- A CBT algorithm has been developed to distribute the GPS sampling load among the cluster of resource-constrained mobile sensors to increases the tracking period, accuracy or both. With the simulated data, the proposed CBT algorithm demonstrated the feasibility of distributing the GPS-sampling load and reducing the energy consumption and position accuracy compared to individual tracking. Experiments provide insights about

usefulness of KF and inertial-sensors in the long-term tracking of resource-constrained nodes for a range of sampling intervals. The thesis identified that KF, in the assumed long-term tracking scenario, is only useful when provided with high-frequency inertial sensor sampling data.

- The CRLB has been derived for localization using multilateration given log-normal distributed errors in the distance measurements due to the underlying shadowing path-loss model for radio propagation and normally distributed errors in the anchor positions. The CRLB provides the minimum achievable variance for an unbiased estimator given the observations along with the errors' statistical properties. Given the resource-constrained scenario, like the one considered in this thesis, this helps with planning the number of observations to be made to achieve the required localization accuracy leading to better utilization of the available energy resources. For example, in the experiments performed, it is noticed that at least six anchor nodes are required to achieve a reasonable localization accuracy using multilateration when there are errors in both anchor positions and distance measurements and only single observations are available.

- The HNL algorithm, minimizing an approximated non-linear cost function using WLS, to solve a multilateration problem was developed and tested. Simulation results show that HNL provides better localization accuracy in significantly less computation time compared to an existing ML-based algorithm, SPEAR, when only single observations of anchor positions and corresponding distances are available.

- The HPL algorithm, a closed form biased compensated solution for multilateration problem. HPL improves an existing similar closed-form solution with similar computational complexity while accounting for errors in anchor node positions as well.

- A multi-mode tracking algorithm for a group of resource-constrained mobile nodes has been developed and analyzed. The proposed algorithm takes the group size and resource availability into consideration and determines the best solution at any particular time instance. The proposed multi-mode algorithm achieves localization performance similar to individual tracking while consuming only half the energy. The proposed algorithm shows that proper accounting for grouping nature and errors in measurements can improve the localization performance significantly.

8.6 Future Work

There are many possible directions to extend the work done in this thesis.

First, HNL algorithm is limited to 2D only and future work could usefully extend it to 3D. In addition, considering that only limited observations are available, the solutions are expected to have a bias. For the combination of poor geometry and limited observations, the bias can be high and its estimation and compensation could lead to significant improvement in the solutions.

Next, both HNL and HPL algorithms assume that the measured RSSI values are measured relative to the reported anchor positions. In practice, however, for mobile nodes, there is always a time gap and RSSI measurements will not be transmitted at exactly the same time that the reported anchor position was estimated. Compensating for the movements of the nodes (both anchors and blind node) in the proposed localization solutions is definitely an interesting direction for future work. In addition, both HNL and HPL algorithms are evaluated in fixed arrangements of anchor nodes. It will be useful to investigate the effect of anchor position geometries on the performance of these algorithms.

The proposed multi-mode algorithm assumes the knowledge of the radio propagation environment and for the case of mobile nodes that may change considerably. Learning radio propagation such as η and σ_{p_i} parameters online will definitely add value to the current work. In addition, within the scope of a PhD thesis, it has not been possible to explore a broader range of mobility models and parameters. Rather the purpose of this thesis is to show the potential of this technique with one specific mobility model and one set of parameters. Rather than explore many models and parameters here, future users of this technique should repeat these experiments for the particular model parameters expected in their specific scenario.

While a single real-world trial is possible, that sufficiently many trials to evaluate the long-term stability of the project would require more resources and time than were available. Therefore, the results reported in this thesis are based on computer simulations.

Bibliography

[1] P. Sommer, B. Kusy, A. McKeown, and R. Jurdak, "The big night out: Experiences from tracking flying foxes with delay-tolerant wireless networking," in *Real-world wireless sensor networks*. Springer, 2014, pp. 15–27. [Online]. Available: http://dx.doi.org/10.1007/978-3-319-03071-5_2

[2] W. Li, Z. Shi, M. Yu, W. Ren, C. Smith, J. H. Epstein, H. Wang, G. Crameri, Z. Hu, and H. Zhang, "Bats are natural reservoirs of SARS-like Coronaviruses," *Science*, vol. 310, no. 5748, pp. 676–679, 2005. [Online]. Available: http://dx.doi.org/10.1126/science.1118391

[3] E. M. Leroy, B. Kumulungui, X. Pourrut, P. Rouquet, A. Hassanin, P. Yaba, A. Délicat, J. T. Paweska, J.-P. Gonzalez, and R. Swanepoel, "Fruit bats as reservoirs of Ebola virus," *Nature*, vol. 438, no. 7068, pp. 575–576, 2005. [Online]. Available: http://dx.doi.org/10.1038/438575a

[4] C. H. Calisher, J. E. Childs, H. E. Field, K. V. Holmes, and T. Schountz, "Bats: important reservoir hosts of emerging viruses," *Clinical Microbiology Reviews*, vol. 19, no. 3, pp. 531–545, 2006. [Online]. Available: http://dx.doi.org/10.1128/CMR.00017-06

[5] E. M. Leroy, A. Epelboin, V. Mondonge, X. Pourrut, J.-P. Gonzalez, J.-J. Muyembe-Tamfum, and P. Formenty, "Human Ebola outbreak resulting from direct exposure to fruit bats in Luebo, Democratic Republic of Congo, 2007," *Vector-borne and Zoonotic Diseases*, vol. 9, no. 6, pp. 723–728, 2009. [Online]. Available: https://doi.org/10.1089/vbz.2008.0167

[6] D. G. Bausch and L. Schwarz, "Outbreak of Ebola virus disease in Guinea: where

ecology meets economy," *PLoS Neglected Tropical Diseases*, vol. 8, no. 7, p. e3056, 2014. [Online]. Available: http://dx.doi.org/10.1371/journal.pntd.0003056

[7] G. F. McCracken, J. K. Westbrook, V. A. Brown, M. Eldridge, P. Federico, and T. H. Kunz, "Bats track and exploit changes in insect pest populations," *PloS One*, vol. 7, no. 8, p. e43839, 2012. [Online]. Available: http://dx.doi.org/10.1371/journal.pone.0043839

[8] J. J. Maine and J. G. Boyles, "Bats initiate vital agroecological interactions in corn," *in Proceedings of National Academy of Sciences*, vol. 112, no. 40, pp. 12 438–12 443, 2015. [Online]. Available: http://dx.doi.org/10.1073/pnas.1505413112

[9] R. Jurdak, P. Sommer, B. Kusy, N. Kottege, C. Crossman, A. Mckeown, and D. Westcott, "Camazotz: multimodal activity-based GPS sampling," in *Proceedings of 12th International Conference on Information Processing in Sensor Networks*. ACM, 2013, pp. 67–78. [Online]. Available: http://dx.doi.org/10.1145/2461381.2461393

[10] A. Oxley, *Uncertainties in GPS Positioning: A Mathematical Discourse*. Academic Press, 2017. [Online]. Available: https://www.elsevier.com/books/uncertainties-in-gps-positioning/oxley/978-0-12-809594-2

[11] D. Bartlett, *Essentials of Positioning and Location Technology*. New York: Cambridge University Press, April 2013, vol. 9781107006218. [Online]. Available: http://dx.doi.org/10.1017/CBO9780511843860

[12] C. W. Reynolds, "Flocks, herds and schools: A distributed behavioral model," *ACM SIGGRAPH computer graphics*, vol. 21, no. 4, pp. 25–34, 1987. [Online]. Available: http://dx.doi.org/10.1145/37402.37406

[13] J. Hemmes, D. Thain, and C. Poellabauer, "Cooperative localization in GPS-limited urban environments," in *Proceedings of International Conference on Ad-Hoc Networks*. Springer, 2009, pp. 422–437. [Online]. Available: http://dx.doi.org/10.1007/978-3-642-11723-7_28

[14] V. K. Garg, *Wireless Network Evolution: 2G to 3G*, T. S. Rappaport, Ed. Upper Saddle River, New Jersey: Prentice Hall PTR, 2001. [Online]. Available: https://dl.acm.org/citation.cfm?id=559259

[15] M. Angjelichinoski, D. Denkovski, V. Atanasovski, and L. Gavrilovska, "SPEAR: Source position estimation for anchor position uncertainty reduction," *IEEE Communications Letters*, vol. 18, no. 4, pp. 560–563, 2014. [Online]. Available: http://dx.doi.org/10.1109/LCOMM.2014.020414.132780

[16] P. Tarrío, A. M. Bernardos, and J. R. Casar, "Weighted least squares techniques for improved received signal strength based localization," *Sensors*, vol. 11, no. 9, pp. 8569–8592, 2011. [Online]. Available: http://dx.doi.org/10.3390/s110908569

[17] C. Edwards, "Taggin along [Communications Radio-Frequency ID]," *Engineering & Technology*, vol. 9, no. 8, pp. 75–79, 2014. [Online]. Available: http://dx.doi.org/10.1049/et.2014.0811

[18] W. Dennis, "Bees kitted out with RFID backpacks for research project," *Engineering & Technology*, vol. 9, no. 1, pp. 20–21, 2014. [Online]. Available: http://dx.doi.org/10.1049/et.2014.0117

[19] K. Pearson, "The problem of the random walk," *Nature*, vol. 72, no. 1867, p. 342, 1905. [Online]. Available: https://doi.org/10.1038/072342a0

[20] J. Broch, D. A. Maltz, D. B. Johnson, Y.-C. Hu, and J. Jetcheva, "A performance comparison of multi-hop wireless ad hoc network routing protocols," in *Proceedings of the 4th annual ACM/IEEE international conference on Mobile computing and networking*. ACM, 1998, pp. 85–97. [Online]. Available: http://doi.org/10.1145/288235.288256

[21] J. Paek, J. Kim, and R. Govindan, "Energy-efficient rate-adaptive GPS-based positioning for smartphones," in *Proceedings of 8th International Conference on Mobile Systems, Applications, and Services*. ACM, 2010, pp. 299–314. [Online]. Available: http://dx.doi.org/10.1145/1814433.1814463

[22] S. Pace, G. Frost, I. Lachow, D. Frelinger, and D. Fossum, "The global positioning system: Assessing national policies," RAND Corporation, Santa Monica, CA, Tech. Rep., 1995. [Online]. Available: http://www.dtic.mil/dtic/tr/fulltext/u2/a305283.pdf

[23] B. Hofmann-Wellenhof, H. Lichtenegger, and J. Collins, *Global Positioning System:*

Theory and Practice. Wien, Austria: Springer Science & Business Media, 2012. [Online]. Available: http://dx.doi.org/10.1007/978-3-7091-3311-8

[24] M. Matosevic, Z. Salcic, and S. Berber, "A comparison of accuracy using a GPS and a low-cost DGPS," *IEEE Transactions on Instrumentation and Measurement*, vol. 55, no. 5, pp. 1677–1683, 2006. [Online]. Available: http://dx.doi.org/10.1109/TIM.2006.880918

[25] M. Lehtinen, A. Happonen, and J. Ikonen, "Accuracy and time to first fix using consumer-grade GPS receivers," in *Proceedings of 16th International Conference on Software, Telecommunications and Computer Networks*. IEEE, 2008, pp. 334–340. [Online]. Available: http://dx.doi.org/10.1109/SOFTCOM.2008.4669506

[26] R. Jurdak, P. Corke, A. Cotillon, D. Dharman, C. Crossman, and G. Salagnac, "Energy-efficient localization: GPS duty cycling with radio ranging," *ACM Transactions on Sensor Networks (TOSN)*, vol. 9, no. 2, p. 23, 2013. [Online]. Available: http://dx.doi.org/10.1145/2422966.2422980

[27] R. Jurdak, B. Kusy, and A. Cotillon, "Group-based motion detection for energy-efficient localization," *Journal of Sensor and Actuator Networks*, vol. 1, no. 3, pp. 183–216, 2012. [Online]. Available: http://dx.doi.org/10.3390/jsan1030183

[28] R. Cardell-Oliver, K. Smettem, M. Kranz, and K. Mayer, "Field testing a wireless sensor network for reactive environmental monitoring [soil moisture measurement]," in *Proceedings of Intelligent Sensors, Sensor Networks and Information Processing Conference*. IEEE, 2004, pp. 7–12. [Online]. Available: http://dx.doi.org/10.1109/ISSNIP.2004.1417429

[29] J. K. Hart and K. Martinez, "Environmental Sensor Networks: A revolution in the earth system science?" *Earth-Science Reviews*, vol. 78, no. 3, pp. 177–191, 2006. [Online]. Available: https://doi.org/10.1016/j.earscirev.2006.05.001

[30] R. Szewczyk, E. Osterweil, J. Polastre, M. Hamilton, A. Mainwaring, and D. Estrin, "Habitat monitoring with sensor networks," *Communications of the ACM*, vol. 47, no. 6, pp. 34–40, 2004. [Online]. Available: http://dx.doi.org/10.1145/990680.990704

[31] L. Blazevic, J.-Y. Le Boudec, and S. Giordano, "A location-based routing method for mobile ad hoc networks," *IEEE Transactions on Mobile Computing*, vol. 4, no. 2, pp. 97–110, 2005. [Online]. Available: http://dx.doi.org/10.1109/TMC.2005.16

[32] A. Swami, Q. Zhao, Y.-W. Hong, and L. Tong, *Wireless Sensor Networks: Signal Processing and Communications*. Chichester, UK: John Wiley & Sons, 2007. [Online]. Available: http://dx.doi.org/10.1002/9780470061794

[33] D. Puccinelli and M. Haenggi, "Wireless Sensor Networks: Applications and Challenges of Ubiquitous Sensing," *IEEE Circuits and Systems Magazine*, vol. 5, no. 3, pp. 19–31, 2005. [Online]. Available: http://dx.doi.org/10.1109/MCAS.2005.1507522

[34] J. S. Esteves, A. Carvalho, and C. Couto, "Generalized geometric triangulation algorithm for mobile robot absolute self-localization," in *Proceedings of International Symposium on Industrial Electronics*, vol. 1. IEEE, 2003, pp. 346–351. [Online]. Available: http://dx.doi.org/10.1109/ISIE.2003.1267272

[35] C. D. Mcgillem and T. S. Rappaport, "A beacon navigation method for autonomous vehicles," *IEEE Transactions on Vehicular Technology*, vol. 38, no. 3, pp. 132–139, 1989. [Online]. Available: http://dx.doi.org/10.1109/25.45466

[36] M. Betke and L. Gurvits, "Mobile robot localization using landmarks," *IEEE Transactions on Robotics and Automation*, vol. 13, no. 2, pp. 251–263, 1997. [Online]. Available: http://dx.doi.org/10.1109/70.563647

[37] D. E. Manolakis, "Efficient solution and performance analysis of 3-D position estimation by trilateration," *IEEE Transactions on Aerospace and Electronic Systems*, vol. 32, no. 4, pp. 1239–1248, 1996. [Online]. Available: http://dx.doi.org/10.1109/7.543845

[38] K. E. Bekris, A. A. Argyros, and L. E. Kavraki, "Angle-based methods for mobile robot navigation: Reaching the entire plane," in *Proceedings of International Conference on Robotics and Automation*, vol. 3. IEEE, 2004, pp. 2373–2378. [Online]. Available: http://dx.doi.org/10.1109/ROBOT.2004.1307416

[39] D. Niculescu and B. Nath, "Ad hoc positioning system (APS) using AOA," in *Proceedings of 22nd Annual Joint Conference of the IEEE Computer and*

Communications Societies, vol. 3. IEEE, 2003, pp. 1734–1743. [Online]. Available: http://dx.doi.org/10.1109/INFCOM.2003.1209196

[40] N. Patwari, J. N. Ash, S. Kyperountas, A. O. Hero, R. L. Moses, and N. S. Correal, "Locating the nodes: cooperative localization in wireless sensor networks," *IEEE Signal Processing Magazine*, vol. 22, no. 4, pp. 54–69, 2005. [Online]. Available: http://dx.doi.org/10.1109/MSP.2005.1458287

[41] A. Ahmed, R. Arablouei, F. de Hoog, B. Kusy, R. Jurdak, and N. Bergmann, "Estimating angle-of-arrival and time-of-flight for multipath components using wifi channel state information," *Sensors*, vol. 18, no. 6, p. 1753, 2018. [Online]. Available: https://doi.org/10.3390/s18061753

[42] B. D. Van Veen and K. M. Buckley, "Beamforming: A versatile approach to spatial filtering," *IEEE ASSP Magazine*, vol. 5, no. 2, pp. 4–24, 1988. [Online]. Available: http://dx.doi.org/10.1109/53.665

[43] B. Ottersten, M. Viberg, P. Stoica, and A. Nehorai, "Exact and large sample ML techniques for parameter estimation and detection in array processing," in *Radar Array Processing*, S. Haykin, J. Litva, and T. Shepherd, Eds. New York: Springer-Verlag, 1993, p. 99–151. [Online]. Available: https://doi.org/10.1007/978-3-642-77347-1_4

[44] W. Li, W. Yao, and P. J. Duffett-Smith, "Comparative study of joint TOA/DOA estimation techniques for mobile positioning applications," in *Proceedings of IEEE Consumer Communications and Networking Conference*. IEEE, 2009, pp. 1–5. [Online]. Available: http://dx.doi.org/10.1109/CCNC.2009.4784819

[45] A. H. Sayed, A. Tarighat, and N. Khajehnouri, "Network-based wireless location: challenges faced in developing techniques for accurate wireless location information," *IEEE Signal Processing Magazine*, vol. 22, no. 4, pp. 24–40, 2005. [Online]. Available: http://dx.doi.org/10.1109/MSP.2005.1458275

[46] N. B. Priyantha, H. Balakrishnan, E. D. Demaine, and S. Teller, "Mobile-assisted localization in wireless sensor networks," in *Proceedings of 24th Annual Joint Conference of the IEEE Computer and Communications Societies.*, vol. 1. IEEE, 2005, pp. 172–183. [Online]. Available: http://dx.doi.org/10.1109/INFCOM.2005.1497889

[47] J. J. Caffery, "A new approach to the geometry of TOA location," in *Proceedings of 52nd Vehicular Technology Conference*, vol. 4. IEEE, 2000, pp. 1943–1949. [Online]. Available: http://dx.doi.org/10.1109/VETECF.2000.886153

[48] X. Wang, Z. Wang, and B. O'Dea, "A TOA-based location algorithm reducing the errors due to non-line-of-sight (NLOS) propagation," *IEEE Transactions on Vehicular Technology*, vol. 52, no. 1, pp. 112–116, 2003. [Online]. Available: http://dx.doi.org/10.1109/TVT.2002.807158

[49] A. R. J. Ruiz and F. S. Granja, "Comparing ubisense, bespoon, and decawave uwb location systems: Indoor performance analysis," *IEEE Transactions on instrumentation and Measurement*, vol. 66, no. 8, pp. 2106–2117, 2017. [Online]. Available: http://dx.doi.org/10.1109/TIM.2017.2681398

[50] B. Kusy, J. Sallai, G. Balogh, A. Ledeczi, V. Protopopescu, J. Tolliver, F. DeNap, and M. Parang, "Radio interferometric tracking of mobile wireless nodes," in *Proceedings of 5th International Conference on Mobile Systems, Applications and Services*. ACM, 2007, pp. 139–151. [Online]. Available: http://dx.doi.org/10.1145/1247660.1247678

[51] S. M. Williams, K. D. Frampton, I. Amundson, and P. L. Schmidt, "Decentralized acoustic source localization in a distributed sensor network," *Applied Acoustics*, vol. 67, no. 10, pp. 996–1008, 2006. [Online]. Available: http://dx.doi.org/10.1016/j.apacoust.2005.12.008

[52] M. Kotaru, P. Zhang, and S. Katti, "Localizing low-power backscatter tags using commodity wifi," in *Proceedings of the 13th International Conference on emerging Networking EXperiments and Technologies*. ACM, 2017, pp. 251–262. [Online]. Available: http://dx.doi.org/10.1145/3143361.3143379

[53] P. Pannuto, B. Kempke, and P. Dutta, "Slocalization: sub-μw ultra wideband backscatter localization," in *Proceedings of the 17th ACM/IEEE International Conference on Information Processing in Sensor Networks*. IEEE Press, 2018, pp. 242–253. [Online]. Available: http://dx.doi.org/10.1109/IPSN.2018.00052

[54] G. Mao, B. Fidan, and B. D. Anderson, "Wireless sensor network localization techniques," *Computer Networks*, vol. 51, no. 10, pp. 2529–2553, 2007. [Online]. Available: http://dx.doi.org/10.1016/j.comnet.2006.11.018

[55] S. Y. Seidel and T. S. Rappaport, "914mhz path loss prediction models for indoor wireless communications in multifloored buildings," *IEEE Transactions on Antennas and Propagation*, vol. 40, no. 2, pp. 207–217, 1992. [Online]. Available: http://dx.doi.org/10.1109/8.127405

[56] R. Peng and M. L. Sichitiu, "Robust, probabilistic, constraint-based localization for wireless sensor networks," in *Proceedings of IEEE Communications Society Conference on Sensor and Ad Hoc Communications and Networks,.* IEEE, 2005, pp. 541–550. [Online]. Available: http://dx.doi.org/10.1109/SAHCN.2005.1557106

[57] T. S. Rappaport, *Wireless communications: principles and practice.* Prentice Hall PTR New Jersey, 1996, vol. 2.

[58] J. Miranda, R. Abrishambaf, T. Gomes, P. Gonçalves, J. Cabral, A. Tavares, and J. Monteiro, "Path loss exponent analysis in wireless sensor networks: Experimental evaluation," in *11th IEEE International Conference on Industrial Informatics (INDIN).* IEEE, 2013, pp. 54–58. [Online]. Available: http://dx.doi.org/10.1109/INDIN.2013.6622857

[59] A. Zanella, "Best practice in rss measurements and ranging," *IEEE Communications Surveys & Tutorials*, vol. 18, no. 4, pp. 2662–2686, 2016. [Online]. Available: http://dx.doi.org/10.1109/INDIN.2013.6622857

[60] A. Payal, C. Rai, and B. Reddy, "Experimental analysis of some radio propagation models for smart wireless sensor networks applications," in *SAI Intelligent Systems Conference (IntelliSys), 2015.* IEEE, 2015, pp. 338–342. [Online]. Available: http://dx.doi.org/10.1109/IntelliSys.2015.7361164

[61] N. Patwari, A. O. Hero, M. Perkins, N. S. Correal, and R. J. O'dea, "Relative location estimation in wireless sensor networks," *IEEE Transactions on Signal Processing*, vol. 51, no. 8, pp. 2137–2148, 2003. [Online]. Available: http://dx.doi.org/10.1109/TSP.2003.814469

[62] I. Ahmad, N. W. Bergmann, R. Jurdak, and B. Kusy, "Towards probabilistic localization using airborne mobile anchors," in *IEEE International Conference on Pervasive Computing and Communication*, 2016, pp. 1–4. [Online]. Available: http://dx.doi.org/10.1109/PERCOMW.2016.7457052

[63] I. Ahmad, N. Bergmann, R. Jurdak, and B. Kusy, "Experiments on localization of wireless sensors using airborne mobile anchors," in *Proceedings of IEEE Conference on Wireless Sensors (ICWiSe)*. IEEE, 2015, pp. 1–6. [Online]. Available: http://dx.doi.org/10.1109/ICWISE.2015.7380344

[64] B. Dawes and K.-W. Chin, "A comparison of deterministic and probabilistic methods for indoor localization," *Journal of Systems and Software*, vol. 84, no. 3, pp. 442–451, 2011. [Online]. Available: https://doi.org/10.1016/j.jss.2010.11.888

[65] A. Leonhardi and K. Rothermel, "A comparison of protocols for updating location information," *Cluster Computing*, vol. 4, no. 4, pp. 355–367, 2001. [Online]. Available: https://doi.org/10.1023/A:1011872831932

[66] A. Leonhardi, C. Nicu, and K. Rothermel, "A map-based dead reckoning protocol for updating location information," 2001. [Online]. Available: http://dx.doi.org/10.1109/IPDPS.2002.1016595

[67] S. Tilak, V. Kolar, N. B. Abu-Ghazaleh, and K.-D. Kang, "Dynamic localization control for mobile sensor networks," in *Proceedings of IEEE International Performance, Computing, and Communications Conference*. IEEE, 2005, pp. 587–592. [Online]. Available: http://dx.doi.org/10.1109/PCCC.2005.1460642

[68] M. B. Kjærgaard, J. Langdal, T. Godsk, and T. Toftkjær, "Entracked: energy-efficient robust position tracking for mobile devices," in *Proceedings of 7th International Conference on Mobile Systems, Applications, and Services*. ACM, 2009, pp. 221–234. [Online]. Available: https://dl.acm.org/citation.cfm?id=1555816.1555839

[69] M. B. Kjærgaard, S. Bhattacharya, H. Blunck, and P. Nurmi, "Energy-efficient trajectory tracking for mobile devices," in *Proceedings of International Conference on Mobile Systems, Applications, and Services*. ACM, 2011, pp. 307–320. [Online]. Available: http://dx.doi.org/10.1145/1999995.2000025

[70] S. Bhattacharya, H. Blunck, M. B. Kjærgaard, and P. Nurmi, "Robust and energy-efficient trajectory tracking for mobile devices," *IEEE Transactions on Mobile Computing*, vol. 14, no. 2, pp. 430–443, 2015. [Online]. Available: http://dx.doi.org/10.1109/TMC.2014.2318712

[71] I. Constandache, S. Gaonkar, M. Sayler, R. R. Choudhury, and L. Cox, "Enloc: Energy-efficient localization for mobile phones," in *Proceedings of 28th Conference on Computer Communications*. IEEE, 2009, pp. 2716–2720. [Online]. Available: http://dx.doi.org/10.1109/INFCOM.2009.5062218

[72] J. Paek, J. Kim, and R. Govindan, "Energy-efficient rate-adaptive GPS-based positioning for smartphones," in *Proceedings of 8th International Conference on Mobile Systems, Applications, and Services*. ACM, 2010, pp. 299–314. [Online]. Available: http://dx.doi.org/10.1145/1814433.1814463

[73] H. Galeana-Zapién, C. Torres-Huitzil, and J. Rubio-Loyola, "Mobile phone middleware architecture for energy and context awareness in location-based services," *Sensors*, vol. 14, no. 12, pp. 23 673–23 696, 2014. [Online]. Available: http://dx.doi.org/10.3390/s141223673

[74] G. M. Djuknic and R. E. Richton, "Geolocation and Assisted GPS," *Communications, Bell Laboratories, Lucent Technologies*, 2001. [Online]. Available: http://dx.doi.org/10.1109/2.901174

[75] H. S. Ramos, T. Zhang, J. Liu, N. B. Priyantha, and A. Kansal, "LEAP: a low energy assisted gps for trajectory-based services," in *Proceedings of 13th international conference on Ubiquitous computing*. ACM, 2011, pp. 335–344. [Online]. Available: http://doi.acm.org/10.1145/2030112.2030158

[76] J. Liu, B. Priyantha, T. Hart, H. S. Ramos, A. a. F. Loureiro, and Q. Wang, "Energy efficient GPS sensing with cloud offloading," *in Proceedings of 10th ACM Conference on Embedded Network Sensor Systems - SenSys '12*, p. 85, 2012. [Online]. Available: http://dl.acm.org/citation.cfm?doid=2426656.2426666

[77] Y.-Y. Chang, C.-Y. Lin, and L.-J. Chen, "A two-layer approach for energy efficiency in mobile location sensing applications," in *Proceedings of International Conference on Research in Networking*. Springer, 2012, pp. 304–315. [Online]. Available: https://doi.org/10.1007/978-3-642-30054-7_24

[78] R. Jirawimut, M. Shah, P. Ptasinski, F. Cecelja, and W. Balachandran, "Integrated DGPS and dead reckoning for a pedestrian navigation system in signal blocked

environments," in *Proceedings of 13th International Technical Meeting of the Satellite Division of The Institute of Navigation, Salt Lake City, UT, USA*, 2000, pp. 19–22. [Online]. Available: http://ave.dee.isep.ipp.pt/~lbf/PINSFUSION/JiAlPtCeBa00.pdf

[79] C. Kee, B. W. Parkinson, and P. Axelrad, "Wide Area Differential GPS," *Navigation*, vol. 38, no. 2, pp. 123–145, 1991. [Online]. Available: http://dx.doi.org/10.1002/j.2161-4296.1991.tb01720.x

[80] Q. Ladetto, V. Gabaglio, and B. Merminod, "Combining gyroscopes, magnetic compass and GPS for pedestrian navigation," in *Proceedings of International Symposium on Kinematic Systems in Geodesy, Geomatics, and Navigation*, 2001, pp. 205–213. [Online]. Available: https://infoscience.epfl.ch/record/29183

[81] S. Y. Cho and C. G. Park, "MEMS based pedestrian navigation system," *The Journal of Navigation*, vol. 59, no. 1, pp. 135–153, 2006. [Online]. Available: http://dx.doi.org/10.1017/S0373463305003486

[82] Y. Lee, J. Lee, S. Dongsoo, and H. Choo, "Energy-efficient adaptive localization middleware based on GPS and embedded sensors for smart mobiles," in *Proceedings of IEEE Fourth International Conference on Consumer Electronics*. IEEE, 2014, pp. 126–130. [Online]. Available: http://dx.doi.org/10.1109/ICCE-Berlin.2014.7034221

[83] K. Nawarathne, F. Zhao, F. C. Pereira, and J. Luo, "Dead reckoning on smartphones to reduce GPS usage," in *Proceedings of 13th International Conference on Control Automation Robotics & Vision (ICARCV)*. IEEE, 2014, pp. 529–534. [Online]. Available: http://dx.doi.org/10.1109/ICARCV.2014.7064360

[84] H.-J. Chu, G.-J. Tsai, K.-W. Chiang, and T.-T. Duong, "GPS/MEMS INS data fusion and map matching in urban areas," *Sensors*, vol. 13, no. 9, pp. 11 280–11 288, 2013. [Online]. Available: http://dx.doi.org/10.3390/s130911280

[85] H. Leppäkoski, J. Collin, and J. Takala, "Pedestrian navigation based on inertial sensors, indoor map, and WLAN signals," *Journal of Signal Processing Systems*, vol. 71, no. 3, pp. 287–296, 2013. [Online]. Available: http://dx.doi.org/10.1007/s11265-012-0711-5

[86] Z. Chen, H. Zou, H. Jiang, Q. Zhu, Y. C. Soh, and L. Xie, "Fusion of WiFi, smartphone sensors and landmarks using the Kalman filter for indoor localization," *Sensors*, vol. 15, no. 1, pp. 715–732, 2015. [Online]. Available: http://dx.doi.org/10.3390/s150100715

[87] V. Vukadinovic and S. Mangold, "Performance of collaborative GPS localization in pedestrian ad hoc networks," in *Proceedings of third ACM International Workshop on Mobile Opportunistic Networks*. ACM, 2012, pp. 45–52. [Online]. Available: http://dx.doi.org/10.1145/2159576.2159587

[88] Y. Lee, Y. Ju, C. Min, S. Kang, I. Hwang, and J. Song, "Comon: Cooperative ambience monitoring platform with continuity and benefit awareness," in *Proceedings of 10th International Conference on Mobile Systems, Applications, and Services*. ACM, 2012, pp. 43–56. [Online]. Available: http://dx.doi.org/10.1145/2307636.2307641

[89] R. Jurdak, P. Corke, D. Dharman, and G. Salagnac, "Adaptive GPS duty cycling and radio ranging for energy-efficient localization," in *Proceedings of 8th ACM Conference on Embedded Networked Sensor Systems*. ACM, 2010, pp. 57–70. [Online]. Available: http://dx.doi.org/10.1145/1869983.1869990

[90] P. H. Mohammadabadi and S. Valaee, "Cooperative node positioning in vehicular networks using inter-node distance measurements," in *Proceedings of 25th Annual International Symposium on Personal, Indoor, and Mobile Radio Communication (PIMRC)*. IEEE, 2014, pp. 1448–1452. [Online]. Available: http://dx.doi.org/10.1109/PIMRC.2014.7136396

[91] T. Higuchi, H. Yamaguchi, and T. Higashino, "Context-supported local crowd mapping via collaborative sensing with mobile phones," *Pervasive and Mobile Computing*, vol. 13, pp. 26–51, 2014. [Online]. Available: http://dx.doi.org/10.1016/j.pmcj.2013.10.012

[92] D. Taniuchi, X. Liu, D. Nakai, and T. Maekawa, "Spring model based collaborative indoor position estimation with neighbor mobile devices," *IEEE Journal of Selected Topics in Signal Processing*, vol. 9, no. 2, pp. 268–277, 2015. [Online]. Available: http://dx.doi.org/10.1109/JSTSP.2014.2382478

[93] L. Doherty, K. Pister, and L. El Ghaoui, "Convex position estimation in wireless sensor networks," *in Proceedings of Twentieth Annual Joint Conference of*

the IEEE Computer and Communications Society (Cat. No.01CH37213), vol. 3, pp. 1655–1663, 2001. [Online]. Available: http://ieeexplore.ieee.org/lpdocs/epic03/wrapper.htm?arnumber=916662

[94] A. Savvides, C.-C. Han, and M. B. Strivastava, "Dynamic fine-grained localization in ad-hoc networks of sensors," in *Proceedings of 7th Annual International Conference on Mobile Computing and Networking*. ACM, 2001, pp. 166–179. [Online]. Available: http://dx.doi.org/10.1145/381677.381693

[95] Y. Shang, W. Ruml, Y. Zhang, and M. Fromherz, "Localization from connectivity in sensor networks," *IEEE Transactions on Parallel and Distributed Systems*, vol. 15, no. 11, pp. 961–974, 2004. [Online]. Available: http://dx.doi.org/10.1109/TPDS.2004.67

[96] C. S. J. Rabaey and K. Langendoen, "Robust positioning algorithms for distributed ad-hoc wireless sensor networks," in *the Proceedings of 2002 USENIX Annual Technical Conference, June 10-15*, 2002, pp. 317–327. [Online]. Available: http://static.usenix.org/event/usenix02/full_papers/savarese/savarese_html/

[97] P. Biswas and Y. Ye, "Semidenite Programming for Ad Hoc Wireless Sensor Network Localization," *Proceedings of Third International Symposium on Information Processing in Sensor Networks*, pp. 46–54, 2004. [Online]. Available: http://dx.doi.org/10.1145/984622.984630

[98] K. Whitehouse, C. Karlof, and D. Culler, "A practical evaluation of radio signal strength for ranging-based localization," *ACM SIGMOBILE Mobile Computing and Communications Review*, vol. 11, no. 1, pp. 41–52, 2007. [Online]. Available: http://dx.doi.org/10.1145/1234822.1234829

[99] N. Patwari and A. O. Hero III, "Using proximity and quantized RSS for sensor localization in wireless networks," in *Proceedings of 2nd ACM International Conference on Wireless Sensor Networks and Applications*. ACM, 2003, pp. 20–29. [Online]. Available: http://dx.doi.org/10.1145/941350.941354

[100] P. Kumar, L. Reddy, and S. Varma, "Distance measurement and error estimation scheme for rssi based localization in wireless sensor networks,"

in *Proceedings of Fifth International Conference on Wireless Communication and Sensor Networks (WCSN)*. IEEE, 2009, pp. 1–4. [Online]. Available: http://dx.doi.org/10.1109/WCSN.2009.5434802

[101] J. A. Costa, N. Patwari, and A. O. Hero III, "Distributed weighted-multidimensional scaling for node localization in sensor networks," *ACM Transactions on Sensor Networks (TOSN)*, vol. 2, no. 1, pp. 39–64, 2006. [Online]. Available: http://dx.doi.org/10.1145/1138127.1138129

[102] J. Zheng and Y.-C. Wu, "Robust joint localization and time synchronization in wireless sensor networks with bounded anchor uncertainties," in *Proceedings of International Conference on Acoustics, Speech and Signal Processing*. IEEE, 2009, pp. 2793–2796. [Online]. Available: http://dx.doi.org/10.1109/ICASSP.2009.4960203

[103] S. Srirangarajan, A. H. Tewfik, and Z.-Q. Luo, "Distributed sensor network localization with inaccurate anchor positions and noisy distance information," in *Proceedings of IEEE International Conference on Acoustics, Speech and Signal Processing*, vol. 3. IEEE, 2007, pp. III–521. [Online]. Available: https://doi.org/10.1007/978-3-642-30054-7_24

[104] S. Srirangaraja, A. H. Tewfik, and Z.-Q. Luo, "Distributed sensor network localization using SOCP relaxation," *IEEE Transactions on Wireless Communications*, vol. 7, no. 12, pp. 4886–4895, 2008. [Online]. Available: http://dx.doi.org/10.1109/T-WC.2008.070241

[105] K. W. K. Lui, W.-K. Ma, H.-C. So, and F. K. W. Chan, "Semi-definite programming algorithms for sensor network node localization with uncertainties in anchor positions and/or propagation speed," *IEEE Transactions on Signal Processing*, vol. 57, no. 2, pp. 752–763, 2009. [Online]. Available: http://dx.doi.org/10.1109/TSP.2008.2007916

[106] G. Naddafzadeh-Shirazi, M. B. Shenouda, and L. Lampe, "Second order cone programming for sensor network localization with anchor position uncertainty," *IEEE Transactions on Wireless Communications*, vol. 13, no. 2, pp. 749–763, 2014. [Online]. Available: http://dx.doi.org/10.1109/TWC.2013.120613.130170

[107] P. Tarrío, A. M. Bernardos, J. a. Besada, and J. R. Casar, "A new positioning technique for RSS-based localization based on a weighted least squares estimator," *in Proceedings*

of IEEE International Symposium on Wireless Communication Systems, pp. 633–637, 2008. [Online]. Available: http://dx.doi.org/10.1109/ISWCS.2008.4726133

[108] Y. T. Chan and K. Ho, "A simple and efficient estimator for hyperbolic location," *IEEE Transactions on Signal Processing*, vol. 42, no. 8, pp. 1905–1915, 1994. [Online]. Available: http://dx.doi.org/10.1109/78.301830

[109] K. Ho, "Bias reduction for an explicit solution of source localization using TDOA," *IEEE Transactions on Signal Processing*, vol. 60, no. 5, pp. 2101–2114, 2012. [Online]. Available: http://dx.doi.org/10.1109/TSP.2012.2187283

[110] K. Ho, L.-o. Kovavisaruch, and H. Parikh, "Source localization using TDOA with erroneous receiver positions," *in Proceedings of IEEE International Symposium on Circuits and Systems*, vol. 3, no. 3, pp. 0–3, 2004. [Online]. Available: http://dx.doi.org/10.1109/ISCAS.2004.1328781

[111] S. Zhu and Z. Ding, "A simple approach of range-based positioning with low computational complexity," *IEEE Transactions on Wireless Communications*, vol. 8, no. 12, pp. 5832–5836, 2009. [Online]. Available: http://dx.doi.org/10.1109/TWC.2009.12.090905

[112] Y. Shi, Q. Cui, and X. Zhang, "Distributed Cooperative Localization with EW-TLS Model in Wireless Networks," in *Proceedings of 79th Vehicular Technology Conference (VTC Spring)*. IEEE, 2014, pp. 1–5. [Online]. Available: http://dx.doi.org/10.1109/VTCSpring.2014.7022883

[113] I. Markovsky, M. L. Rastello, A. Premoli, A. Kukush, and S. Van Huffel, "The element-wise weighted total least-squares problem," *Computational Statistics & Data Analysis*, vol. 50, no. 1, pp. 181–209, 2006. [Online]. Available: http://dx.doi.org/10.1016/j.csda.2004.07.014

[114] A. Premoli and M. L. Rastello, "The parametric quadratic form method for solving tls problems with elementwise weighting," in *Total Least Squares and Errors-in-Variables Modeling*. Springer, 2002, pp. 67–76. [Online]. Available: http://dx.doi.org/10.1007/978-94-017-3552-0_7

[115] S. Li and K. Ho, "Accurate and Effective Localization of an Object in Large Equal Radius Scenario," *IEEE Transactions on Wireless Communications*, vol. 15, no. 12, pp. 8273–8285, 2016. [Online]. Available: http://dx.doi.org/10.1109/TWC.2016.2613534

[116] Y. Weng, W. Xiao, and L. Xie, "Total least squares method for robust source localization in sensor networks using TDOA measurements," *International Journal of Distributed Sensor Networks*, 2011. [Online]. Available: http://dx.doi.org/10.1155/2011/172902

[117] J. Wan, N. Yu, R. Feng, Y. Wu, and C. Su, "Localization refinement for wireless sensor networks," *Computer Communications*, vol. 32, no. 13, pp. 1515–1524, 2009. [Online]. Available: http://dx.doi.org/10.1016/j.comcom.2009.05.011

[118] Y. Zhou, J. Li, and L. Lamont, "Multilateration localization in the presence of anchor location uncertainties," in *Proceedings of Global Communications Conference (GLOBECOM)*. IEEE, 2012, pp. 309–314. [Online]. Available: http://dx.doi.org/10.1109/GLOCOM.2012.6503131

[119] A. Noroozi and M. A. Sebt, "Weighted least squares target location estimation in multi-transmitter multi-receiver passive radar using bistatic range measurements," *IET Radar, Sonar & Navigation*, 2016. [Online]. Available: http://dx.doi.org/10.1049/iet-rsn.2015.0446

[120] A. Noroozi and A. Mohammad, "Target Localization in Multistatic Passive Radar Using SVD Approach," *IEEE Transactions on Aerospace and Electronic Systems*, 2017. [Online]. Available: http://dx.doi.org/10.1109/TAES.2017.2669558

[121] I. Markovsky and S. Van Huffel, "Overview of total least-squares methods," *Signal processing*, vol. 87, no. 10, pp. 2283–2302, 2007. [Online]. Available: http://dx.doi.org/10.1016/j.sigpro.2007.04.004

[122] T. Abatzoglou and J. Mendel, "Constrained total least squares," in *Proceedings of IEEE International Conference on Acoustics, Speech, and Signal Processing*, vol. 12. IEEE, 1987, pp. 1485–1488. [Online]. Available: http://dx.doi.org/10.1109/ICASSP.1987.1169438

[123] M. Petovello, "How does a GNSS receiver estimate velocity?" *Inside GNSS*, pp. 38–41, 2015.

[124] S. B. L. Rice, "Mathematical Analysis of Random Noise Part III: statistical properties of random noise currents," pp. 46–156, 1945. [Online]. Available: http://dx.doi.org/10.1002/j.1538-7305.1944.tb00874.x

[125] A. AlSaammare, M. Shaqfeh, and H. Alnuweiri, "A simple and efficient approximation to the modified bessel functions and its applications to Rician fading," in *Proc. IEEE 7th GCC Conference and Exhibition*, 2013, pp. 351–354. [Online]. Available: http://dx.doi.org/10.1109/IEEEGCC.2013.6705802

[126] R. Jurdak, B. Kusy, and A. Cotillon, "Group-based Motion Detection for Energy-Efficient Localisation," *Journal of Sensor and Actuator Networks*, vol. 1, no. 3, pp. 183–216, 2012. [Online]. Available: http://dx.doi.org/10.3390/jsan1030183

[127] V. Kumar, N. W. Bergmann, I. Ahmad, R. Jurdak, and B. Kusy, "Cluster-based position tracking of mobile sensors," in *Proceedings of IEEE Conference on Wireless Sensors (ICWiSE)*. IEEE, 2016, pp. 7–14. [Online]. Available: http://dx.doi.org/10.1109/ICWISE.2016.8187754

[128] D. Denkovski, M. Angjelichinoski, V. Atanasovski, and L. Gavrilovska, "Geometric interpretation of theoretical bounds for RSS-based source localization with uncertain anchor positions," *Digital Signal Processing*, vol. 68, pp. 167–181, 2017. [Online]. Available: http://dx.doi.org/10.1016/j.dsp.2017.06.003

[129] C. Jiang, D. Yuan, and Y. Zhao, "Towards clustering algorithms in wireless sensor networks-a survey," in *Proceedings of Wireless communications and networking conference*. IEEE, 2009, pp. 1–6. [Online]. Available: http://dx.doi.org/10.1109/WCNC.2009.4917996